NUREG/CR-1339
EGG-2020

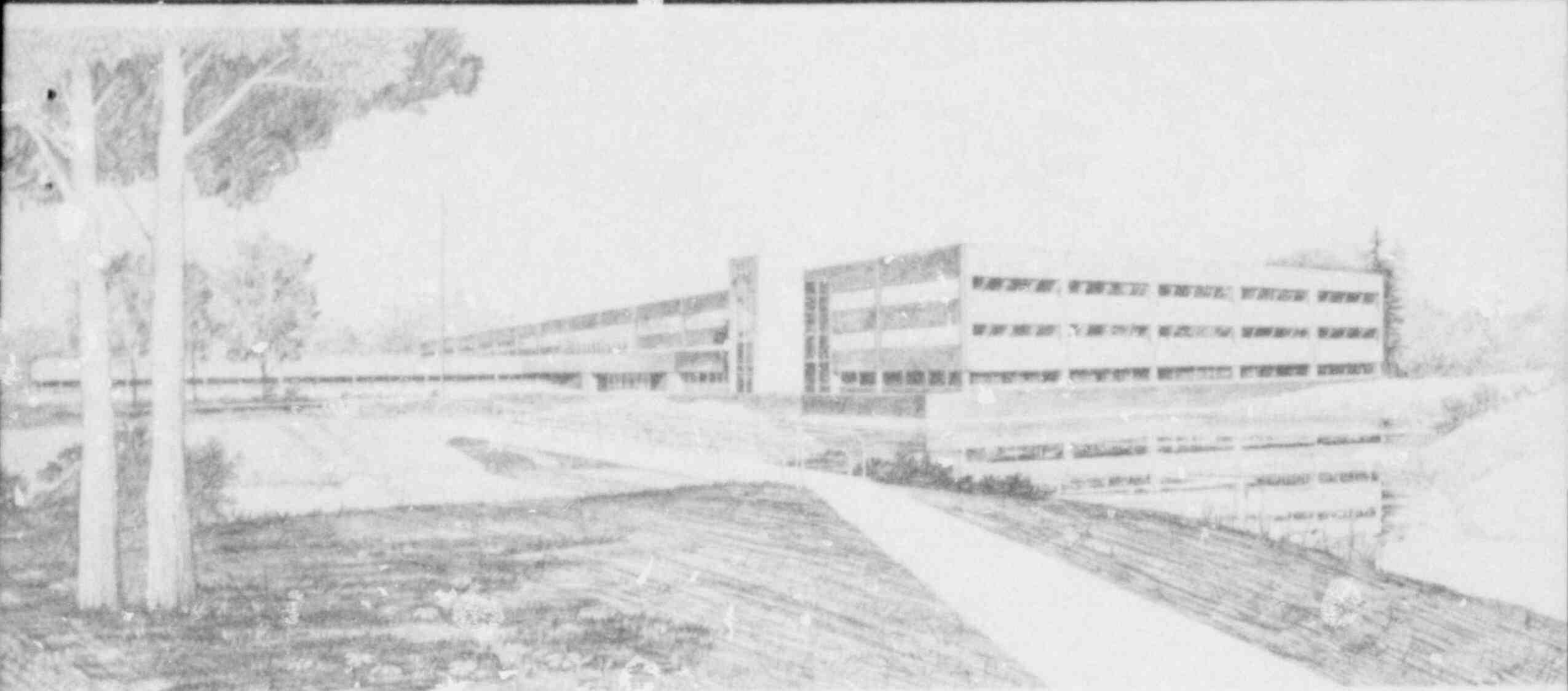

U.S. Department of Energy
Idaho Operations Office • Idaho National Engineering Laboratory

Independent Assessment Of The Steady State Fuel Rod Analysis Code FRAPCON-1

E. Thomas Laats
G. Bob Peeler
Nora R. Scofield

May 1980

Prepared for the
U. S. Nuclear Regulatory Commission
Under DOE Contract No. DE-AC07-76IDO1570

EG&G Idaho

Available from

GPO Sales Program
Division of Technical Information and Document Control
U.S. Nuclear Regulatory Commission
Washington, D.C. 20555

and

National Technical Information Service
Springfield, Virginia 22161

NUREG/CR-1339
EGG-2020
Distribution Category: R3 and R4

INDEPENDENT ASSESSMENT OF THE STEADY STATE FUEL ROD ANALYSIS CODE FRAPCON-1

E. Thomas Laats
G. Bob Peeler
Nora R. Scofield

Published May 1980

EG&G Idaho, Inc.
Idaho Falls, Idaho 83415

Prepared for the
U. S. Nuclear Regulatory Commission
Washington, D. C. 20555
Under DOE Contract No. DE-AC07-76IDO1570
FIN No. A6046

ABSTRACT

The predictive capabilities of the steady state fuel rod behavior program, FRAPCON-1, have been independently assessed. FRAPCON-1 code predictions of fuel behavior are compared with experimental data for test rods and with predictions from the FRAP-S3 code for commercial design rods. The code-to-data comparisons are used to assess the accuracy of fuel rod thermal, pressure, deformation, and corrosion models under steady state operating conditions. The code-to-code comparisons are used to identify the effects of model differences between FRAPCON-1 and the previously assessed fuel behavior code, FRAP-S3. On the basis of results of these studies, conclusions are given regarding present model capabilities and future development needs.

ACKNOWLEDGMENTS

The authors acknowledge the many people and organizations who assisted in the performance of the FRAPCON-1 assessment. G. A. Berna provided timely model development support, and N. L. Hampton assisted in data processing and report preparation. Much of the data used to assess the FRAPCON-1 code was obtained from preliminary data reports describing tests conducted at the Power Burst Facility at the Idaho National Engineering Laboratory and the OECD Halden reactor test facility in Halden, Norway.

SUMMARY

The steady state fuel rod analysis program, FRAPCON-1, has been independently assessed for the United States Nuclear Regulatory Commission by the Code Assessment and Applications Program of EG&G Idaho, Inc. The primary objectives of this assessment were to demonstrate where best estimate model capabilities exist and to provide guidance for model development where improvements seem warranted. FRAPCON-1 is a derivation of the FRAP-S3 code developed by EG&G Idaho, Inc., and the GAPCON-Thermal-3 code developed by Battelle Pacific Northwest Laboratories. This new code is the first of a series of FRAPCON codes intended to calculate the effects of power and burnup on fuel behavior under normal (as opposed to transient or hypothesized accident-related) operating conditions. The primary application of FRAPCON-1 is to supply initial conditions to the FRAP-T5 transient fuel rod analysis program.

Two general types of analyses were conducted during the assessment of FRAPCON-1. First, an analysis of fuel behavior for commercial rods was used to evaluate general code performance characteristics. Second, a comparative analysis between FRAPCON-1 predictions and the measured behavior of test rods was used to evaluate model accuracy.

During the studies involving commercial rods, predictions of FRAPCON-1 and the previously assessed FRAP-S3 code were compared for a core-average rod. The rod was assumed to operate in either a boiling or a pressurized water reactor (BWR, PWR) from beginning-of- to end-of-life. This comparison shows (a) the effect of model differences between FRAPCON-1 and FRAP-S3, and (b) the capability of FRAPCON-1 for modeling a full scale commercial fuel rod. General conclusions from this study are:

1. Modeling differences cause FRAPCON-1 to predict higher fuel temperatures than FRAP-S3 for these low density 94% theoretical density (TD) fuel rods.
2. Use of the new permanent fuel restructing model decreases predicted fuel temperatures during the rod lifetime.
3. FRAPCON-1 prediction of higher fuel temperatures produced prediction of higher internal pressures, increased fuel swelling, and reduced cladding creepdown.

During the studies in which FRAPCON-1 results were compared with experimental data (in-pile measurements and postirradiation examination data from about 700 test rods), FRAPCON-1 exhibited better calculational accuracy than FRAP-S3. Results from this study are summarized as follows. The thermal model results are discussed first, due to the governing influence of rod temperature on the fission gas release, internal pressure, and mechanical deformation models. Then, the pressure, deformation and corrosion model results are presented, respectively.

1. Fuel centerline temperature is generally overpredicted for rods with low density (< 95% TD) fuel, and underpredicted for rods with high density fuel (>95% TD). Better agreement is noted for certain situations, namely, (a) for unpressurized rods rather than pressurized rods, (b) pellet-cladding gap sizes less than 2% of the pellet diameter, and (c) power levels greater than 45 kW/m. The standard deviation between centerline temperature measurements and predictions is 170 K for unpressurized rods and 294 K for pressurized rods.
2. The predicted radial temperature profile is too steep in the inner part of the fuel pellet and too flat near the pellet surface.
3. FRAPCON-1 accurately predicts gap conductance during hard gap closure conditions, but overpredicts the measured value during soft gap closure. The standard deviation is about 11 000 $W/m^2 \cdot K$ for unpressurized rods and 21 000 $W/m^2 \cdot K$ for pressurized rods.
4. Fission gas release fraction is generally overpredicted when the measured fraction

is less than about 20%. The overall standard deviation is 16%. Although the gas release model includes cumulative burnup effects, a burnup enhancement factor is required.

5. Rod internal pressure is generally overpredicted for prepressurized fuel rods, especially when the rod power level is high or the pellet-cladding gap is closed. The standard deviation is 1.6 MPa.

6. The onset of thermal gap closure is predicted to occur within the range of measured values. Best agreement between FRAPCON-1 and the data occurs for power levels between 20 and 25 kW/m. FRAPCON-1 overpredicts the amount of relocation for large gap sizes (>2%) and underpredicts relocation for small gap sizes (<2%). The standard deviation is 11 kW/m.

7. Predictions are in close agreement with fuel axial thermal expansion measurements and for strains less than 0.3% of the stack length, when the pellet-cladding gap is usually open. For strains above 0.3% when the pellet-cladding gap is closed, FRAPCON-1 overestimates the measured expansion. The standard deviation is 0.37% of the stack length.

8. For open or soft gap closure conditions, the extent of permanent fuel deformation is underestimated, probably due to the lack of a fuel compression model or of a fuel stack slippage model, or both. The standard deviation between the permanent deformation measurements and the predictions is 0.45% of the measurement.

9. FRAPCON-1 generally predicts negative cladding strain trends well, but overestimates the extent of creepdown, even though fission gas release, internal pressure, and fuel temperature are generally overestimated, which tends to retard creepdown. The standard deviation between measured and predicted cladding strain is 0.5% in the radial direction and 0.2% in axial direction.

10. Cladding corrosion and hydrogen uptake rates are slightly underpredicted. The standard deviations for these models are 6 μm and 37 ppm, respectively.

CONTENTS

FIGURES

TABLES

INDEPENDENT ASSESSMENT OF THE STEADY STATE FUEL ROD ANALYSIS CODE FRAPCON-1

1. INTRODUCTION

Before a computer code can be used with a known degree of confidence for conducting reactor safety analyses, the accuracy of its constituent models must be demonstrated on basic physical grounds. This report discusses the results of model assessment studies addressing the steady state fuel rod behavior code, FRAPCON-1.[a] This code, the first of a series of FRAPCON codes, is a derivation of the FRAP-S3[1] code developed by EG&G Idaho, Inc., and the GAPCON-Thermal-3[2] code developed by Battelle Pacific Northwest Laboratories. The assessment of FRAPCON-1 was conducted by the Code Assessment and Applications Program of EG&G Idaho, Inc., and is part of the Safety Code Development Program sponsored by the Office of Water Reactor Safety Research of the United States Nuclear Regulatory Commission.

FRAPCON-1 calculates the effects of power and burnup on fuel rod behavior under steady state operating conditions. The code treats the coupled effects of fuel rod thermal and mechanical changes. Burnup effects modeled by FRAPCON-1 include fission gas release, fuel swelling and densification, cladding collapse, and cladding corrosion buildup. The primary application of FRAPCON-1 is to supply the transient fuel rod analysis program, FRAP-T5[3], with initial conditions which reflect operation prior to the occurrence of hypothesized transients.

a. FRAPCON MOD 001, MATPRO Version 10A, Idaho National Engineering Laboratory, EG&G Idaho, Inc., Code Configuration Control Number H00730IB.

The primary objectives of the FRAPCON assessment effort were to demonstrate where best estimate model capabilities exist and to provide guidance for model development where improvements seem warranted. Model capabilities to be assessed are chosen to correspond with fuel behavior phenomena which are both amenable to experimentation and are expected to impact reactor safety analyses.

Model assessment studies consist of comparing FRAPCON-1 predictions with experimental data for test rods and with FRAP-S3 code predictions for rods of commercial design. The code-to-data comparisons are used to assess the accuracy of fuel rod thermal, pressure, deformation, and corrosion models under steady state operating conditions. The code-to-code comparisons are used to identify the effects of model differences between FRAPCON-1 and the previously assessed code, FRAP-S3. In all, some 700 runs were generated for the independent assessment of FRAPCON-1.

This report briefly describes the FRAPCON-1 code, the procedures, and the general assessment approach. The individual computer runs, experiment data sources, rod design and operating conditions, and the model parameters evaluation are identified. The general requirements for FRAPCON-1 analyses and interpretation of results are explained. The results are discussed for each assessment category and conclusions of these assessments are presented. User recommendations are given. General text references and source material for data comparison runs are listed.

2. CODE DESCRIPTION

The FRAPCON-1 code calculates thermal and mechanical fuel behavior responses occurring during steady state operation. FRAPCON-1 has models which account for temperature- and burnup-dependent changes in fuel and cladding properties, gap and surface heat transfer, rod internal pressure, and fuel and cladding deformation. Fuel dimensions are influenced by thermal expansion, relocation, swelling, and densification models. Cladding deformation models account for thermal expansion, hydrostatic pressure differences, creep collapse, irradiation growth, and gap closure. Fission gas production and release, rod deformation, and temperature models impact rod internal pressure. The buildup of cladding corrosion layers affects surface heat transfer models. Unless sustained closed gap and high temperature conditions exist, running time and convergence are usually not limiting considerations. Detailed descriptions of the FRAPCON-1 code and its materials properties package are provided in References 4 and 5.

The main user-supplied input for FRAPCON-1 describes fuel design and fabrication history, operating history, and axial nodalization. The operating history includes system coolant conditions, axial power distributions, and time-dependent rod average power.

3. ASSESSMENT PROCEDURE AND RATIONALE

As background to the discussion of results, this section presents a general description of (a) the procedure used to assess FRAPCON-1, (b) the rationale pertaining to the data sample, and (c) the input conventions used for computer runs.

3.1 Functional Procedure

The procedure used to assess FRAPCON-1 is summarized in Table 1. Basically, the procedure involves acquiring fuel rod experimental data, reviewing and cataloging the data, generating code predictions, and comparing the code predictions and experimental data to determine the code predictive capabilities. A large experimental data sample is used to provide a statistical base for quantitative model evaluation. Many measurements, model calculations, and results of supporting analyses were independently generated and then interrelated with other experiments and the computer code on a consistent basis. Present status of each activity in Table 1 is assigned a letter designation, A or B, which indicates currently implemented and planned activities, respectively.

3.2 Rationale for Using Large Sets of Data Samples

Various incentives exist for maximizing the sample sizes considered in code-to-data comparisons. These incentives all stem from the reliability desired for safety analysis codes. In general, data requirements have not been completely met until the point is reached when either (a) consideration of new data does not change

TABLE 1. FUEL BEHAVIOR ASSESSMENT STANDARD PROCEDURES

General Procedure	Activities	Status
Data Acquisition	Fuel Research Programs Followed	A[a]
	Literature Reviewed	A
	Assessment Aspects identified	A
Experiment Review	Design Operating Conditions Identified	A
	Data Reduction, Physical Evaluation	A
	Data Presentation Formulated	A
	Measured Values Cataloged	A
Generation of Results	Input Deck Set Up	A
	FRAP Computer Run	A
	Debug Activity	A
	Predictions Cataloged	A
Analysis of Results	Comparative Presentation Formulated	A
	Physical Interpretation, Diagnosis	A
	Results Consolidated, Trends Established	A
	Best Estimate Comparison ($\mu_m \rightarrow \mu_p$)	B[b]
	Uncertainty Comparison ($\mu_m \leftrightarrow \mu_p$)	B
	Model Capability Stated	

a. = Currently used.

b. = Potentially used.

measurement distributions, or (b) current model uncertainties are found to be acceptable on the basis of sensitivity studies.

The probability exists that inherent model design characteristics may either be physically unrealistic or somehow provide compensation for undiscovered model errors. Such a condition may be undetected by the code assessment process, unless data other than that used for correlation, or data which may reflect as yet unmodeled basic principles are continually added to the sample.

For each category of code-to-data comparison, identifying the mean, range, and distribution of the fuel behavior measurements is dependent on having many data points applicable to a given design configuration and range of operating conditions. This requirement arises because scatter in the data suggests that the range reflecting reproducibility of fuel rod measurements is quite large. An additional reason for generating large numbers of code-to-data comparisons is based on intended application of the code to commercial power reactor conditions. Assessment conclusions based on measurements from large numbers of rods are considered most likely to be applicable to the case of typical fuel behavior variation in a large power reactor core with 40 to 50 thousand rods. That is, data scatter is thought to be necessary for describing the wide range of core conditions which will exist.

Measurement distributions characterized by many data points can also indicate whether integral calculations of the corresponding model output uncertainty are physically valid. Figure 1 shows an idealized schematic of how the relationship between measured and predicted distributions can be used to either characterize model capabilities or make development recommendations. Defining these distributions for fuel behavior parameters requires large sets of data samples.

3.3 Input Conventions

Certain input conventions were common to all FRAPCON-1 runs. Radial nodalization consisted of 10 fuel intervals, one gap interval, and two cladding intervals. Central holes were specified for test rods with fuel centerline thermocouples. Axially, test rods were divided into three or five intervals, commercial rods were divided into nine intervals. A single-channel thermal-hydraulic analysis was used with enthalpy rise calculated internally based on inlet coolant conditions. When not reported in detail, hydraulic parameters and channel geometry were input to allow surplus cooling conditions to exist. (Surface heat transfer was usually not a limiting factor for the experiments considered.) Radial power distributions were based on the FRAPCON-1 simplified diffusion theory model for low enrichment commercial design rods and most of the highly enriched rods[6], and on test predictions for rods irradiated in the Power Burst Facility.[7] The Ross and Stoute gap conductance model, coupled with the Coleman fuel relocation and effective fuel conductivity models[1], was selected.

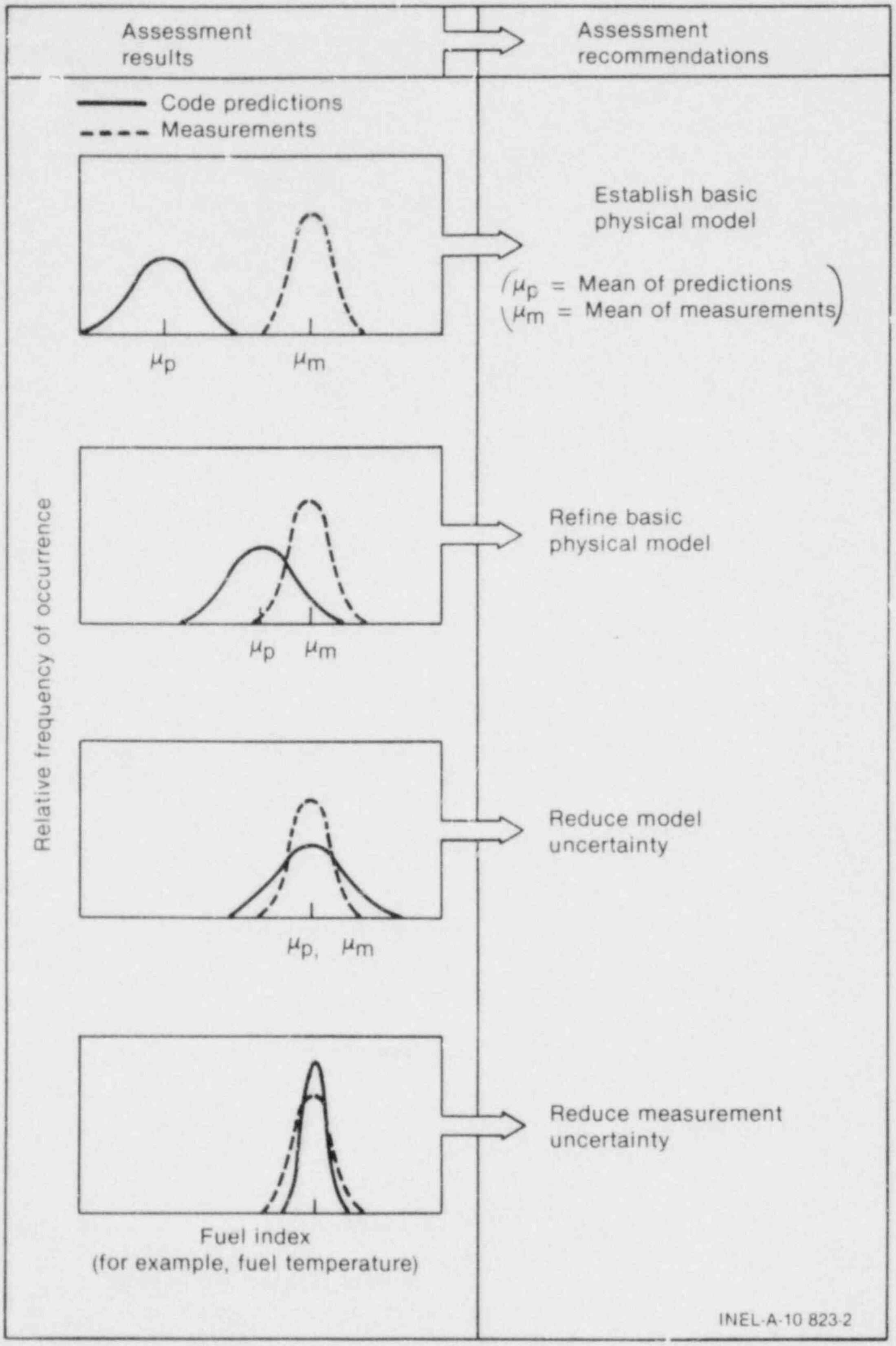

Figure 1. Idealized application of assessment functions.

4. RUN IDENTIFICATION

Nominal input data and data sources for all assessment runs are summarized in Table 2. Presented herein are the computer run number and experimental data source, reference numbers, rod design and operating data, and relevant output parameters for all runs in each rod analysis category. Best-estimate input values were assumed whenever geometry, system condition, or fabrication input details were not given in the reference material.

The scope of the FRAPCON-1 assessment effort is summarized in Table 3. Listed are the various assessment categories, the experimental data source, and the models which were evaluated within each category.

Dish Volume (%)	Fuel Length (ft)	Loop Pressure (psia)	Mass Flow (10^6 lb/hr-ft^2)	Inlet Temperature (°F)	Peak Power (kW/ft)	Peak Average (axial)	Operating hours	Output
0.0	12.0	1035.0	1.3	533.0	10.3[c]	1.4	32000.0	Standard[d]
0.0	12.3	1055.0	1.3	533.0	8.8[c]	1.4	32000.0	Standard[d]
1.5	12.0	2250.0	2.5	552.0	9.8[c]	1.4	21000.0	Standard[d]
1.5	11.9	2250.0	2.5	552.0	7.6[c]	1.4	21000.0	Standard[d]
1.3	5.625	406.0	0.39	446.0	--	1.3	10,4400.0	TF,hg
2.0	1.6,1.2	1100.0	2.1	414.0	20.6,20.2	1.0[f]	1810.0.5.0,3.0	ε'_{cr}
3.6,0.0	1.736	485.0	0.35	463.0	22.6	1.2	2140.0	ε'_{cr},ε'_{fx},ε'_{cx}
2.1	2.0-2.15	490.0	0.36	460.0,467.0	12.0,15.0	1.36,1.07	4820.0	TF,P',ε_{cx}
0.9	2.0	490.0	0.36	460.0	15.6	1.1	4820.0	ε'_{cx}
0.9	2.14-2.18	490.0	0.36	467.0	11.8	1.4	4820.0	P'
0.0	1.77	490.0	0.27	467.0	17.8	1.26	14.0	ε'_{fx},ε_{cx}
1.0,0.0	1.76	490.0	0.33	467.0	15.8	1.26	14.0	ε'_{fx}
1.4	1.77	485.0	0.32	460.0	14.7-16.3	1.07	14.0	TF,ε'_{cx}
0.0	0.46	2000.0[f]	0.0	375.0-813.0	14.1	1.0[f]	3830.0	TF
2.2	1.64	1000.0	0.0	563.0[e]	20.8	1.2	1692.0	TF
2.0,0.0	1.98	490.0	0.36	467.0,460.0	21.5,23.8	1.4,1.3	6450.0,20.0	TF,ε'_{fx},ε'_{cx}
2.0,0.0	1.98	490.0	0.36	467.0,460.0	21.5,23.8	1.4,1.3	20.0	ε'_{fx},ε'_{cx}
0.0	0.37	15.0[f]	0.0	150.0-290.0	22.9,25.7	1.0	24.0,30.0	TF,hg, TFOC
0.0	1.52	485.0	0.39	464.0	19.4	1.5	20,1500.0	TF
0.0	1.8	485.0	0.46	464.0	32.0,40.3	1.5[f]	2740.0,130.0	P',ε'_{cx}
0.0	0.24	0.0	0.0	650.0[e]	14.0-26.0	1.02-1.05	1800.0-18000.0	GR
1.5	9.0-8.7	2360.0	2.5[f]	550.0	7.4[f]	1.4[f]	20000.0	ε_{cr},ε_{fx}
1.9	2.9-3.05	2000.0	2.8	515.0	4.2-8.4	1.32	1200.0-7800.0	H_2
1.9	3.05	2000.0-2250.0	2.7	515.0,480.0	8.4-18.3	1.32	2200.0-10400.0	ε_{cr},ε_{cx},GR,ZrO_2,H_2
1.9	3.05	2000.0-2250.0	2.7	515.0,480.0	7.3-24.3	1.32	12600.0-18000.0	ε_{cr},ε_{cx},GR,ZrO_2,H_2
2.4	5.5	406.0	0.39-0.51	440.0	3.2-16.0	1.24	900.0-7700.0	ε_{cr},ε_{cx},GR,ZrO_2,H_2,ε'_{cx}
1.8	0.52	1407.0	0.0	126.0-324.0	19.6-36.6	1.0-1.13	600.0	ε_{cr},ε_{cx},GR
0.0	0.51-1.01	1421.0	0.0	100.0-177.0	9.5-16.8	1.0	14000.0	ε_{cr},ε_{cx},GR
1.5,0.0	2.6-5.6	406.0	0.3-0.48	440.0	9.3-18.8	1.28	500.0-1900.0	TF
0.0	0.50	1180.0	2.4	480.0	16.6-17.4	1.0	2800.0	ε_{cr},ε_{cx},GR
--	2.46-2.85	1000.0	3.2-6.8	344.0	27.4-47.3	1.3-1.5	480.0-1560.0	GR,ε_{cr}
2.3	3.0	2080.0-2200.0	0.94-2.0	590.0,620.0	19.9-24.9	1.35	10.0	TF,ε_{cx},P',hg',ZrO_2,ε_{cr}
4.1	2.89	2160.0	0.61-2.6	540.0-620.0	19.2-20.3	1.32,1.34	23.0,33.0	TF,ε'_{cx},P',hg
1.1[f]	7.38	1050.0	1.5	500.0	9.5-12.1	1.28	5500.0-7900.0	GR,GRMOL,GLOMP,ε_{cr}
1.0,1.1	4.89	1050.0	1.5	500.0	12.1-21.4	1.28	500.0-3260.0	GR,GRMOL,GCOMP,ε_{cx},ε_{cr}
1.8	1.56	490.0	0.96	454.0,464.0	13.2-19.4	1.08-1.39	5060.0	GR
2.6	1.58	490.0	0.96	454.0,464.0	18.6,19.8	1.04,1.18	7070.0	GR
1.8	4.81	490.0	0.26	454.0	11.3	1.28	5500.0	GR
1.8,1.9	4.81	490.0	0.26	454.0	11.4,11.6	1.28	9700.0	GR
0.0,1.2	1.66	490.0	0.27	454.0	20.2,21.0	1.11	2100.0	GR, P
0.0,1.8	4.82	490.0	0.33	454.0	22.8-24.9	1.34	3200.0	ε_{cx},ε_{cr},ε'_{fx},ε'_{cx},GR
1.1	1.64	490.0	0.32	454.0	24.1	1.04	4000.0	P, TF, GR

TABLE 2. FRAPCON-I MODEL ASSESSMENT RUN IDENTIFICATION AND NOMINAL INPUT

Run	Source	Number of Rods	Cladding Inside Diameter^a (in.)	Diametral Gap (mils)	Fuel Density (%)	Enrichment (%)	Fill Gas Pressure (psia)	
Commercial Rod Study								
46	7 x 7 SAR	1	0.4990	12.0	94.0	2.2	15.0	1
47	8 x 8 SAR	1	0.4250	9.0	95.0	2.2	15.0	1
48	15 x 15 SAR	1	0.3740	7.5	94.0	2.8	345.0	
49	17 x 17 SAR	1	0.3290	6.5	95.0	2.6	300.0	
Data Comparison Study								
1 - 6	Halden[8]	6	0.4957-0.4961	2.0-6.7	95.2-97.8	5.0	15.0	1.
29, 30	NRU[9]	2	0.7349	4.3	97.6,95.8	1.4,1.6	15.0	0
31, 32	Halden IFA-225	2	0.4992	5.9	95.0	5.9	15.0	0.
33 - 36	Halden IFA-226[10]	4	0.3743-0.3746	7.9-9.9	91.6-95.9	7.3(U+Pu)	15.0	5.
37 - 39	Halden IFA-226[10]	3	0.3737-0.3741	3.6-7.8	95.5	7.3(U+Pu)	15.0	.7
50 - 52	Halden IFA-226[10]	3	0.3743-0.3746	8.2-8.4	90.6-95.1	7.3(U+Pu)	15.0	4.
40	Halden[11]	1	0.4922	5.9	95.0	5.8	15.0	1.
41, 42	Halden[11]	2	0.4921	7.5	95.7	5.8	15.0	0.
43 - 45	Halden[11]	3	0.5535	8.4	96.9,91.3	6.0	15.0	0.
53	RISO	1	0.6929(SS)	3.9	95.7	1.35	15.0	0.
54	RISO	2	0.5043	7.1	94.0	1.45	15.0	1.
57, 59,60	Halden IFA-223	3	0.4988,0.4992	5.9,6.3	94.7	6.0	15.0	3.
58, 61	Halden IFA-223	2	0.4992,0.4994	6.5,6.3	94.7	6.0	15.0	3.
62 - 64	Plum Brook[12,13]	3	1.2745(SS)	24.5	95.0	0.6,0.8	15.0	0.
65 - 69	Halden IFA-130,131[14]	5	0.5024-0.5035	5.9-12.3	90.0-94.0	6.0	15.0	1.
70, 71	Halden IFA-132[14]	2	0.5512	9.9	94.7,94.9	10.0	15.0	9.
73 - 87	LRC[15]	16	0.370	4.0,8.0	93.5	3.0	15.0	1.
88 - 89	KWO[16]	2	0.3661	8.6	94.3	2.8,3.1	15.0,329.0	5.
90 - 94	Saxton I[17]	5	0.3435	6.5	95.0	5.1-7.3	15.0(.1N)	0.
95A-107	Saxton II[18]	13	0.3444	7.1	94.0	5.9(U+Pu)	15.0(.1N)	0.
108-123	Saxton III[19]	16	0.3444	7.1	94.0	5.9(U+Pu)	15.0(.1N)	0.
124-152	Halden[20]	29	0.574-0.5745	5.1-9.5	95.9-97.0	7.0	15.0	1.
205-212	NRX[21]	8	0.7811	33.1	96.6	4.34	15.0(air)^f	0.
213-217	NRX[22]	5	0.8005-0.8044	4.0-8.0	93.1-95.0	1.85	15.0(Ar)	0.
219-221	Halden[6]	3	0.5024-0.4969	6.0-6.7	96.0-96.3	15.0-6.0	15.0	0.
232-239	NRX[23]	8	0.6497-0.6505	7.2-8.0	95.0-97.9	2.4	15.0(air)^f	0.0
251-270	GETR[24]	20	0.5003-0.5103	4.3-8.9	94.8	1.5-3.8	15.0	2.1
273-275, 277-278	PBF[25]	5	0.374	8.0	93.0,94.0	20.0	550.0,375.0	2.0
276, 279-281	PBF[26]	4	0.346	9.9	92.0	9.5	380.0(He,Ar)	3.0
286-288	PRTR[27]	3	0.5078	12.0	94.5	1.2	15.0	7.0
289-298	PRTR[27]	10	0.505,0.5078	12.0	94.5	2.4,2.6	15.0	7.0
299-304	Halden	6	0.7472	3.5,5.1	94.0	4.0	15.0	0.1
305, 306	Halden	7	0.7441	6.3	94.0	4.0	15.0	0.1
307-309	Halden	3	0.4264	11.7	95.1	10.1	15.0	5.6
310-313	Halden	4	0.4264	5.8-11.8	95.1	10.1	15.0	5.6
314, 315	Halden[28]	2	0.4922	3.9,5.9	95.0	5.76	15.0^f	1.4
316-318	Halden IFA-208[29]	3	0.4992	11.8	94.9	7.0	15.0^f	3.7
319, 320	Halden IFA-116[30]	2	0.5537,0.5538	8.6,8.7	96.9,91.3	6.0	5.7,11.4^f	0.9

TABLE 2. (Continued)

Run	Source	Number of Rods	Cladding Inside Diameter[a] (in.)	Diametral Gap (mils)	Fuel Density (%)	Enrichment (%)	Fill Gas[b] Pressure (psia)	Cold Plenum (in.)	V
321 -324	Halden IFA-117[31]	4	0.5531-0.5539	8.0-8.8	96.9,91.3	6.0	11.4	1.06-1.41	1.1
325	Halden	1	0.6309	8.5	95.9	9.65	15.0	5.5[f]	2.1[f]
326, 327	Halden	2	0.5034,0.5036	9.0,12.2	94.0	6.0	15.0	1.68	0.0
328	Halden	1	0.5512	9.9	95.0	10.0	15.0	5.0	0.9
331 -334	Halden IFA-178[32]	4	0.5189	11.9	93.8	6.0	15.0	1.77	0.0
335 -339	Halden IFA-181[33]	5	0.4921	11.2	94.0	11.0	15.0	2.7,3.2	2.5
340 -345	Halden IFA-162[34]	6	0.5059	7.5-13.0	94.8	5.1	15.0	3.9	0.0,
346, 347	Halden IFA-150[35]	2	0.4264	5.9,11.8	95.1	10.1	15.0	5.6	1.8
348	Halden IFA-208[29]	1	0.4992	11.8	94.9	7.0	15.0	3.2	0.0
351	Halden IFA-224[29]	1	0.4992	11.8	90.1	7.0	15.0	3.2	3.7
352, 353	Halden IFA-230[29]	2	0.4992	9.8,13.8	94.9	6.0	15.0	3.2	0.0,
359 -362	WPWR, Saxton West[36]	4	0.374	7.5	92.0	2.8	345.0	6.8	1.5
363 -366	BRR B&W[37]	4	0.380	10.0-13.0	92.5-96.5	5.0[f]	15.0	2.0[f]	2.2
367	Halden IFA-166	1	0.4922	5.9	95.0	5.8	15.0	1.42	0.0
370, 371	Halden IFA-116[30]	2	0.5530,0.5539	7.9,8.8	91.3,96.9	6.01	15.0[f]	1.06,2.04	1.1
372, 373	Halden IFA-142[32]	2	0.7480	4.7	94.3	3.0	15.0[f]	0.12	2.0,
381	Halden IFA-180[38]	2	0.5531	9.2	87.3,91.3	11.0	15.0[f]	1.05	0.0
386	Halden IFA-181[33]	1	0.4921	11.2	94.0	11.0	15.0[f]	2.73	2.5
387 -389	Halden IFA-225	3	0.4992	11.8	95.0	5.9	15.0[f]	0.84	3.7
390 -401	Halden IFA-401 II[39]	11	0.5000	2.8,13.8	86.8-94.5	7.0	15.0	1.4[f]	2.4
402 -404	Halden IFA-404 I	3	0.5000	2.4-3.9	94.8	7.0	15.0[f]	2.8[f]	2.4
405, 406	Halden IFA-414	1	0.3933	2.0-8.7	95.0	7.0	15.0[f]	1.0[f]	2.7[f]
407	Halden IFA-173	1	0.4921	10.6	91.6	6.1	15.0[f]	0.96	1.8[f]
408 -410	Halden IFA-404 II	3	0.4988	2.4	90.1-95.8	7.0	15.0[f]	2.8[f]	2.4
411 -414	MTR[40,41]	4	0.2483-0.2498	0.3,1.0	95.7-97.4	43.0-49.9	15.0	0.04-0.06	10.2,
415 -423	Halden IFA-429[42]	9	0.374	8.0	91.0-95.0	13.0	375.0	1.0	1.1
424 -429	Halden IFA-431[43-5]	6	0.4291	1.9-14.9	92.0,95.0	10.0	15.0	0.59-0.94	0.0
430	PBF	1	0.3460	5.9	92.0	9.5	386.0	3.04	1.3
431, 432	PBF	2	0.4252	7.9	95.0	10.0	15.0	2.17	0.0
433 -436	PBF	4	0.3740	8.0	93.3	20.0	376.0,550.0	2.0	1.0
437 -440	PBF[46]	4	0.3740	8.0	93.3	20.0	376.0	2.0	1.0
441 -445	Halden IFA-418,419	5	0.3661	9.0	91.6-95.0	6.0	514.0,323.0	4.15	2.7
446 -449	PBF	4	0.3740	7.9	93.3	20.0	376.0,550.0	2.0	1.0
450 -453	PBF	4	0.4248	8.7,3.9	97.0,95.0	10.0	374.0(Xe,He,Ar)	2.17	0.0
454 -457	PBF	4	0.3443	3.7,13.6	94.0	12.5	363.0,390.0(Xe)	2.25	1.3,
458 -459	PBF	2	0.3444	8.6	94.0	12.5	389.0,377.0(Xe)	2.0	1.6
460A-463A	PBF	4	0.3443,0.3444	3.3-3.9	94.0	12.5	1204.0,377.0(Xe)	2.0	1.3
464A	PBF[47]	1	0.3445	8.7	92.0	12.5	175.0(Xe)	2.0	1.4
460 -462	Saxton[48]	3	0.3435	7.5	92.0	12.5,9.5	314.0	3.0	1.33
463 -465	Saxton[48]	3	0.3435	7.5	92.0	12.5	12.9(air)	2.0	1.33
466, 467	Saxton[48]	2	0.3435	7.5	92.0	9.5,12.5	185.0,314.0	3.0	1.41
468	Saxton[48]	1	0.3435	7.5	92.0	12.5	12.9(air)	2.0	1.41
469 -472	Saxton[48]	4	0.3435	7.5	92.0	12.5	314.0	3.0	1.41
473 -475	Saxton[48]	3	0.3435	7.5	92.0	12.5	12.9(air)	2.0	1.41
476 -478	Saxton[48]	3	0.3435	7.5	92.0	12.5	314.0	3.0	1.41
479 -481	Saxton[48]	3	0.3435	7.5	92.0	12.5	12.9(air)	2.0	1.41
482 -489	Saxton[48]	8	0.3445	6.5	94.0	5.7	12.9(air)	1.8	1.42
490, 491	Saxton[48]	2	0.3430,0.3435	9.0,9.5	94.0	12.5	185.0,430.0	3.0	1.41
492 -499	Maine Yankee[49]	8	0.3880	8.5	92.2-93.3	2.4	14.7	5.8	1.37
500 -507	Maine Yankee[49]	8	0.3880	8.5	92.3-93.6	2.4	14.7	5.8	1.37
508 -514	Maine Yankee[49]	7	0.3880	8.5	91.7-93.8	2.01	14.7	5.8	1.37
515 -521	Maine Yankee[49]	7	0.3880	8.5	92.7-94.0	2.95	14.7	5.8	1.37
522 -542	Y. B. Robinson[50-8]	21	0.3734	6.5	92.0	3.1	275.0	6.83	1.47
543 -548	Big Rock Point[59,60]	6	0.4825	11.5	92.0,95.0	1.92-2.29	14.7	5.68	2.86
549, 550	EL3[61]	2	0.5256,0.5145	11.8,3.5	95.1	2.98	4.4	0.246	0.0
551, 552	WR1[61]	2	0.5456	9.6	97.8	4.5	14.7(Ar,He)	0.058	1.49

ish lume (%)	Fuel Length (ft)	Loop Pressure (psia)	Mass Flow (10^6 lb/hr-ft^2)	Inlet Temperature (°F)	Peak Power (kW/ft)	Peak Average (axial)	Operating hours	Output
	1.64	490.0	0.32	454.0	21.7-26.0	1.04-1.27	4450.0	P,TF,GR
	1.64	490.0	0.36	454.0	41.8	1.14	1650.0	GR
	1.52	490.0	0.39	454.0	20.4	1.03	5440.0	GR
	2.21	490.0	0.90	454.0	25.2	1.32	4250.0	GR
	1.71	490.0	0.30	464.0,464.0	16.3-17.1	1.11,1.15	7400.0	P',GR
	4.83	490.0	0.28	454.0	18.5	1.25	5790.0	P',ϵ'_{fx},ϵ'_{cx},GR
.4,1.8	5.48	490.0	0.32	454.0	16.0	1.25	5280.0	ϵ_{fx},H_2
	4.81	490.0	0.26	454.0	13.8	1.28	9700.0	ϵ'_{cx}
	4.82	490.0	0.33	454.0	21.7	1.34	3180.0	ϵ_{cr},ϵ_{cx}
	4.82	490.0	0.34	454.0	17.6	1.34	150.0	ϵ'_{fx}
.3	4.92	490.0	0.34	454.0	16.3	1.34	60.0	ϵ'_{cx},ϵ'_{fx}
	12.0	2250.0	2.5	552.0	5.9,13.7	1.40	5000.0,10000.0	ϵ_{fx}
	0.83	500.0[f]	0.0	400.0	4.5	1.12	1200.0,2000.0	ϵ'_{fx}
	1.66	490.0	0.27	454.0	18.0	1.11	12.0	ϵ'_{fx}
	1.64	490.0	0.32	464.0	13.5,14.5	1.26	15.0	TF
.2	1.57	490.0	0.31	464.0	20.3	1.14	4180.0	P'
	1.74	490.0	0.20	454.0	20.0,20.4	1.11	1070.0,10400.0	GRMOL,GR
	4.83	490.0	0.38	454.0	18.5	1.25	5790.0	ϵ'_{fx},ϵ',cx,P
	1.60	490.0	0.35	464.0	15.2	1.27	39.0	P
	0.82	490.0	0.34	454.0,464.0	12.9,17.5	1.04,1.14	7170.0	ϵ'_{fx}
	1.64	490.0	0.17	454.0	17.9	1.08	1640.0	ϵ'_{cr}
	1.31	2000.0	0.12	491.0[f]	14.0	1.20	810.0	ϵ'_{fx},ϵ'_{cr},ϵ'_{cx}
	1.66	490.0	0.34	464.0	12.9	1.16	36.0	ϵ'_{fx}
	1.64	490.0	0.17	454.0	16.3	1.08	3900.0	ϵ'_{cr}
1.9	0.41	2000.0	0.39	518.0	13.0-15.6	1.23	285.0,320.0	ϵ_{cx},ϵ_{cr},ϵ'_{cr},ϵ'_{cx},GR
	0.80	490.0	0.56	464.0	7.2-17.0	1.02-1.30	960.0	TF,P
	1.86-1.89	490.0	0.36	464.0	5.6-8.2	1.08	17.0	TF,hg'
	2.89	2160.0		540.0	13.6	1.345	33.1	TF
	2.98	1040.0	1.9	401.0	11.2,10.8	1.348	2.25,2.0	TF,hg', TFOC
	2.99	2160.0	2.5,2.6	590.0	11.1-12.0	1.349	2.0,2.8	TF,hg',P',ϵ'_{cx}
	2.99	2220.0	2.4	590.0	12.5-13.7	1.349	2.9,5.0	TF,hg',P',ϵ'_{cx}
	2.46	490.0	2.9	460.0	10.1,7.84	1.20	3601.0,4501.0	TF
	3.0	2200.0	2.5	590.0	11.5-15.5	1.348	3.6	TF,P',ϵ'_{cx}
	3.0	1040.0	0.14-0.63	510.0	10.9-11.8	1.348	6.0	TF,hg',TFOC
.4	2.89	2205.0	1.3-3.6,1.6	630.0	6.3-15.7	1.348	22.5-39.0	TF,hg'
	3.89	2205.0	1.6	540.0	4.8,4.4	1.348	3.5	hg'
	2.89	2205.0	3.6,1.6-3.1	630.0	8.2-14.9	1.348	10.0-12.0	TF,P',ϵ'_{cx}
	2.89	2205.0	1.6	540.0	5.0	1.348	1.5	hg'
	2.88	2250.0	2.7	480.0	6.16-6.7	1.49	13571.0	ϵ_{cr},VO,GCOMP,P
-1.41	2.97	2250.0	2.7	483.0	6.20-6.54	1.49,1.42	13571.0	ϵ_{cr}
	2.88	2250.0	2.7	480.0	5.54,6.06	1.42	13571.0	ϵ_{cr}
	2.97	2250.0	2.7	480.0	6.2	1.37	13571.0	ϵ_{cr}
	2.88	2250.0	2.7	480.0	6.15-6.45	1.37	13571.0	ϵ_{cr}
	2.97	2250.0	2.7	480.0	6.48-6.77	1.37,1.43	13571.0	ϵ_{cr}
	2.88	2250.0	2.7	480.0	6.65-6.92	1.43	13571.0	ϵ_{cr}
	2.97	2250.0	2.7	480.0	6.77-6.99	1.36-1.43	13571.0	ϵ_{cr},VO,GCOMP,P
	3.0	2250.0	2.7	480.0	1.23-3.11	1.22-1.28	13571.0	ϵ_{cr}
	2.92	2250.0	2.7	480.0	2.73,5.78	1.42,1.28	13571.0	VO,GCOMP,P
	11.4	1866.0	2.3	525.0	6.09-7.35	1.191	11821.0	GR,ϵ_{fx},ϵ_{cr},VO,GCOMP
	11.4	1866.0	2.3	525.0	6.63-7.34	1.191	11821.0	GR,ϵ_{fx},ϵ_{cr},VO,GCOMP
	11.4	1866.0	2.3	525.0	6.18-6.71	1.91	11821.0	GR,ϵ_{fx},ϵ_{cr},VO,GCOMP
	11.4	1866.0	2.3	525.0	5.20-6.87	1.91	11821.0	GR,ϵ_{fx},ϵ_{cr},VO,GCOMP
	11.98	2250.0	2.3	536.0	7.00-7.65	1.135	19177.0	ϵ_{fx},ϵ_{cr},VO,GCOMP,P
.0.0	5.72	1350.0	1.2	540.0	9.0-10.6	1.19-1.31	6468.0,13420.0	GR,ϵ_{fx},ϵ_{cr},ϵ_{cx},GCOMP
	0.403	50.0	0.0	172.0,162.0	21.58,16.06	1.00	1689.0	GR
	0.53	1120.0	2.6	471.0,483.0	15.22,21.33	1.29,1.19	2015.0	ϵ'_{cr},ϵ_{cx},ϵ'_{cx}

TABLE 2. (Continued)

Run	Source	Number of Rods	Cladding Inside Diameter[a] (in.)	Diametral Gap (mils)	Fuel Density (%)	Enrichment (%)	Fill Gas[b] Pressure (psia)	Co Ple (i
553	Halden IFA-418[61]	1	0.3660	12.0	96.0	6.0	320.0	4.0
555	R2[61]	1	0.4205	8.3	94.4	2.05	14.7	5.5
55[illegible]-585	VBWR,Dresden[62]	30	0.3803-0.3808	6.3-6.8	94.0-96.0	2.76-3.49	14.7	1.90
586	Halden IFA-206	1	0.5941	11.4	95.0	6.0	14.7	4.27
587	Halden IFA-208	1	0.4992	11.8	94.9	7.0	14.7	3.15
588, 589	Halden IFA-211	2	0.4992	11.6	94.3	6.0	14.7	5.20
590A,590B	Halden IFA-224	2	0.4992	11.8	89.3	7.0	14.7	3.15
591	Halden IFA-220	1	0.4992	9.8	94.9	6.0	14.7	5.20
592-594	Halden IFA-410	3	0.4890	7.9-15.8	94.8	7.09	14.7	1.75
595, 598,599	Halden IFA-411	3	0.4249	6.8	94.8	7.09	14.7	5.2
596, 597	Halden IFA-418	2	0.3661	12.2	95.7	12.0,6.0	323.0	3.97
600-602	Halden IFA-409 II	3	0.4252	9.1	92.6-92.9	2.73,2.89	14.7	6.0
603-605	Halden IFA-418	3	0.3661	12.2,9.0	95.7,92.1	12.0,6.0	514.0	4.0
606, 607	Halden IFA-419	2	0.3661	9.0	91.2,94.3	6.0	323.0	4.0
608-610	Halden IFA-427	3	0.3661	7.4,12.2	93.0	3.95,12.0	323.0,514.0	4.0
611	Halden IFA-207	1	0.5941	11.4	95.0	6.0	14.7	4.27
612, 613	Halden IFA-233	2	0.4992,0.4988	6.3,5.9	94.7	6.01	14.7	3.66
614A-615B	DR3	4	0.6929	3.9	95.7	1.35	14.7(Xe)	0.44
616A,616B	Halden IFA-227 I	2	0.5520	8.7,2.8	96.6	2.4	14.7	0.28
617B	Halden IFA-227 II	1	0.5522	3.0	96.5	2.4	14.7	0.28
618A,618B	Halden IFA-227 III	2	0.5520	2.8	96.6	2.4	14.7	0.28
619A,619B	Halden IFA-227 IV	2	0.5512	2.8	90.0,95.0	2.4	14.7	0.59
620-628	Halden IFA-106[63]	9	0.4252	5.2,7.2	94.8-95.5	10.02	14.7	3.31
629-632	Halden IFA-107[63]	4	0.4252	5.2,7.2	94.8,95.5	10.02	14.7	3.31
633-639	Halden IFA-138	7	0.7480	7.1,4.3	93.9	3.0	14.7(Xe)	0.20
640-644	Halden IFA-142	5	0.7480	4.7	94.3	3.0	14.7(Xe)	0.20
645, 646	Halden IFA-206	2	0.5941	11.4	95.0	6.0	14.7	4.27
647-650	BRP[64]	4	0.4820-0.4824	9.8-12.4	90.7-94.6	1.92-2.29	14.7	5.59
651-657	BRP[64]	7	0.4820	11.0	92.0	2.16-8.86	14.7	5.7[f]
658-665	Halden IFA-118 I	8	0.5522-0.5525	1.5-4.1	96.7	6.0	14.7	1.53
666-669	Halden IFA-118 II	4	0.5522-0.5525	3.8-4.1	96.0	6.0	14.7	1.57
670-675	Halden IFA-118 III	6	0.5521-0.5528	1.3-3.9	96.7	6.0	14.7	1.52
676-686	Halden IFA-402	11	0.500	2.4-9.8	94.8-89.8	7.0	14.7	2.95
687-691	Halden IFA-215	5	0.5512	4.0	96.0	6.0	14.7	2.9[f]
692, 693	Halden IFA-216	2	0.5126	6.7	90.1,94.8	91.7	14.7	2.9[f]
694-697	Halden IFA-413	4	0.4988	2.3-9.8	95.6	7.0	14.7	1.5[f]
698, 699	Halden IFA-410	2	0.489	7.9	94.8,96.9	7.09	14.7	1.75
700-702	Halden IFA-411	3	0.4249	6.8	94.8	7.09	14.7	5.2[f]
703-704	PBF GC2-2	2	0.4248	9.1,3.9	97.0	10	374(Xe),(Ar)	2.17
705-706	PBF GC2-2	2	0.4248	3.9,14.2	95.0	10	374	2.17
707-708	PBF GC2-3	1	0.4248	3.9	92.0,95.0	10	374,(Xe)	2.17
709-710	PBF GC2-3	4	0.4248	13.8,9.1	97.0,92.0	10	374,(Ar)	2.17
711	PBF GC1-3	1	0.4248	7.9	95.0	10	15.0	2.17

a. Zircaloy unless otherwise noted.

b. Helium unless otherwise noted.

c. Core average rod power.

d. Standard design package (versus time): centerline temperature, gas release fraction, h_{gap}, internal pressure void volume, ga

e. Cladding surface temperature specified.

f. Assumed.

' (prime)	- denotes instrumented rod data	GRMOL	- gas content
TF	- fuel centerline temperature	GCOMP	- gas composition
ε_{cr}	- cladding circumferential deformation	VO	- void volume
ε_{cx}	- cladding axial deformation	ε_{fx}	- fuel axial deformation
GR	- gas release fraction	ZrO_2	- cladding corrosion thickness
P	- rod internal pressure	H_2	- cladding hydrogen concentration
hg	- gap conductance		

d um .)	Dish Volume (%)	Fuel Length (ft)	Loop Pressure (psia)	Mass Flow (10^6 lb/hr-ft^2)	Inlet Tempgrature (°F)	Peak Power (kW/ft)	Peak Average (axial)	Operating hours	Output
	2.17	2.45	490.0	0.29	460.0	10.8	1.04-1.07	5936.0	TF
	1.21	1.67	1160.0	3.4	491.0	16.37	1.22,1.23	1817.0	TF,GR
	0.0	3.08	1017.0	1.2	528.0	4.53-7.45	1.10-1.48	28187.0-47350.0	GR,ϵ_{cr},ZrO_2,H_2,GCOMP,VO,ϵ_{cx}
	2.85	5.05	490.0	0.84	460.0	14.51	1.22	6576.0	TF
	0.0	4.92	490.0	0.33	460.0	18.7	1.22	2706.0	TF
	1.06	4.92	490.0	0.34	460.0	17.67	1.22	10285.0	TF,GR
	0.0	4.82	490.0	0.34	460.0	16.15	1.22	2556.0	TF
	0.0	4.92	490.0	0.34	460.0	17.67	1.22	9596.0	TF
	--	--	--	--	--	--	--	--	--
	0.0	4.92	490.0	0.34	460.0	13.4	1.22	3491.0-5496.0	TF,ϵ_{fx},ϵ_{cx}
	1.47	2.46	490.0	0.29	464.0	15.24,13.25	1.05	1686.0,2800.0	TF
	1.93	0.82	490.0	0.24	460.0	6.55	1.07	4525.0	ϵ_{fx}
	1.47	2.46	490.0	0.29	460.0	10.06-15.54	1.05	6631.0	ϵ_{fx}
	1.47	2.46	490.0	0.29	460.0	7.01	1.05	5341.0	ϵ_{fx}
	1.47	2.46	490.0	0.29	460.0	9.14	1.05	2001.0	ϵ_{fx}
	2.85	5.05	490.0	0.84	460.0	13.7	1.22	2785.0	TF
	0.0,2.03	1.98	490.0	0.36	460.0,465.0	22.41,17.67	1.26,1.45	5925.0,10720.0	TF
	0.0	0.46	500.0	0.0	205.0-880.0	20.0	1.00	2870.0,16725.0,16705.0	TF, TFOC
	0.0	1.72	490.0	0.20	460.0	17.45	1.15	54.4	ϵ'_{cr}
	0.33	1.72	490.0	0.20	460.0	19.5	1.15	45.6	ϵ'_{cr}
	26.0,0.0	1.72	490.0	0.20	460.0	13.62	1.15	38.8	ϵ'_{cr}
	0.45	1.61	490.0	0.20	460.0	11.43	1.08	32.6	ϵ'_{cr}
	0.0	2.38	490.0	1.2	464.0	9.02-14.32	1.31,1.15	9506.0	TF,P',GR,ϵ_{fx},ZrO_2,ϵ_{cx}
	0.0	2.38	490.0	1.2	464.0,460.0	9.46-15.26	1.35,1.08	3375.0	TF,P',GR,ZrO_2
	2.14	1.43	490.0	0.31	460.0,464.0	15.43-18.49	1.21,1.23	11960.0	GR
	2.16,2.02	1.43	490.0	0.31	464.0,460.0	16.3-21.41	1.15,1.20	8900.0	GR
	2.85,0.0	5.05	490.0	0.84	460.0	12.26,13.12	1.22	6560.0	GR
-5.80	2.85,0.0	5.70	1350.0	1.2	540.0	6.90-9.23	1.28	27811.0	ϵ_{fx},ϵ_{cr},ϵ_{cx}
	0.0	5.84,5.70	1350.0	1.2	540.0	8.96-11.55	1.37	21343.0	ϵ_{fx},ϵ_{cr},ϵ_{cx}
	0.0,0.712	1.64	490.0	0.28	465.0,460.0	15.7-19.4	1.35,1.20	1728.0	ϵ'_{cx}
-1.90	0.0-1.02	1.64	490.0	0.28	465.0,460.0	12.4-15.7	1.34,1.10	1344.0	ϵ'_{cx}
-1.70	0.0,0.714	1.64	490.0	0.28	465.0,460.0	14.1-16.7	1.30,1.20	2736.0	ϵ'_{cx}
	2.38,2.37	1.64	490.0	0.34	460.0	9.3-9.75	1.17,1.16	70.0	ϵ'_{cx}
	0.711	1.64	490.0	0.32	465.0	10.06-14.66	1.30,1.20	78.0	ϵ'_{cx}
	0.0	1.64	490.0	0.36	465.0,460.0	20.0,14.26	1.30,1.20	193.0,137.0	ϵ'_{cx}
	0.0,2.38	1.64	490.0	0.34	460.0,465.0	8.23-10.42	1.17,1.16	98.0	ϵ'_{cx}
	0.0	1.64	490.0	0.33	464.0	12.19	1.12	50.0	ϵ'_{cx}
	0.0	4.92	490.0	0.34	460.0	12.19	1.22	50.0	ϵ'_{fx}, ϵ'_{cx}
	0.0	3.0	1040	2.77	455	11.6,11.5	1.345	7.4	TF, TFOC
	0.0	3.0	1040	2.77	455	12.0,9.62	1.345	7.4	TF, TFOC
	0.0	3.0	1040	2.77	455	11.7,12.8	1.345	5.6	TF, TFOC
	0.0	3.0	1040	2.77	455	11.5,12.1	1.345	5.6,4.6	TF, TFOC
	0.0	3.0	1040	1.9	401	10.8	1.348	2.0	TF, TFOC

abundance, gap size, gas helium fraction.

TABLE 3. MATRIX FOR THE ASSESSMENT OF FRAPCON-1

Assessment Category	Data Analysis Effort	Data Source	Model Evaluation							
			Fuel Temperature	Gap Conductance	Gas Release	Internal Pressure	Fuel Deformation	Cladding Deformation	Cladding Oxidation	Cladding Hydrogen Uptake
Commercial Rod	--	Not Applicable	X	--	--	X	X	X	--	--
Thermal Model	X	Halden, RISO, Plum Brook, PBF, R2, DR3	X	X						
Pressure Model	X	Halden, Saxton, NRX, R2, VBWR, Dresden, LRC, GETR, PBF, PRTR, MTR, Maine Yankee, H. B. Robinson, BRP, EL3	--	--	X	X	--	--	--	--
Deformation Model		Halden, NRU, KWO, Saxton, NRX, GETR, PBF, PRTR, WPWR, BRR B&W, MTR, Maine Yankee, H. B. Robinson, BRP, WR1, VBWR, Dresden	--	--	--	--	X	X	--	--
Corrosion Model		Saxton, PBF, VBWR, Dresden, Halden	--	--	--	--	--	--	X	X

5. ASSESSMENT RESULTS

The results of FRAPCON-1 assessment activities are discussed in the following two sections. The first section establishes FRAPCON-1 performance for modeling typical commercial fuel rod designs and operating conditions as compared to the previously assessed FRAP-S3 code. The second section presents the predictive capabilities of FRAPCON-1 on the basis of comparisons between FRAPCON-1 calculations and experimental data.

5.1 Commercial Rod Studies

Commercial rod studies have been performed with FRAPCON-1 using input representing fuel rod design and operating conditions typical of commercial power reactors. The main objectives are (a) to establish FRAPCON-1 performance characteristics for commercial sized rods, and (b) to determine the integral effects of model and correlation revisions which were used in the development of FRAPCON-1.

FRAPCON-1 predictions for 7 x 7 boiling water reactor (BWR) and 15 x 15 pressurized water reactor (PWR) fuel types were examined to identify the behavior of important variables representing fuel rod thermal and mechanical properties as functions of burnup and power. Previous results have shown that output trends for the more recent 8 x 8 BWR and 17 x 17 PWR fuel types are consistent with those identified for the 7 x 7 and 15 x 15 types, with minor differences due to the lower heat rating, fuel temperature, and sensitivity to burnup of the new fuel types.

Comparisons were made between FRAPCON-1 and FRAP-S3 results. The version of FRAP-S3 used in this study is identical to the previously assessed version, except that an error in the fission gas production model present in the assessed version, was corrected in the version used for this study. This allowed consistency between the FRAP-S3 and FRAPCON-1 gas production models, thus allowing any comparisons between these two codes to indicate the effects of model changes and updates, other than the code performance changes resulting from the correction of the gas production model.

The FRAPCON-1/FRAP-S3 code comparisons represent steady state operation of core average PWR and BWR rods. The power history consists of a power ramp at beginning-of-life (BOL), a long period of steady state operation at full reactor power, concluded by a power ramp at end-of-life (EOL). The rod average heat rating during the long period of steady state operation is 23 and 24.3 kW/m for the PWR and BWR cases, respectively. Rod average burnup is about 2.8×10^6 MWs/kg for EOL ramps. All local results presented here, such as fuel temperature, gap size, and cladding deformation, will correspond to the axial peak power location. The axial peaking factor is 1.4.

Figures 2 and 3 compare FRAP-S3 and FRAPCON-1 calculated fuel centerline temperature as a function of power for 7 x 7 and 15 x 15 rods. These curves represent the startup ramp for BOL fuel rods. FRAPCON-1 temperatures are greater than the FRAP-S3 temperatures, due principally to the effect of one model revision. The Maxwell-Euken porosity correction-factor for determining fuel thermal conductivity, was copied from FRAP-S3 into FRAPCON-1, and then changed. Model developers expected this change to increase fuel temperatures for rods with low fuel density (< 95% TD) and decrease temperatures in high density fuel rods (> 95% TD). As expected, the 94% TD fuel assumed for the commercial rods, resulted in slightly higher fuel temperatures, and higher stored energy as shown on Figures 4 and 5.

The calculated internal pressure during BOL startup as a function of power is shown on Figures 6 and 7. The consistently higher pressures predicted by FRAPCON-1 relative to FRAP-S3 result from (a) higher FRAPCON-1 fuel temperatures, and (b) a modification to the pressure model as incorporated into FRAPCON-1 to more accurately model porosity and pellet-cladding gap pressures. Most of the difference between the FRAPCON-1 and FRAP-S3 values is attributed to the pressure model modification, since the small void volume being directly affected by the temperature increase produces a very small pressure increase.

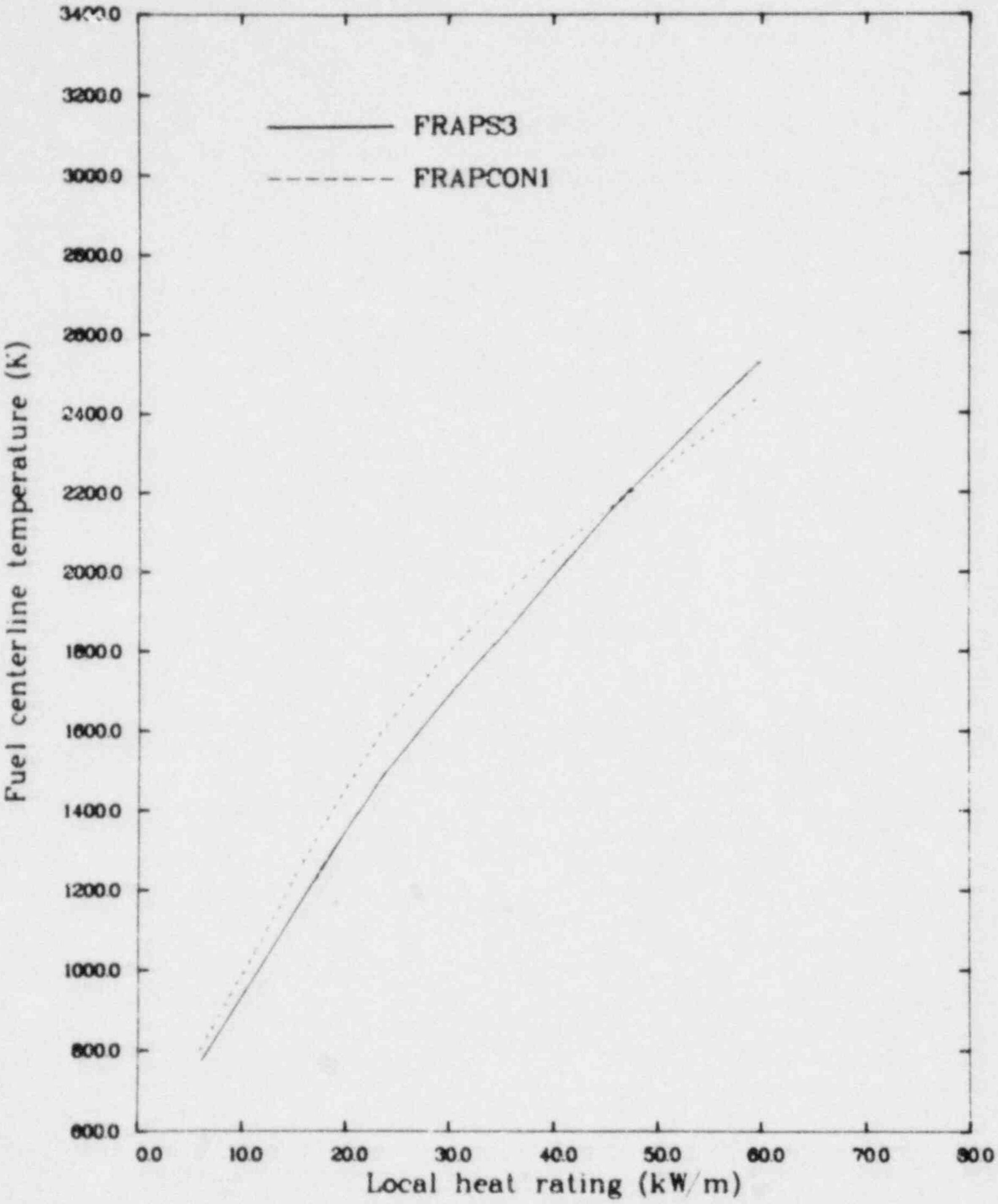

Figure 2. Comparison of FRAPCON-1 and FRAP-S3 fuel centerline temperature ramp for a 7 x 7 rod at beginning-of-life.

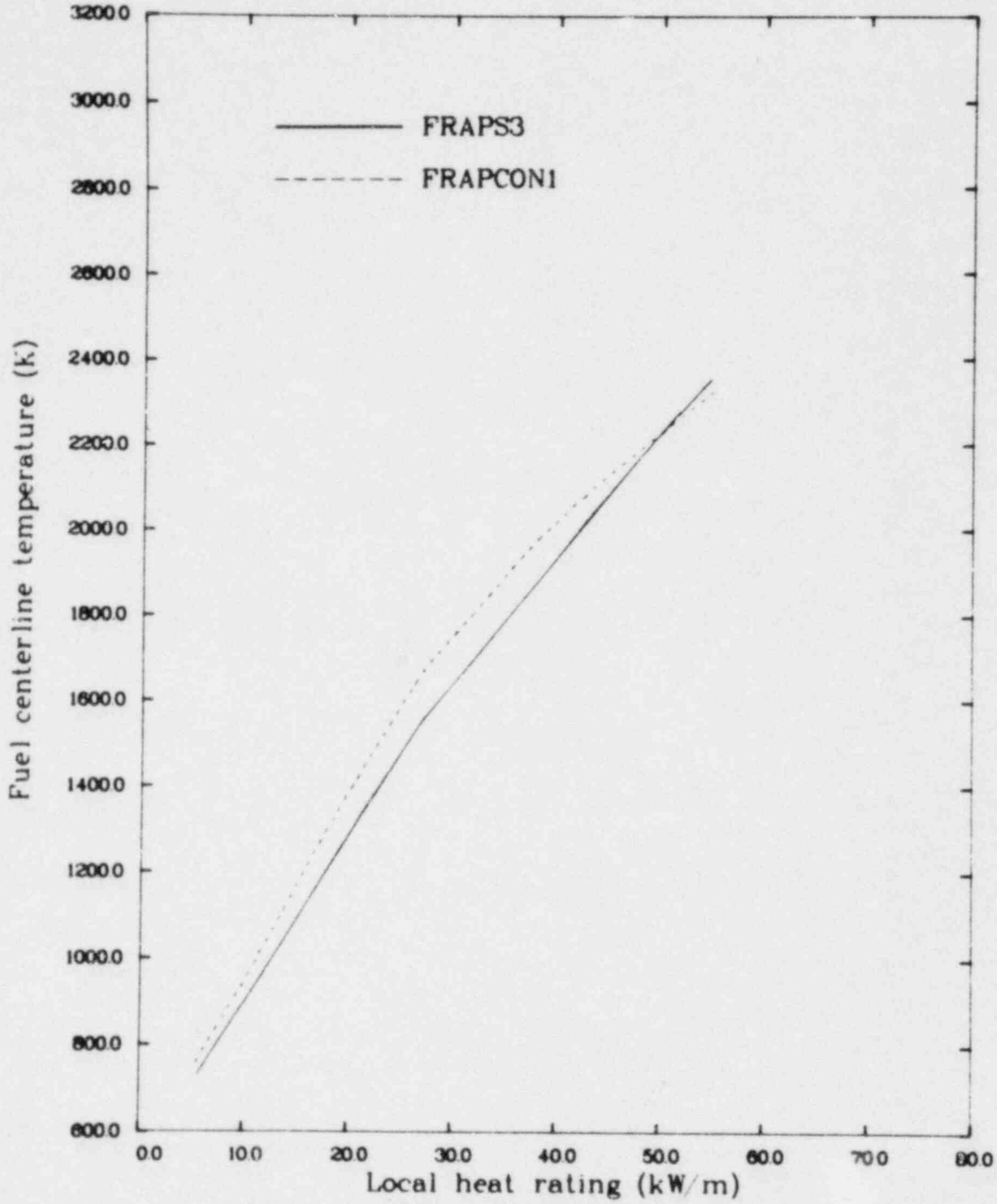

Figure 3. Comparison of FRAPCON-1 and FRAP-S3 fuel centerline temperature ramp for a 15 x 15 rod at beginning-of-life.

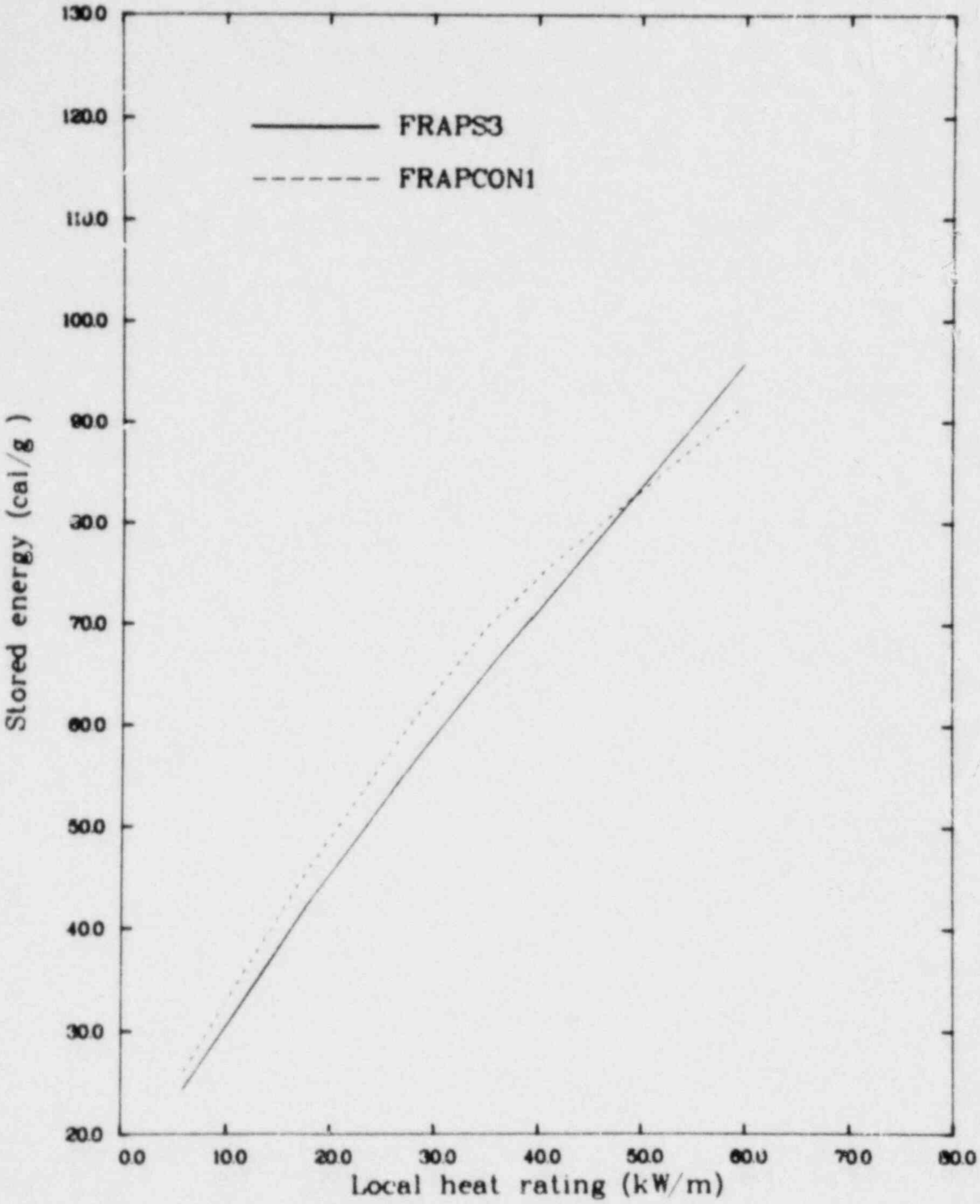

Figure 4. Comparison of FRAPCON-1 and FRAP-S3 stored energy for a 7 x 7 rod at beginning-of-life.

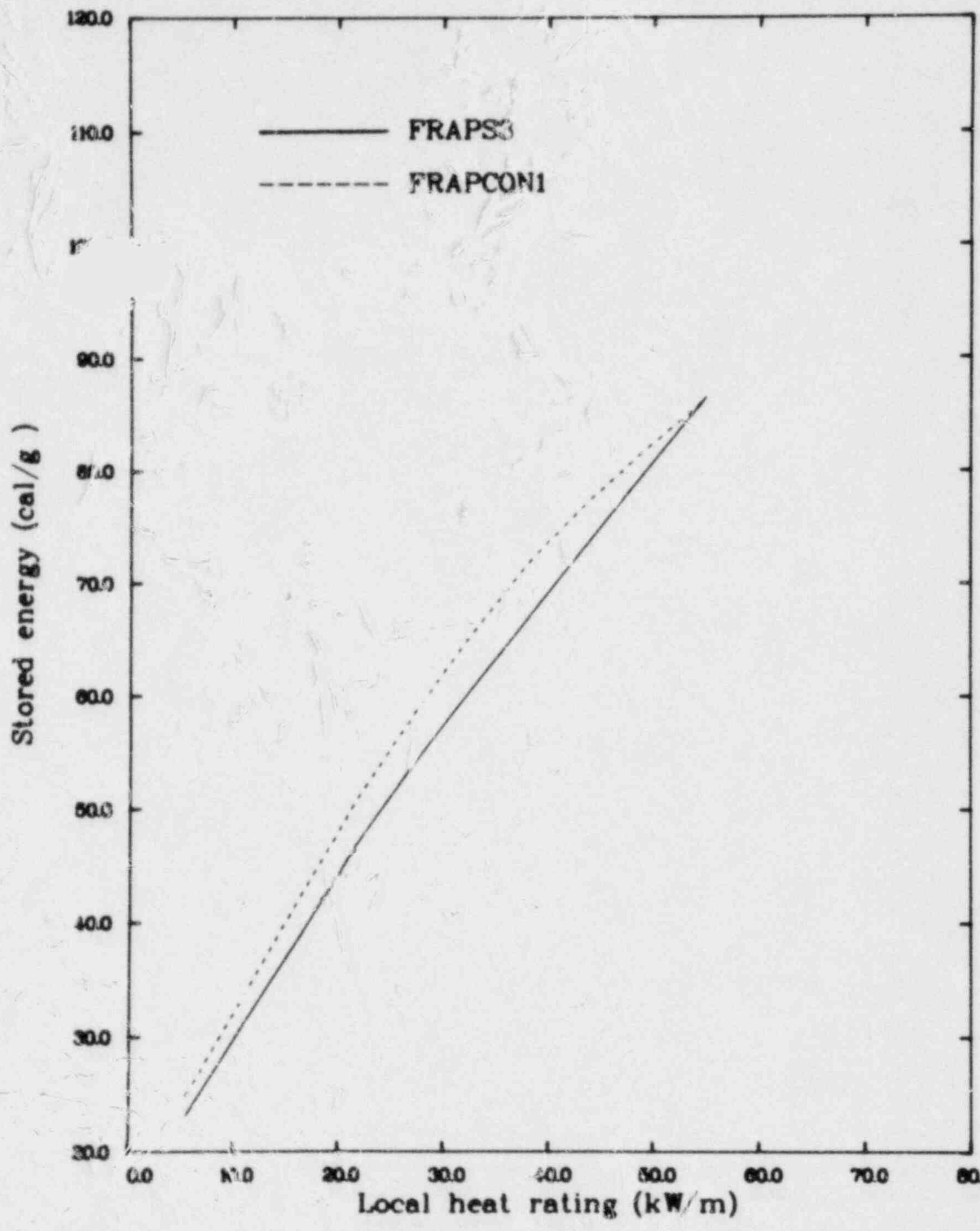

Figure 5. Comparison of FRAPCON-1 and FRAP-S3 stored energy for a 15 x 15 rod at beginning-of-life.

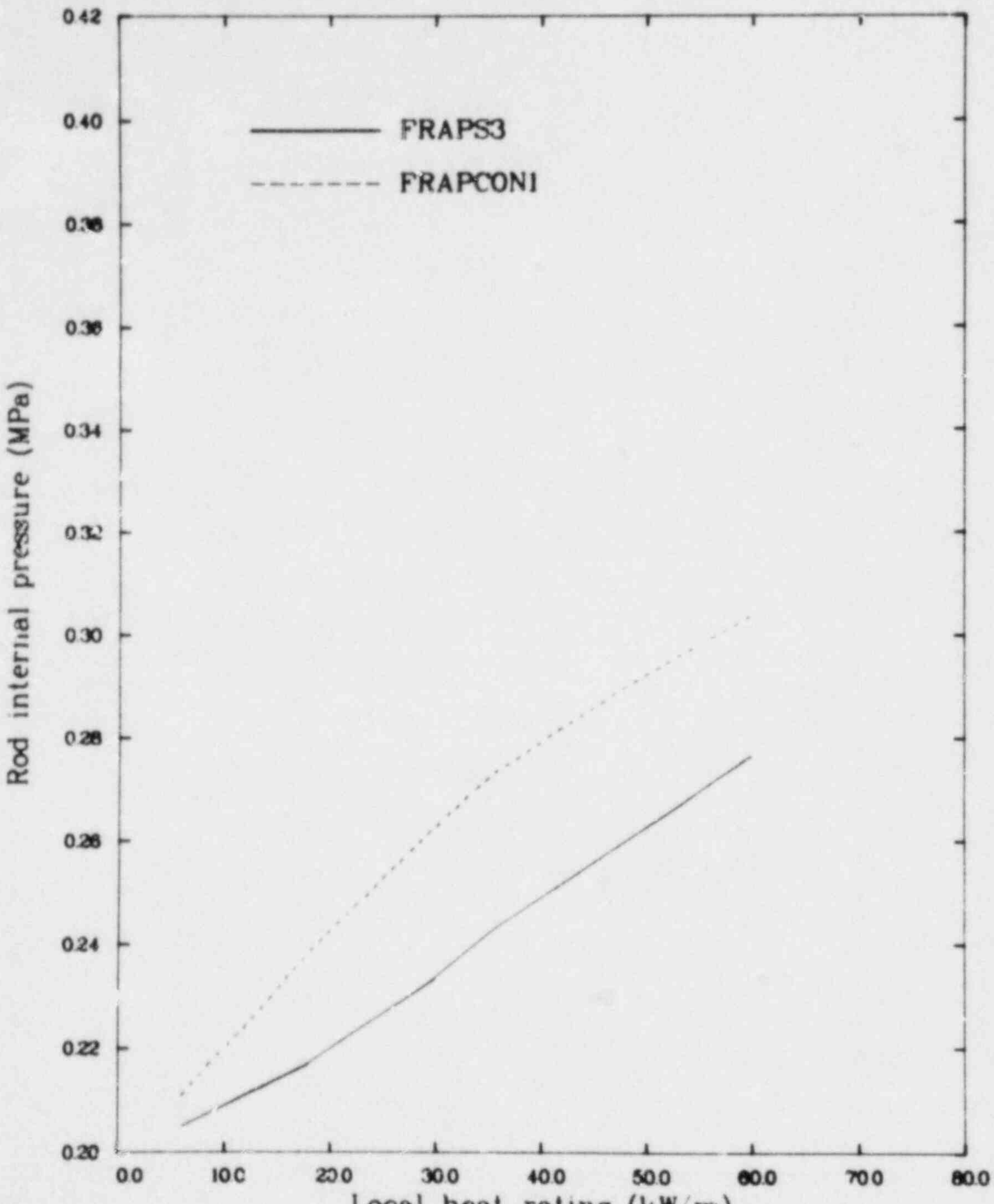

Figure 6. Comparison of FRAPCON-1 and FRAP-S3 rod internal pressure ramp for a 7 x 7 rod at beginning-of-life.

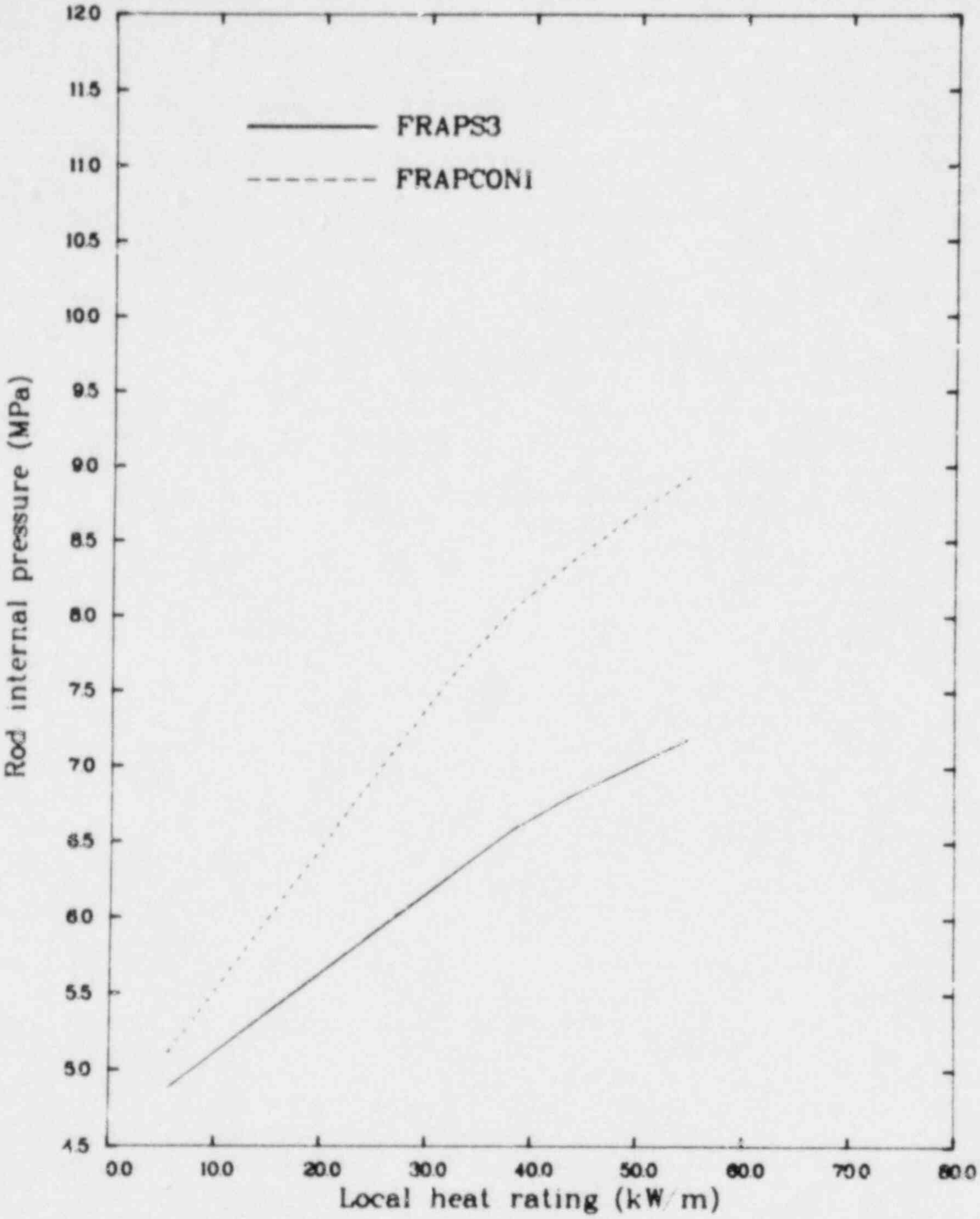

Figure 7. Comparison of FRAPCON-1 and FRAP-S3 rod internal pressure ramp for a 15 x 15 rod at beginning-of-life.

Figures 8 and 9 compare FRAP-S3 and FRAPCON-1 predicted cladding hoop strain as a function of power for 7 x 7 and 15 x 15 rods during the BOL power ramp. For both fuel designs, greater cladding strains are calculated by FRAPCON-1. Even though the percent increase in internal pressure from FRAP-S3 to FRAPCON-1 was comparable for both fuel types, the absolute increase for PWR rods was more than an order of magnitude greater than for the BWR rods. Figures 8 and 9 reflect this difference. Correspondingly, the increased cladding hoop strain from FRAP-S3 to FRAPCON-1 for the PWR rods was about an order of magnitude greater than the observed increase for BWR rods.

The combined influence upon diametral gap size from higher fuel temperature and greater cladding hoop strain is shown on Figures 10 and 11. For both fuel types, FRAPCON-1 predicts slightly smaller gap sizes. Since higher fuel temperatures tend to close the gap and greater cladding hoop strains reduce creepdown (that is, keep the gap open), higher fuel temperature is apparently the dominant parameter affecting gap size, during the BOL power ramp.

The predicted fuel centerline temperature histories for 7 x 7 and 15 x 15 rods during extended steady state operation are shown on Figures 12 and 13, respectively. Three curves are shown on each figure—the FRAP-S3 prediction, the FRAPCON-1 prediction with the permanent fuel restructuring model not used, and the FRAPCON-1 prediction using the permanent fuel restructuring model. Two FRAPCON-1 curves (one with and one without fuel restructuring) are given to enable better characterization of the permanent fuel restructuring model, which is the only completely new model added since FRAP-S3. Also, presenting two curves allows a more direct comparison of FRAP-S3 and FRAPCON-1 differences from model updates alone, without the additional influence of permanent fuel restructuring.

The permanent restructuring model assumes a permanent increase in the fuel thermal conductivity, as a result of fuel restructuring which occurs at elevated temperatures. The fuel probably recracks if the temperature subsequently decreases; however, cracking, following fuel restructuring, is assumed to have negligible effect upon fuel conductivity.

Comparison of the FRAP-S3 and FRAPCON-1 without the permanent restructuring model (Curves 1 and 2) indicates that model updates have produced an increased fuel centerline temperature throughout fuel rod lifetime. Also, the rate of temperature decrease noted for the FRAPCON-1 curve is less, due principally to thermal feedback to the gas release and gap conductance models and to use of a nonburnup-dependent radial power profile model in FRAPCON-1. The burnup-dependent model used in FRAP-S3 depressed the relative power factor at fuel centerline as burnup increased. Thus, the influence of this model caused FRAP-S3 centerline temperatures to decrease as burnup accumulated, a phenomenon not modeled in FRAPCON-1.

As fuel temperatures increased during the BOL startup ramp, prior to the extended steady state operation (Figures 2 and 3), fuel restructuring was assumed to occur for that portion of the fuel pellet whose temperature exceeded 90% of the fuel fabrication sintering temperature. Centerline temperatures reached 2430 and 2350 K for the 7 x 7 and 15 x 15 rods, respectively. Fuel fabrication sintering temperature was 1873 K for both cases. Curves 2 and 3 on Figures 12 and 13 represent, respectively, the centerline temperature histories when (a) the restructured fuel is allowed to crack upon subsequent temperature reduction, thus reducing the effective fuel conductivity, and (b) the restructured fuel is considered permanently restructured and the effective fuel conductivity is not allowed to decrease. As expected, when the permanent fuel restructuring model is used, centerline temperatures during steady state operation are consistently lower than the case for which this model is not used.

The FRAPCON-1 and FRAP-S3 stored energy histories exhibit the same general trends as the temperature histories. These trends are shown on Figures 14 and 15 for BWR and PWR rods, respectively. However, for both FRAPCON-1 cases, a slight increase is observed in the stored energy with operating time, and the FRAP-S3 results show a decrease in stored energy with operating time. This difference in stored energy history is due primarily to the burnup dependent radial power profile model which is available in FRAP-S3 and not available in FRAPCON-1. The slight increase in the FRAPCON-1 predictions are

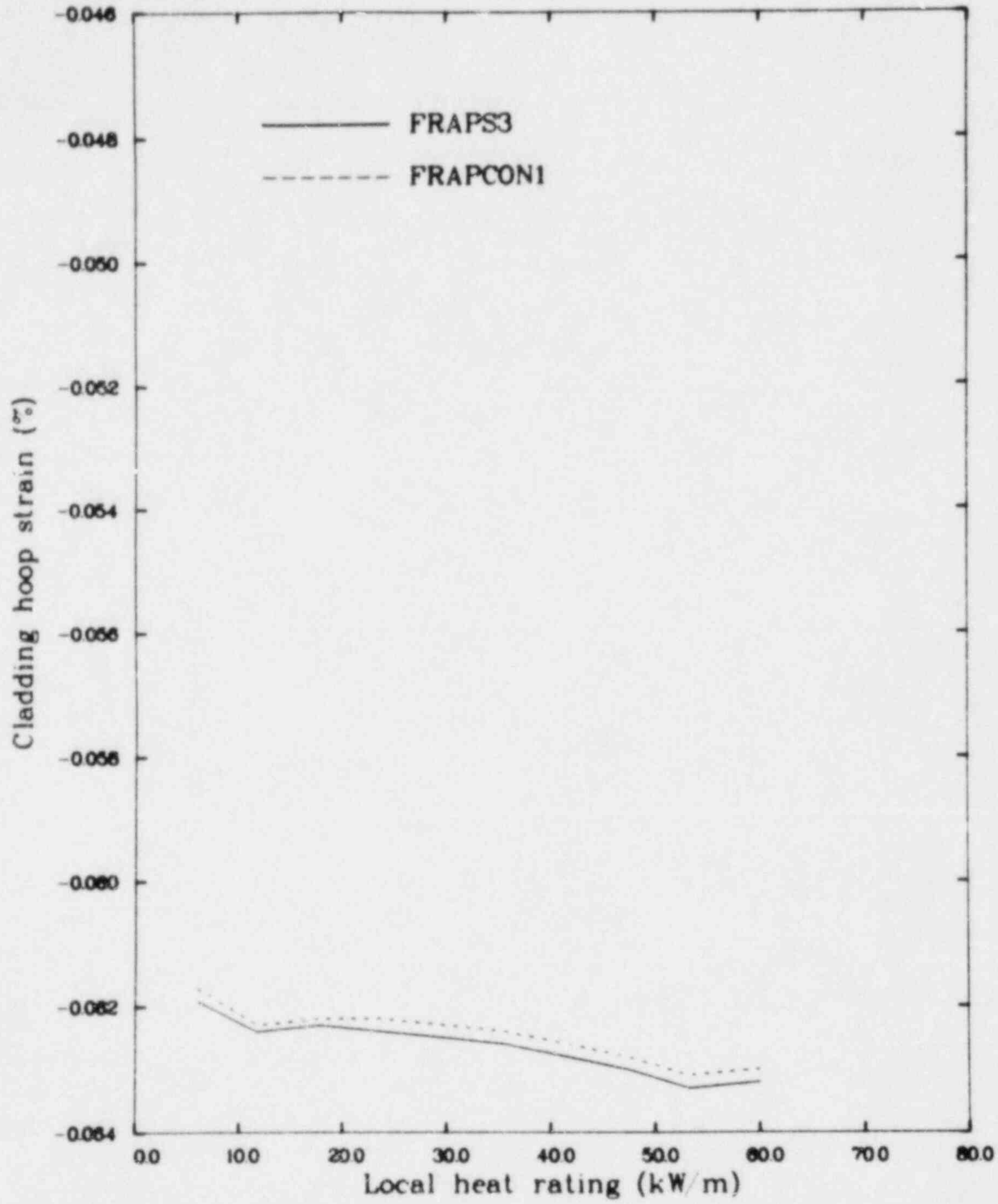

Figure 8. Comparison of FRAPCON-1 and FRAP-S3 cladding hoop strain ramp for a 7 x 7 rod at beginning-of-life.

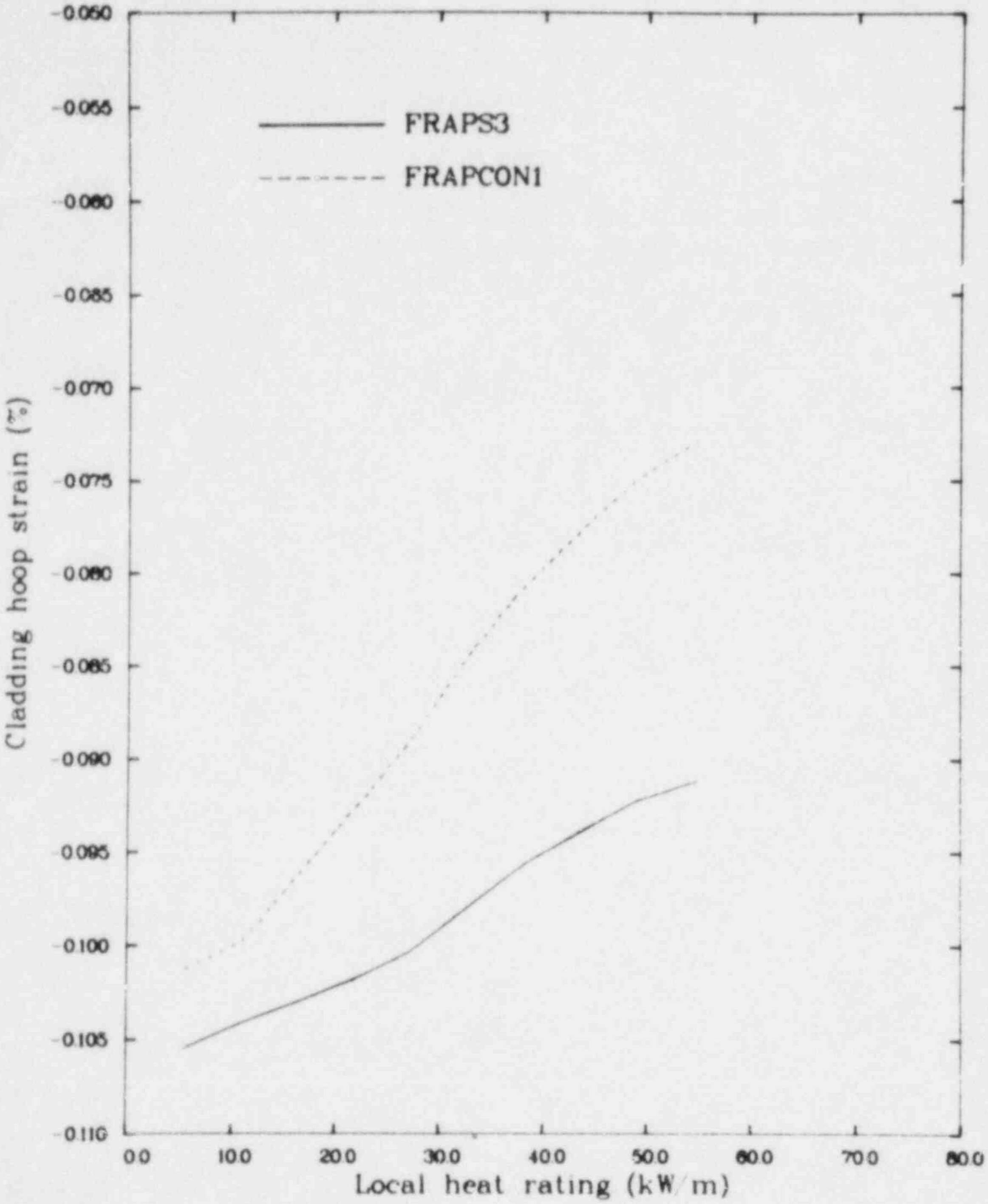

Figure 9. Comparison of FRAPCON-1 and FRAP-S3 cladding hoop strain ramp for a 15 x 15 rod at beginning-of-life.

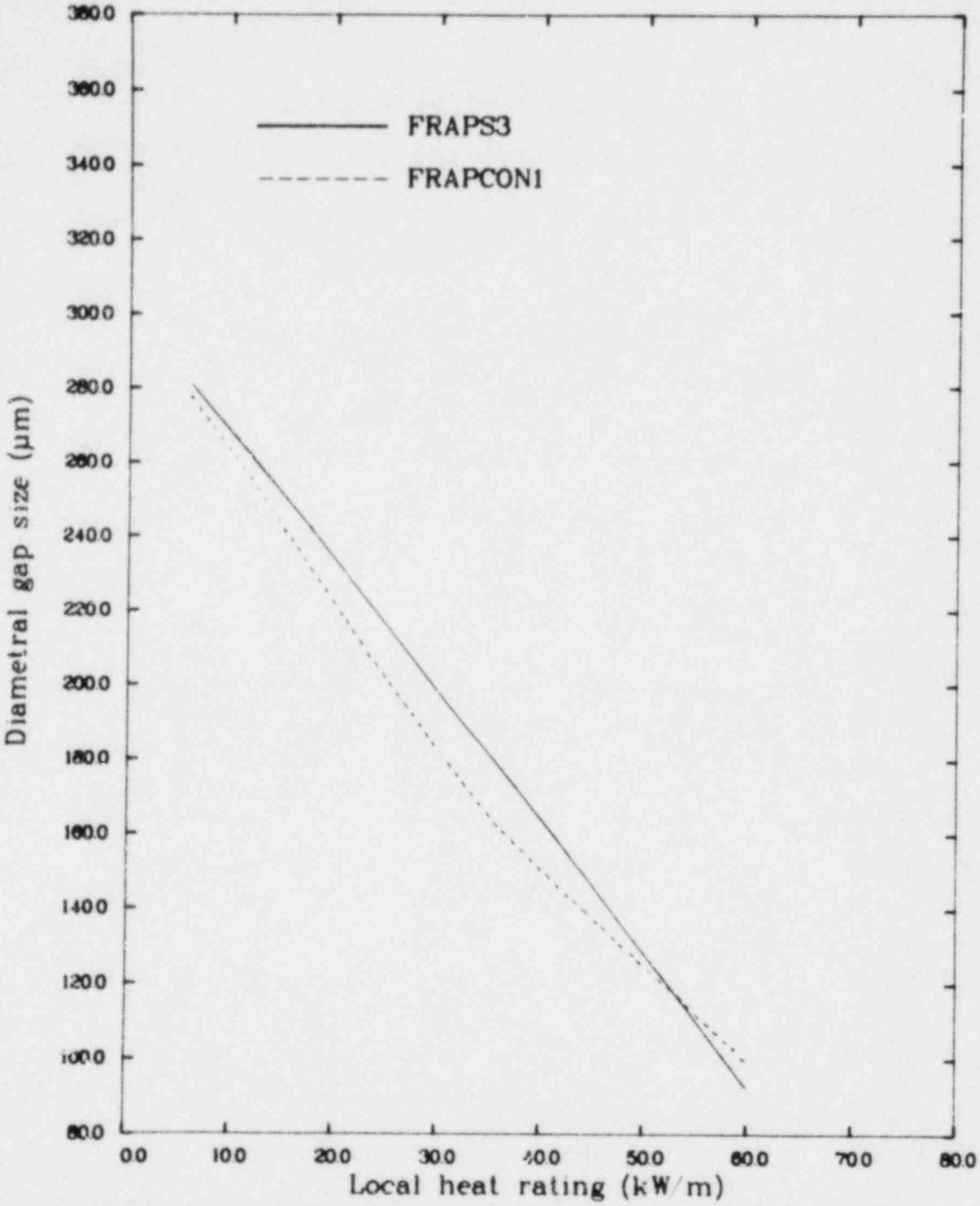

Figure 10. Comparison of FRAPCON-1 and FRAP-S3 diametral gap size for a 7 x 7 rod at beginning-of-life.

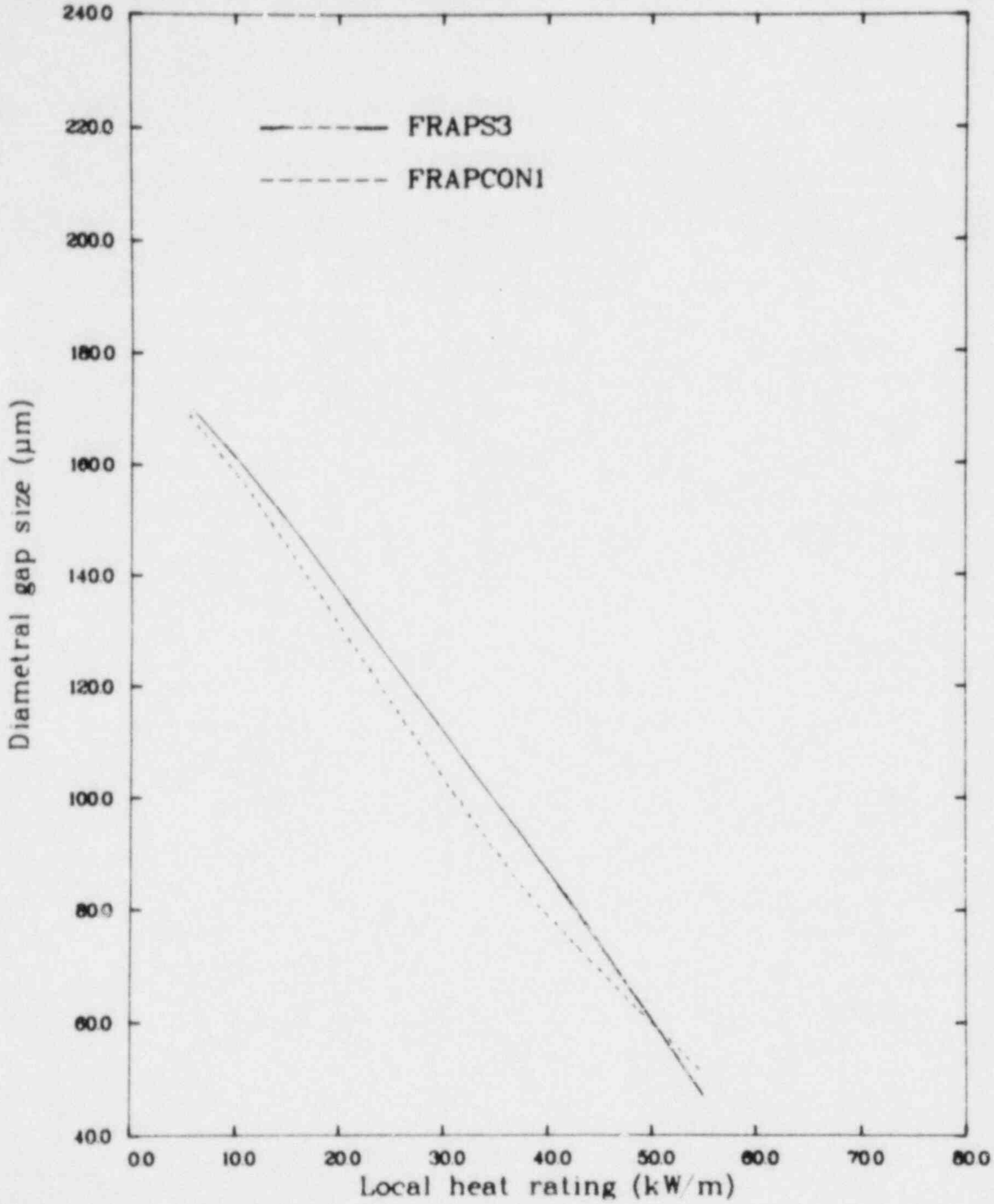

Figure 11. Comparison of FRAPCON-1 and FRAP-S3 diametral gap size for a 15 x 15 rod at beginning-of-life.

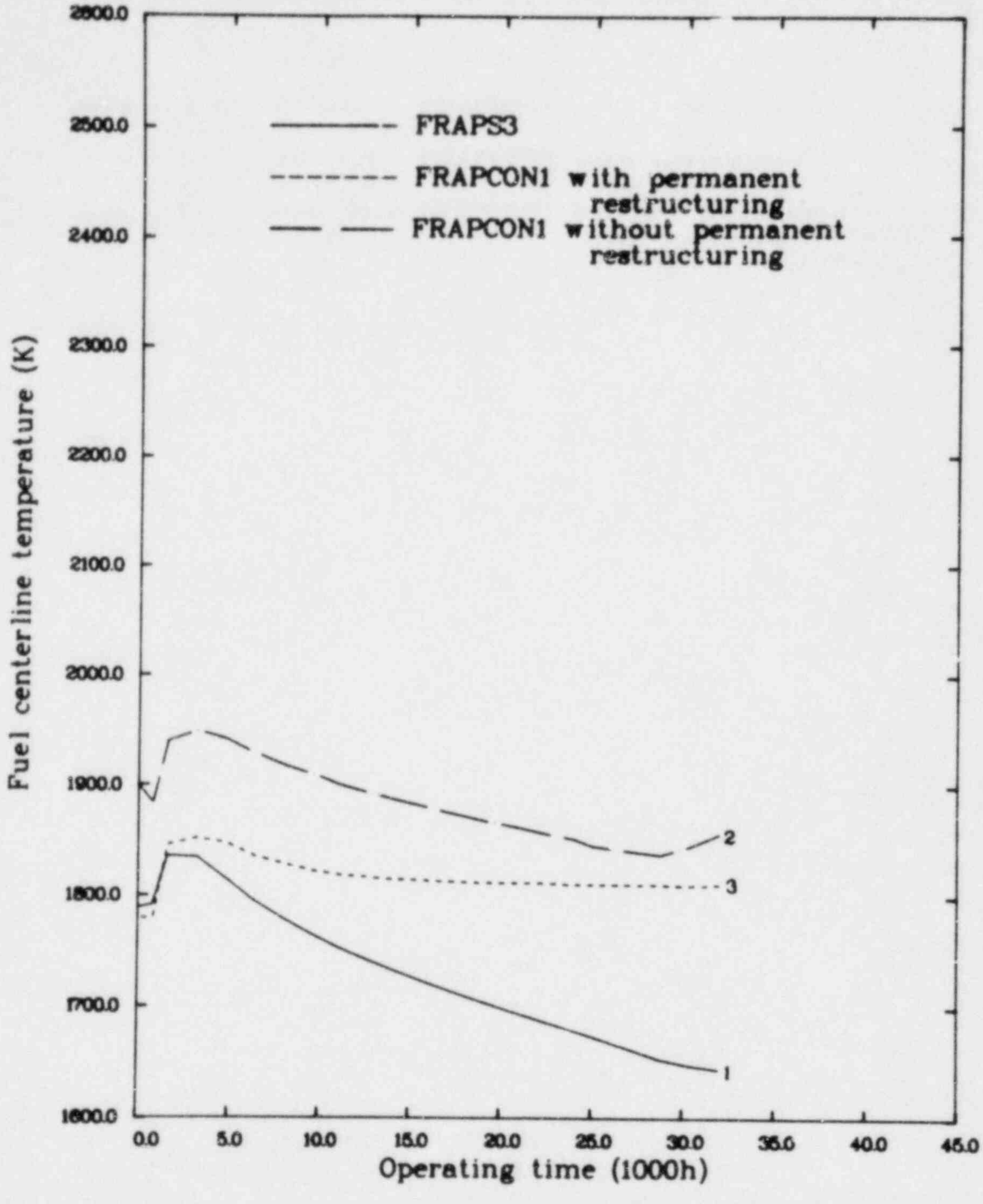

Figure 12. FRAPCON-1 and FRAP-S3 fuel centerline temperature history for a 7 x 7 rod.

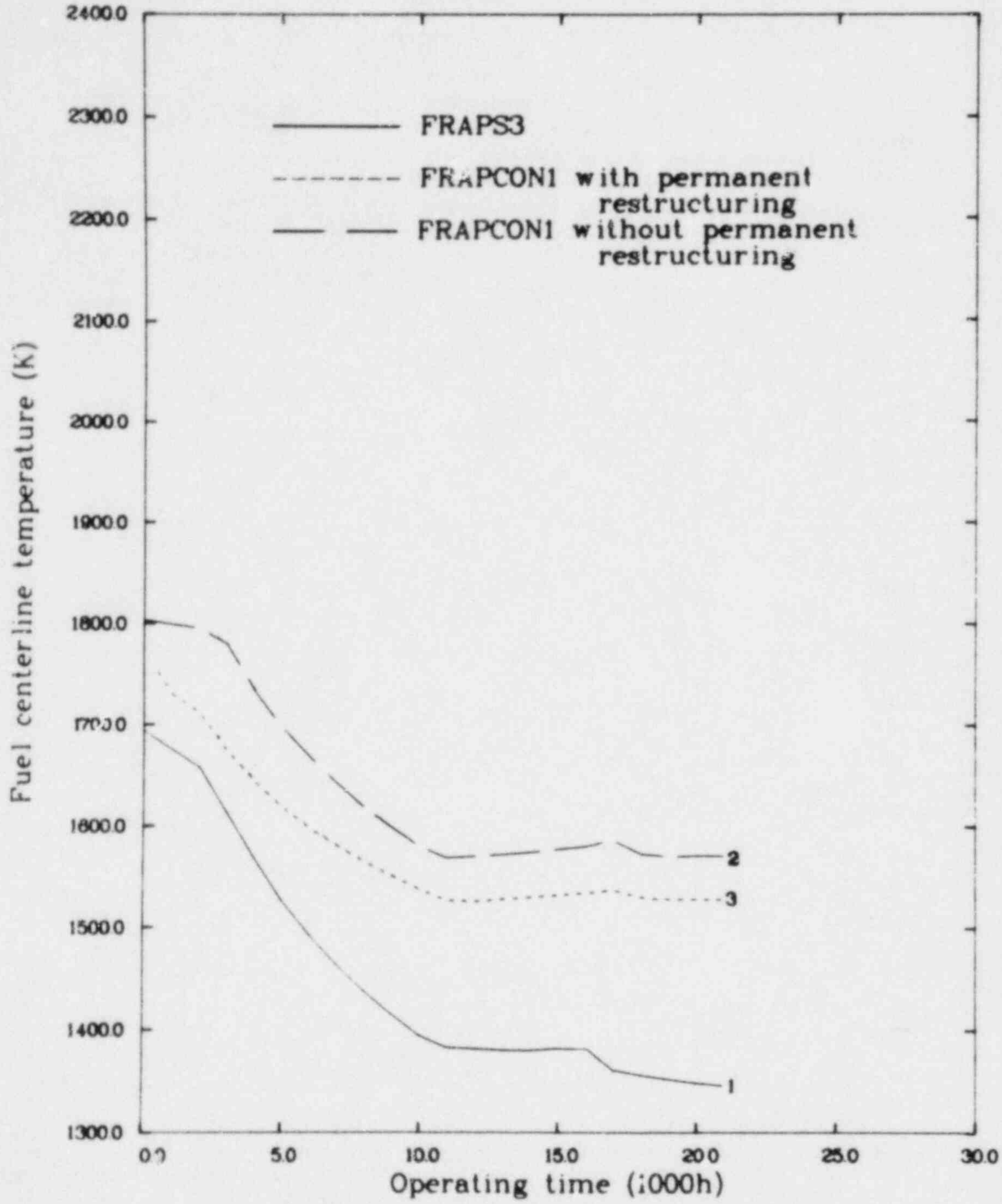

Figure 13. FRAPCON-1 and FRAP-S3 fuel centerline temperature history for a 15 x 15 rod.

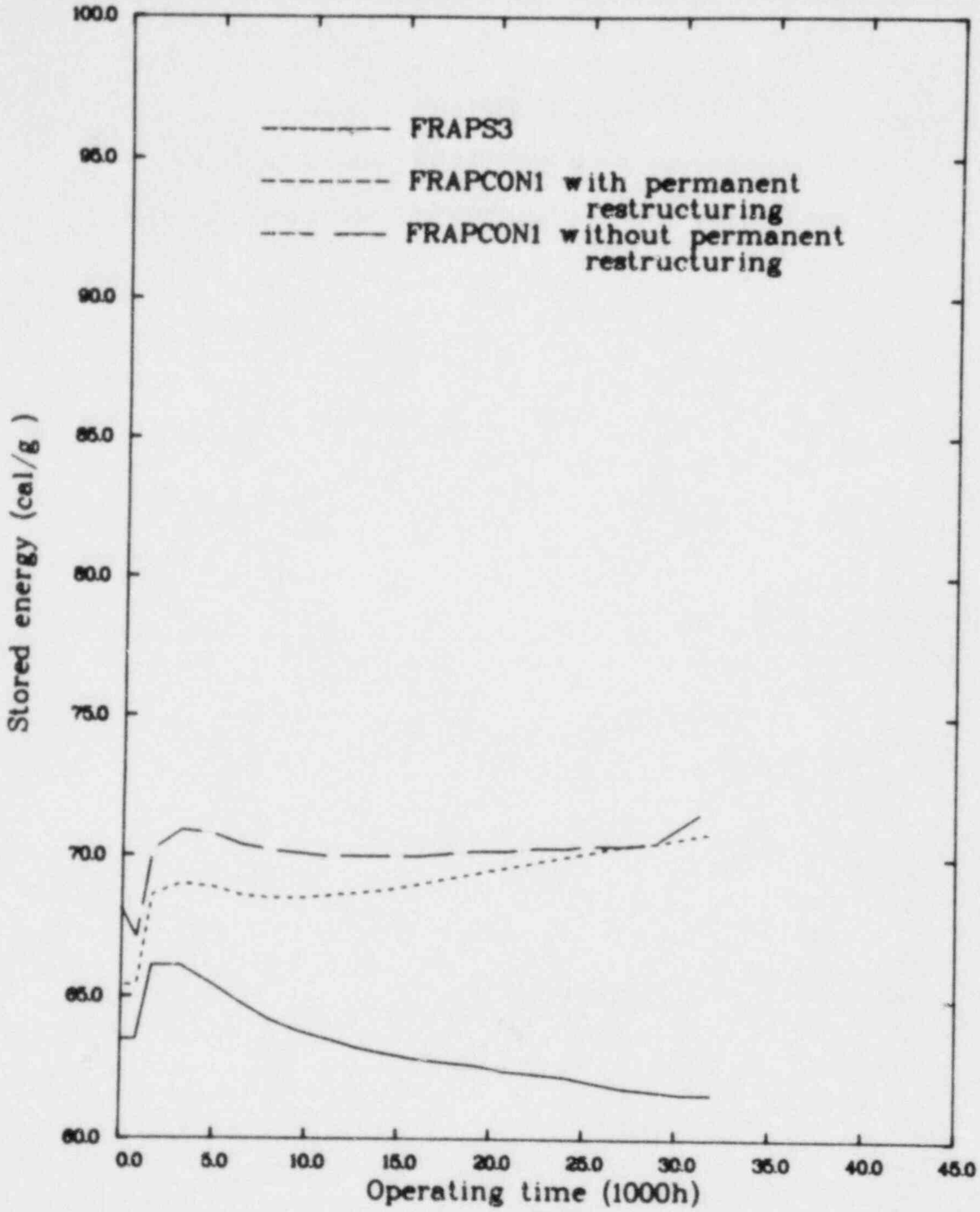

Figure 14. FRAPCON-1 and FRAP-S3 stored energy history for a 7 x 7 rod.

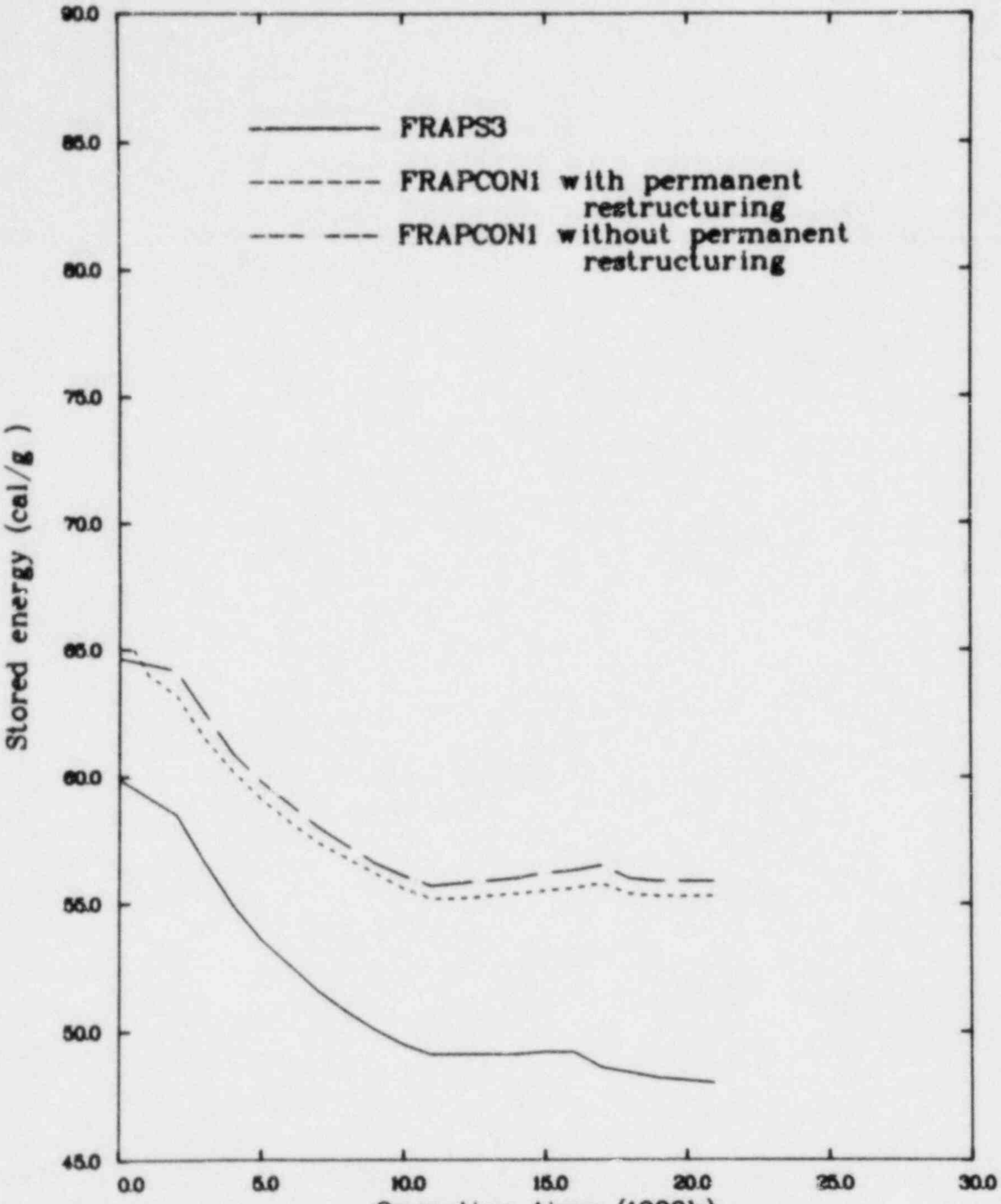

Figure 15. FRAPCON-1 and FRAP-S3 stored energy history for a 15 x 15 rod.

due to radial temperature profile changes as a result of gap size, gap conductance, and effective fuel conductivity changes that occur during the extended steady state operation.

As was previously seen, FRAPCON-1 predicts higher internal pressures than FRAP-S3 at BOL. The same tendency is evident throughout rod lifetime, as shown on Figures 16 and 17. The increased pressure in the 7 x 7 rod is not of sufficient magnitude to greatly alter the predicted cladding creepdown behavior, shown on Figure 18. However, the increased pressure in the 15 x 15 rod is of sufficient magnitude to affect the predicted large cladding creepdown behavior, as shown in Figure 19.

The cumulative effect of higher FRAPCON-1 fuel temperatures and pressures on diametral gap size is shown on Figures 20 and 21. For the BWR rod, higher FRAPCON-1 fuel temperatures during steady state operation cause more fuel swelling to occur, with no significant change in cladding creepdown. For the PWR case (Figure 21), FRAPCON-1 initially predicts a smaller gap size, due to higher temperatures. During extended operation, the greater fuel expansion resulting from higher temperatures is slightly outweighed by the reduced cladding creepdown rate, producing a larger FRAPCON-1 gap size during the latter 75% of the operating history.

The temperature, pressure, and strain trends observed during the BOL ramp are essentially identical for the EOL power ramp. The absolute values have changed, resulting from prior burnup effects. Figures 22 through 29 show the fuel rod centerline temperature, internal pressure, cladding hoop strain, and diametral gap size as a function of power for the BWR and PWR cases during an EOL power ramp. A noteworthy trend resulting from prior steady state operation is shown on Figures 28 and 29, which present diametral gap size. For the BWR rod, higher FRAPCON-1 fuel temperatures during prior steady state operation caused more fuel swelling to occur, with no significant change in cladding creepdown (strain). As a result of more fuel swelling and higher EOL fuel temperatures, FRAPCON-1 closes the diametral gap at a lower EOL power level. For the PWR rod, both codes predicted about the same amount of fuel swelling but much less cladding creepdown (strain) was noticed from FRAPCON-1 during prior steady state operation, thus tending to keep the diametral gap much larger. As a result, FRAPCON-1 calculates diametral gap closure at a higher power level. Figure 29 shows that for FRAPCON-1, the reduced amount of cladding creepdown was more dominant than fuel swelling effects on diametral gap size during extended steady state operation. This trend is evident because the diametral gap size at the beginning of the EOL ramp for FRAPCON-1 was larger than for FRAP-S3.

5.2 Code-to-Data Comparisons

The results of code-to-data comparisons are discussed in this section. FRAPCON-1 calculations have been graphically compared with experimental data to assess the accuracy of fuel rod thermal, pressure, deformation, and corrosion models. Different graphical symbols have been used to distinguish between test programs or test series listed previously in Table 2. The data base used to assess FRAPCON-1 is essentially the same as was used to assess FRAP-S3, except that new data were added to aid in the assessment of the permanent fuel restructuring model.

5.2.1 Thermal Models. Results of the code-to-data comparisons for the thermal models are discussed first, due to the governing influence of fuel rod temperature and temperature distribution on the fission gas release, internal pressure, and mechanical deformation models. The thermal model variables considered are fuel temperature and gap conductance.

5.2.1.1 Fuel Temperature Profile – Prior assessment results[1] established the fact that a fuel relocation model with associated pellet conductivity feedback, and the Ross and Stoute gap conductance model provided the most realistic or best estimate option presently available for simulating the current experimental data base. However, the tendency of prior assessment results to overpredict fuel centerline temperatures provided an incentive to evaluate the effect on the effective fuel conductivity of a permanent fuel restructuring model. Also, the data base of fuel temperature experiments having both centerline and radially distributed fuel pellet thermocouples was recently expanded, thus lending itself to such an analysis. As shown on Figure 30, the predicted temperature decrease from the fuel centerline to a radially positioned thermocouple is somewhat greater than the

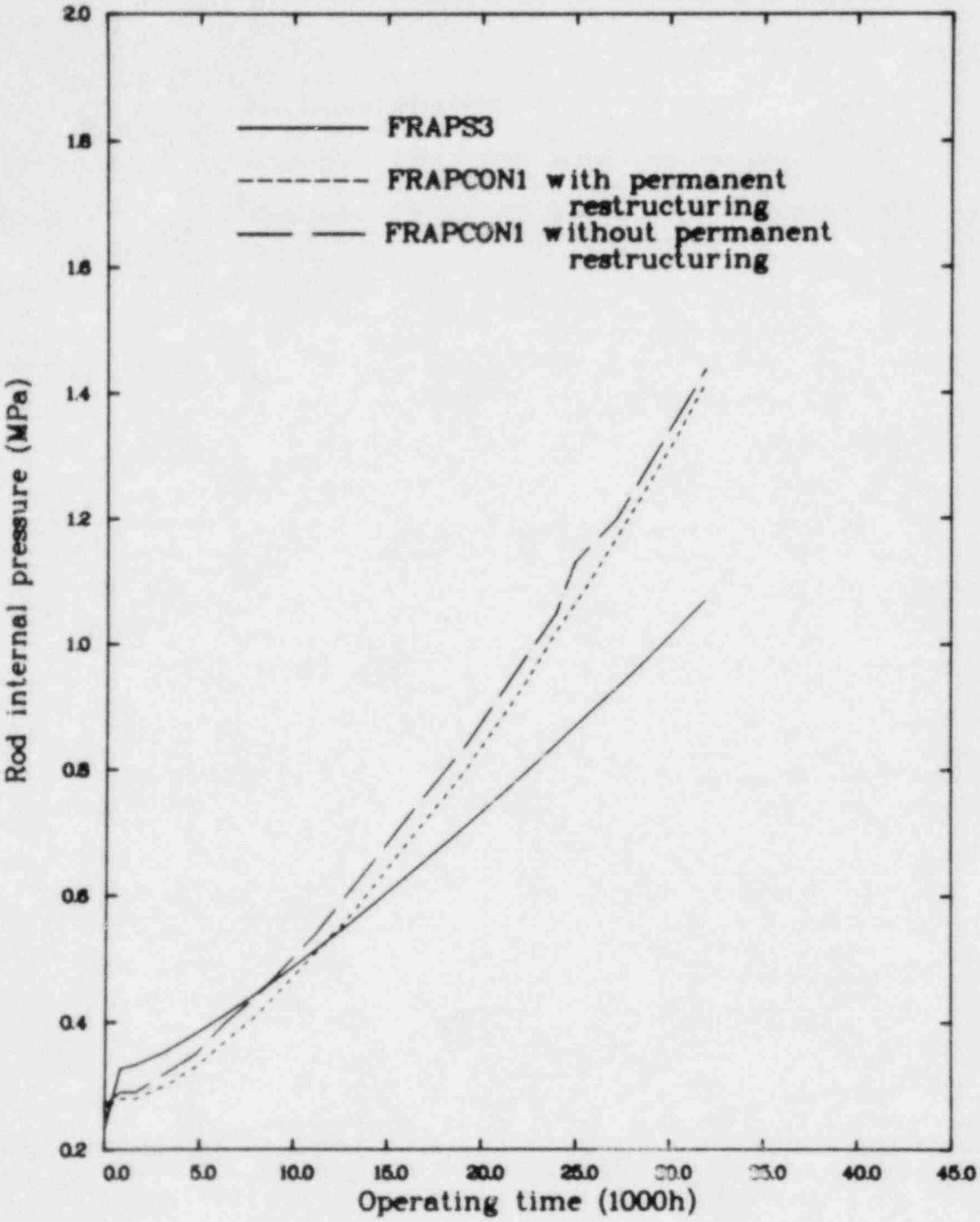

Figure 16. FRAPCON-1 and FRAP-S3 rod internal pressure history for a 7 x 7 rod.

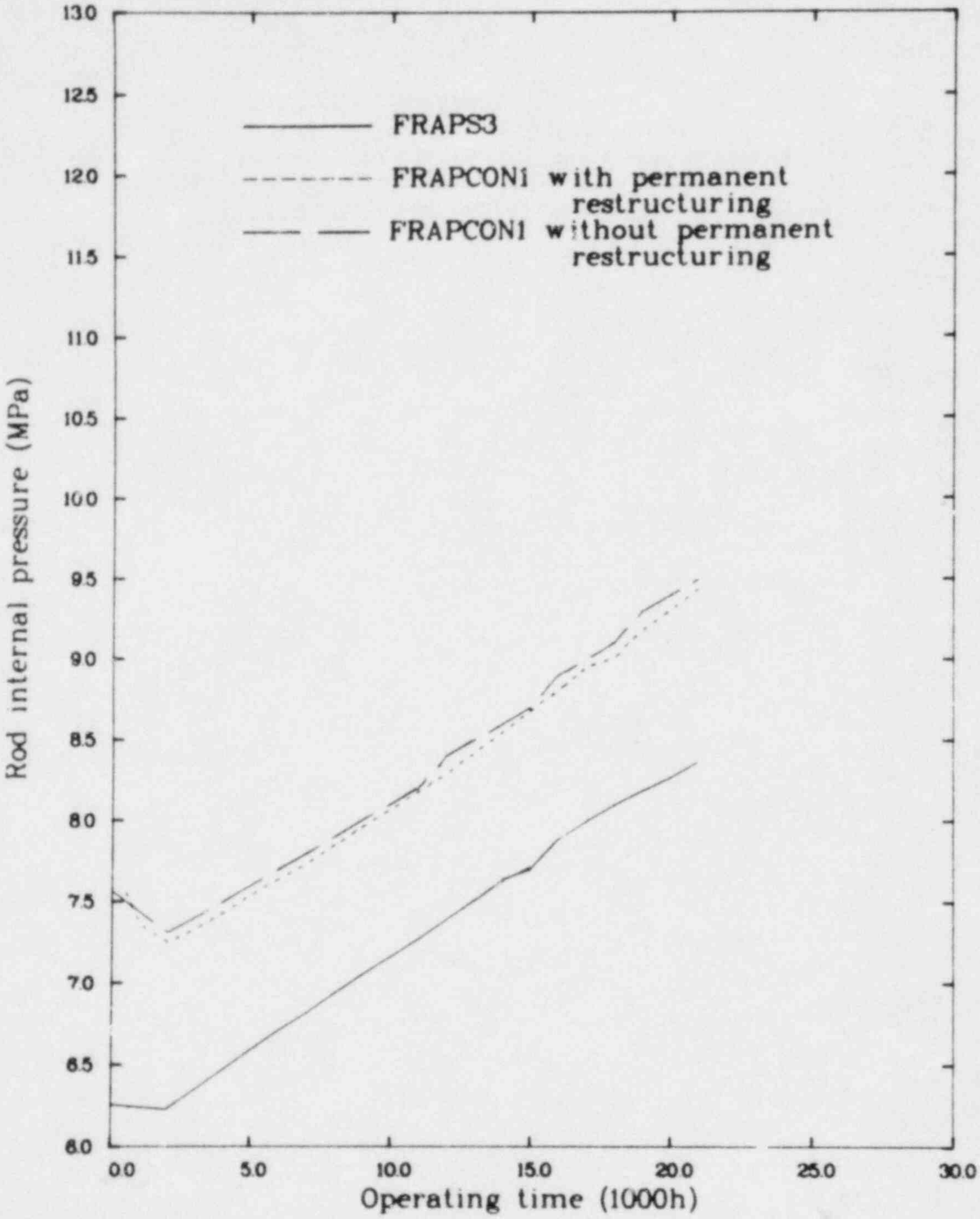

Figure 17. FRAPCON-1 and FRAP-S3 rod internal pressure history for a 15 x 15 rod.

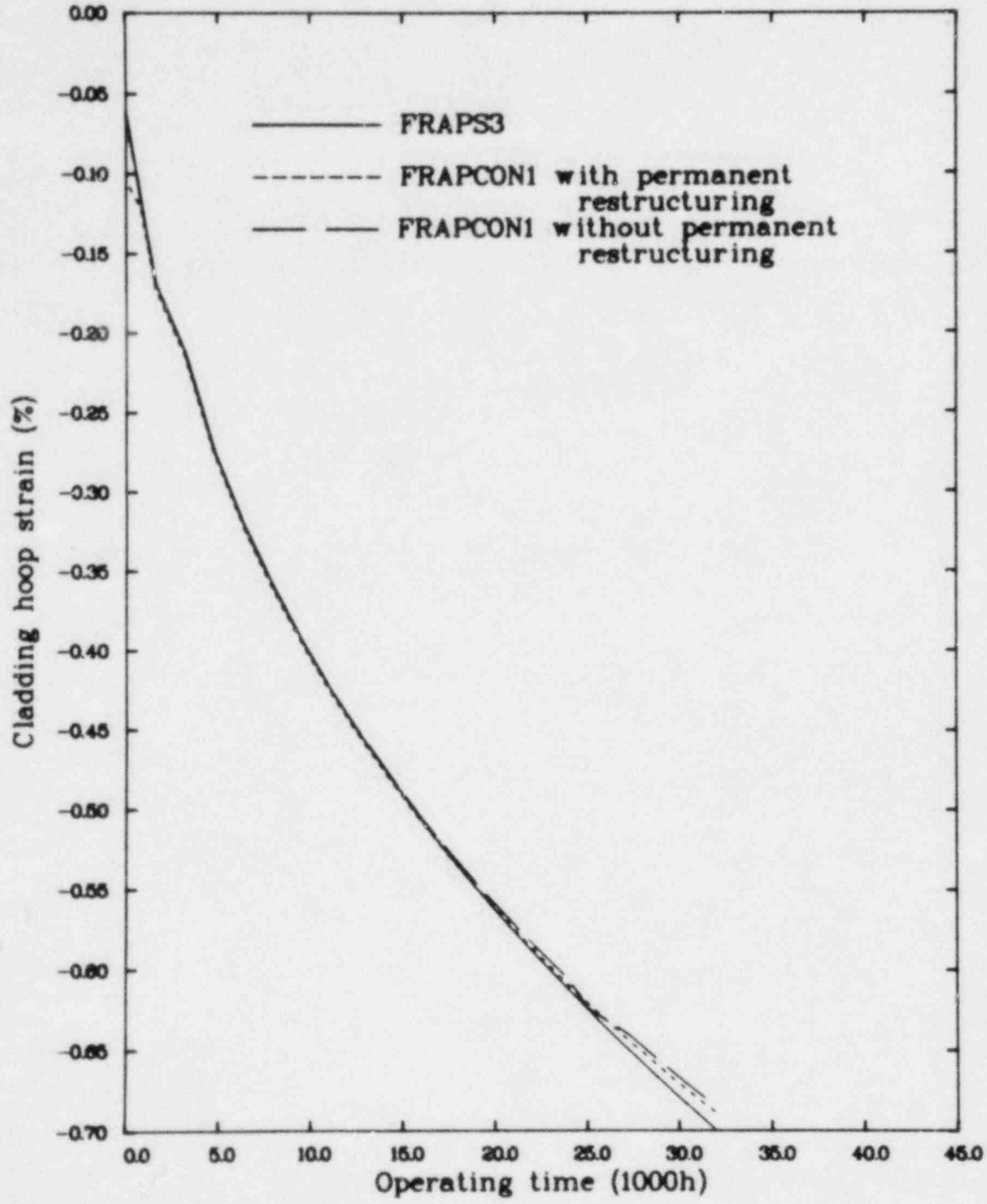

Figure 18. FRAPCON-1 and FRAP-S3 cladding hoop strain history for a 7 x 7 rod.

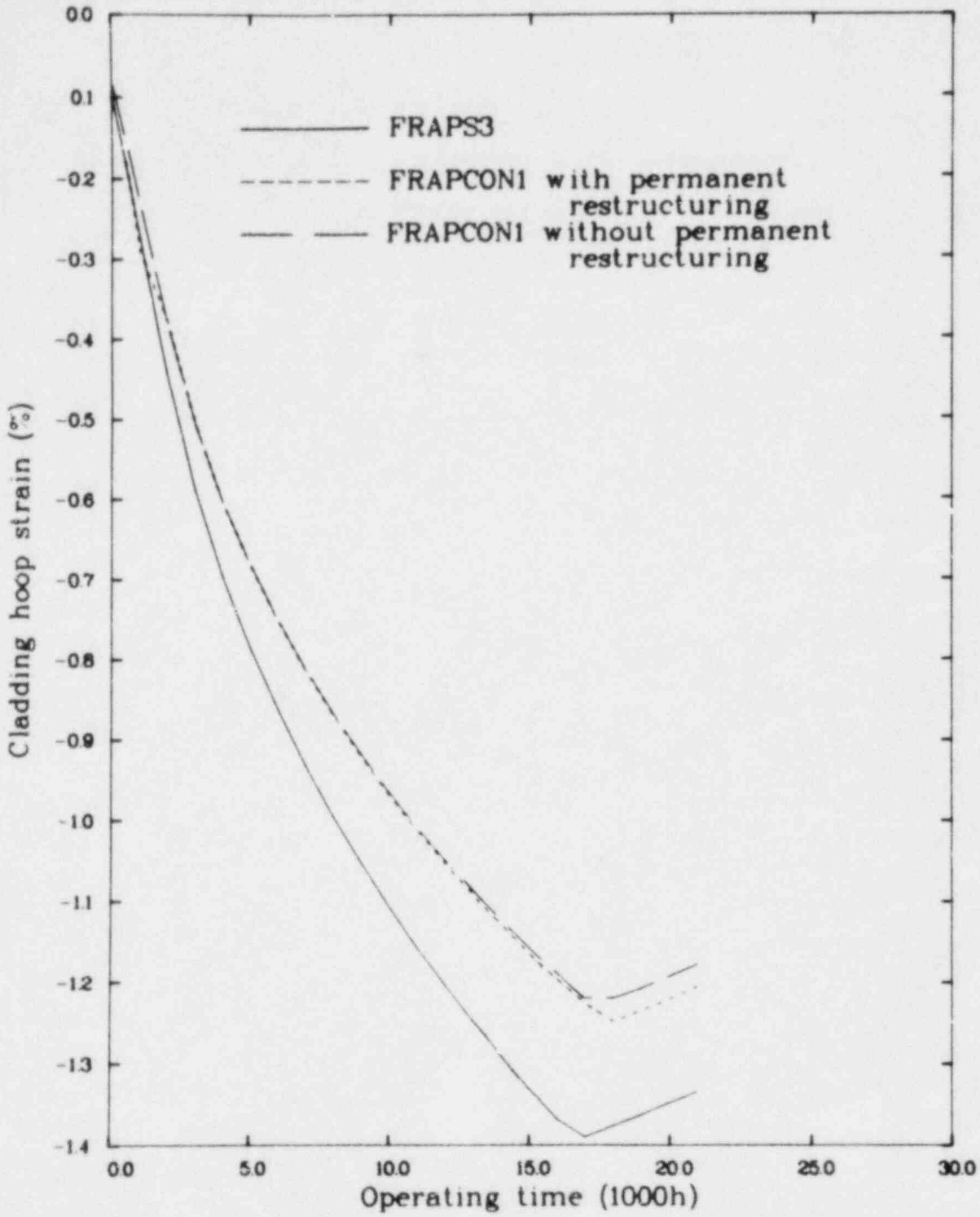

Figure 19. FRAPCON-1 and FRAP-S3 cladding hoop strain history for a 15 x 15 rod.

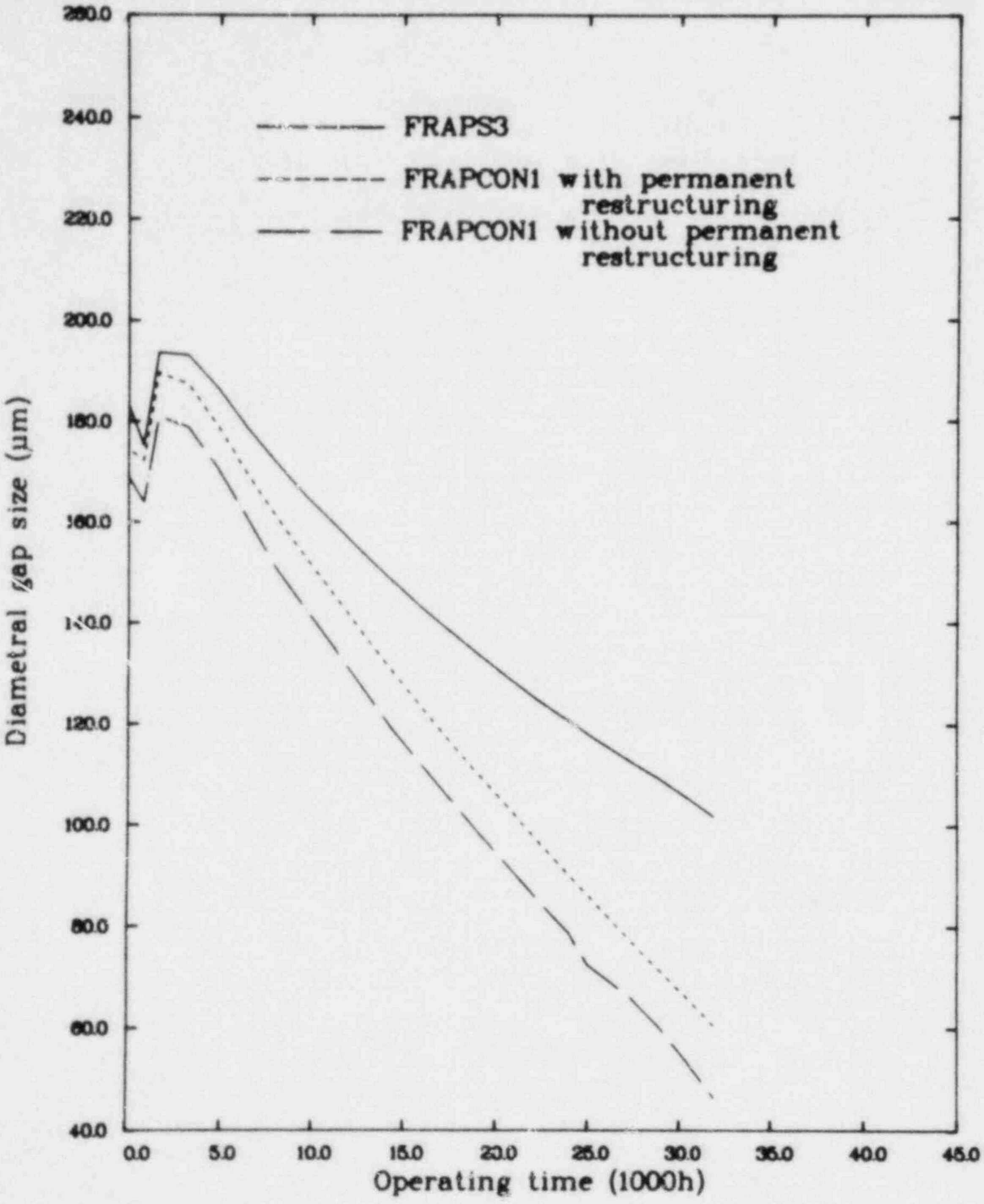

Figure 20. FRAPCON-1 and FRAP-S3 diametral gap size history for a 7 x 7 rod.

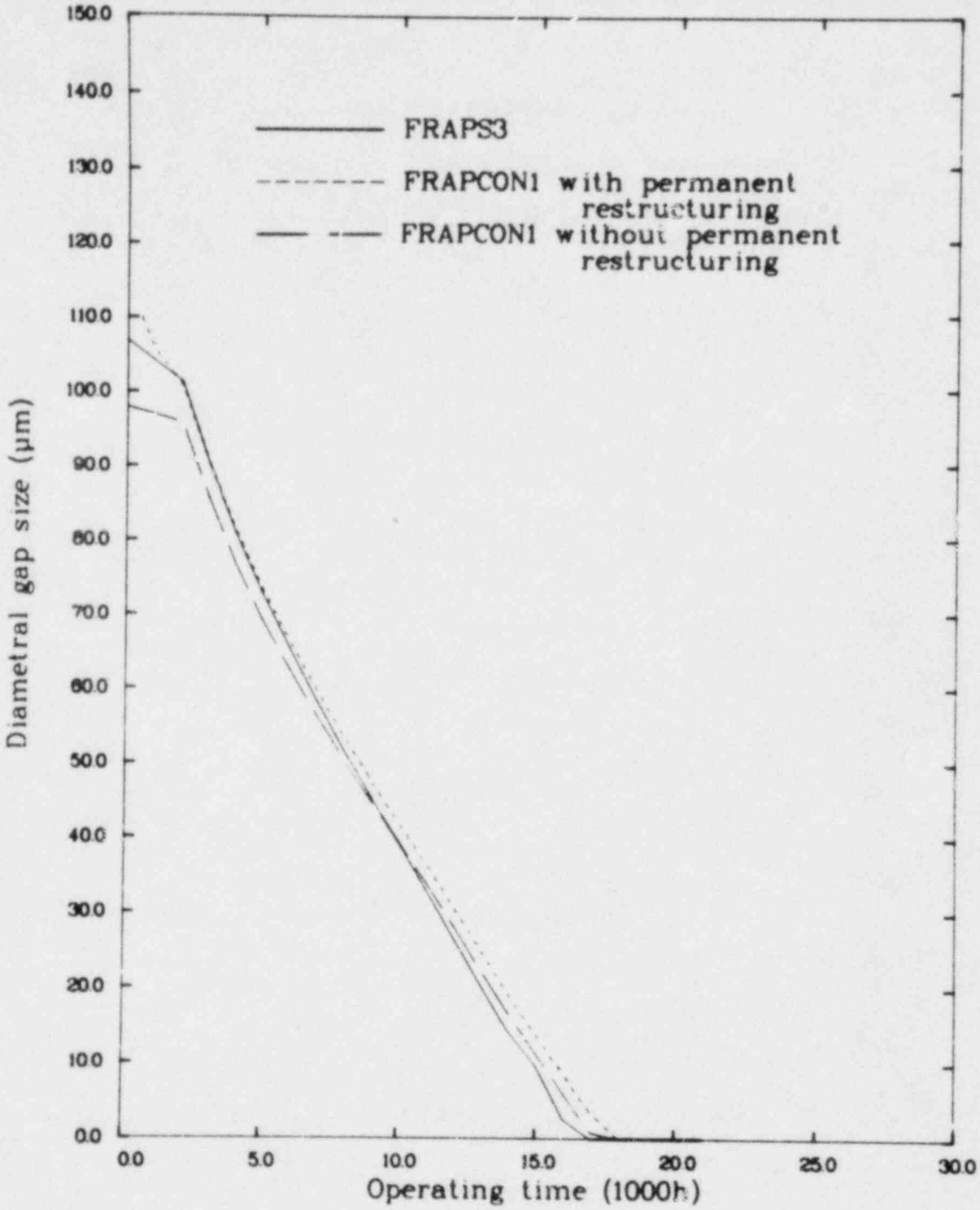

Figure 21. FRAPCON-1 and FRAP-S3 diametral gap size history for a 15 x 15 rod.

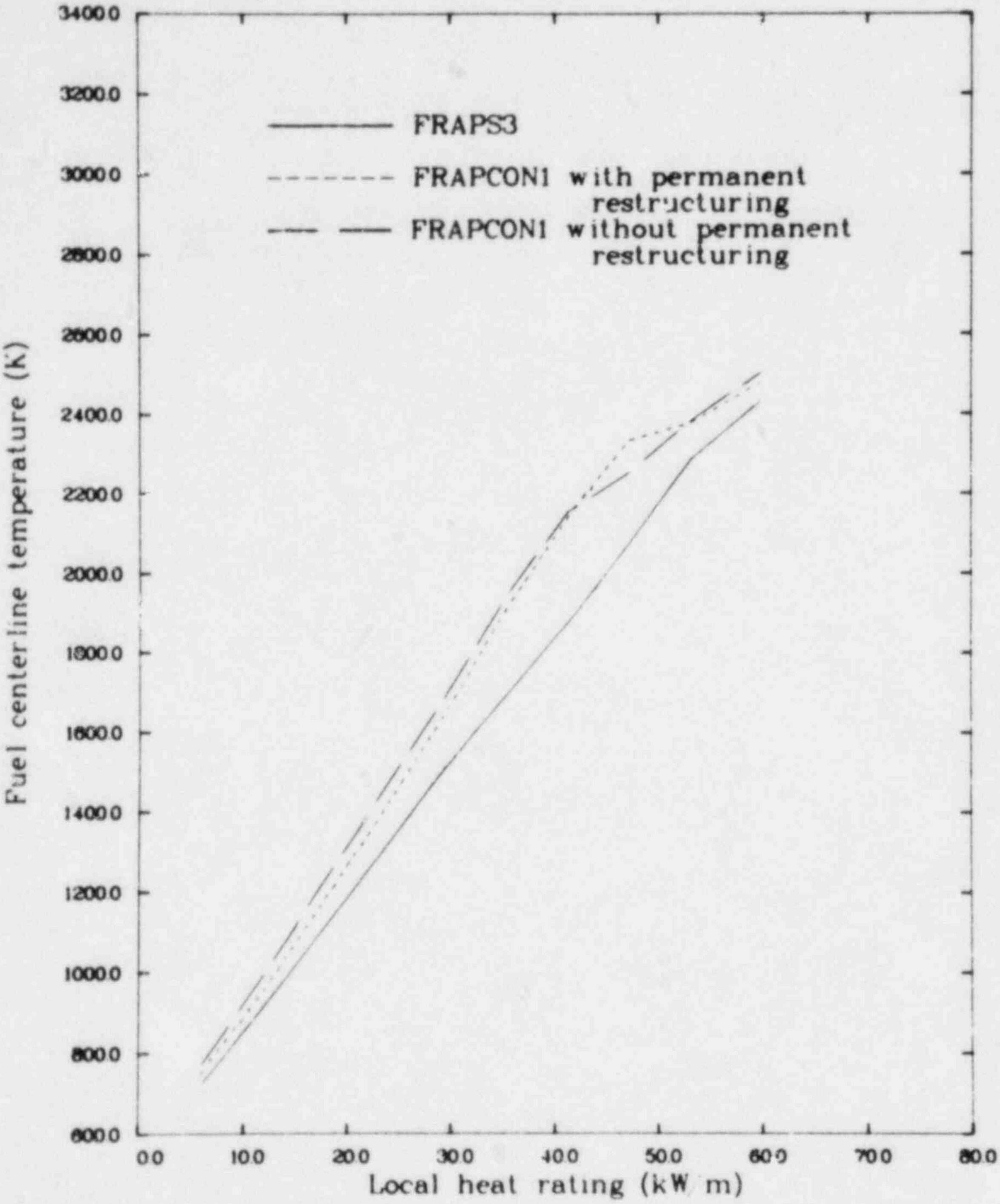

Figure 22. Comparison of FRAPCON-1 and FRAP-S3 fuel centerline temperature ramp for a 7 x 7 rod at end-of-life.

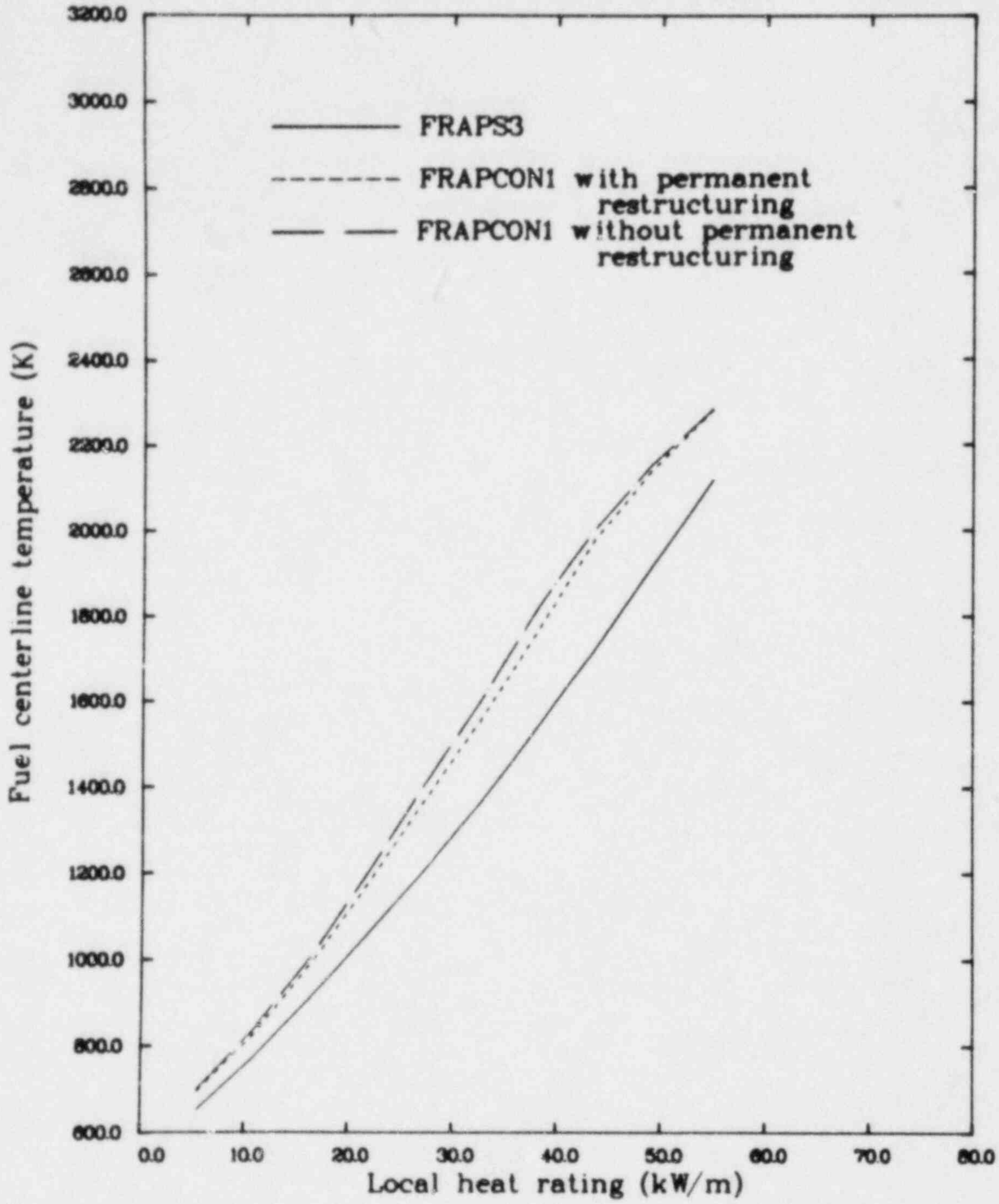

Figure 23. Comparison of FRAPCON-1 and FRAP-S3 fuel centerline temperature ramp for a 15 x 15 rod at end-of-life.

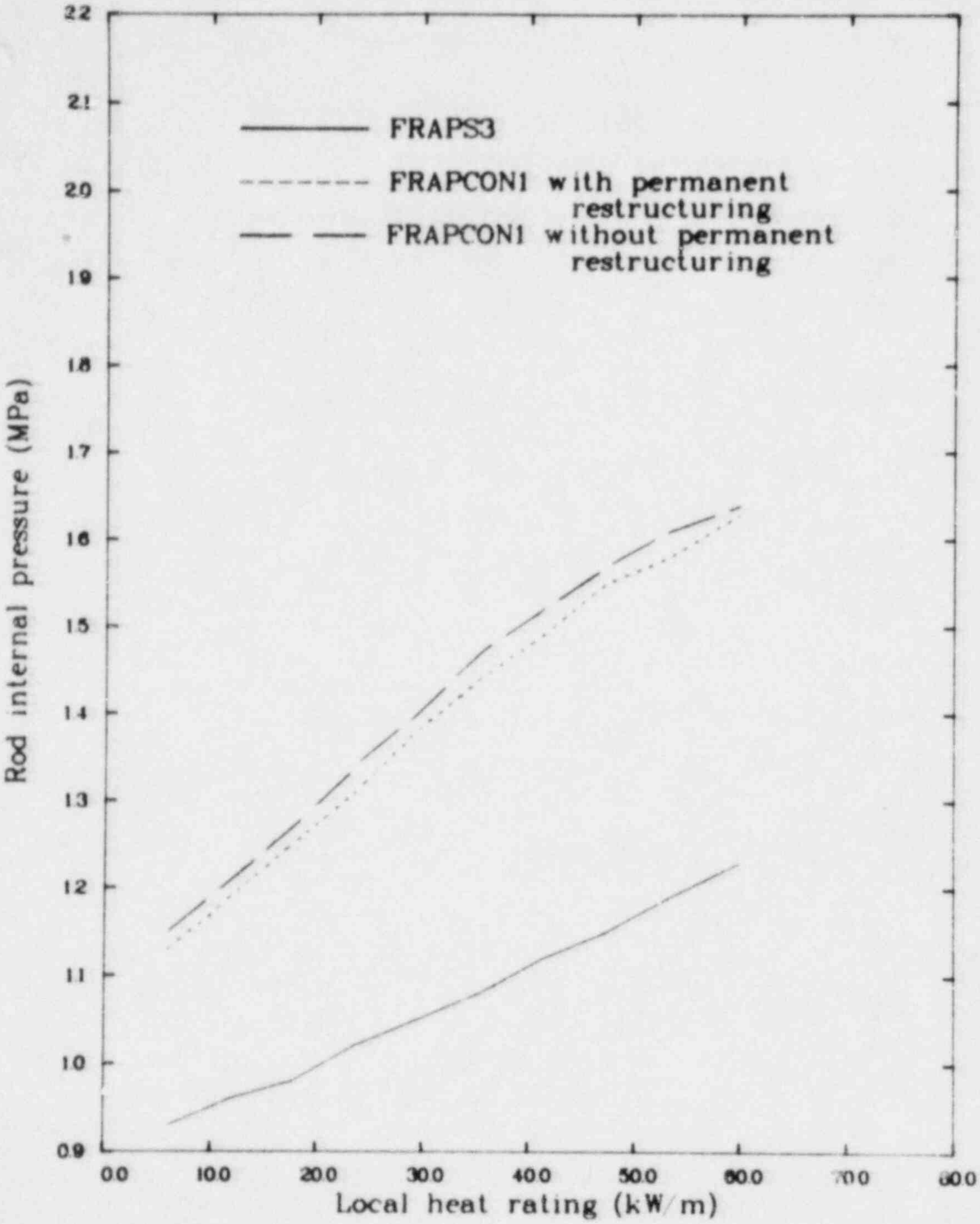

Figure 24. Comparison of FRAPCON-1 and FRAP-S3 rod internal pressure ramp for a 7 x 7 rod at end-of-life.

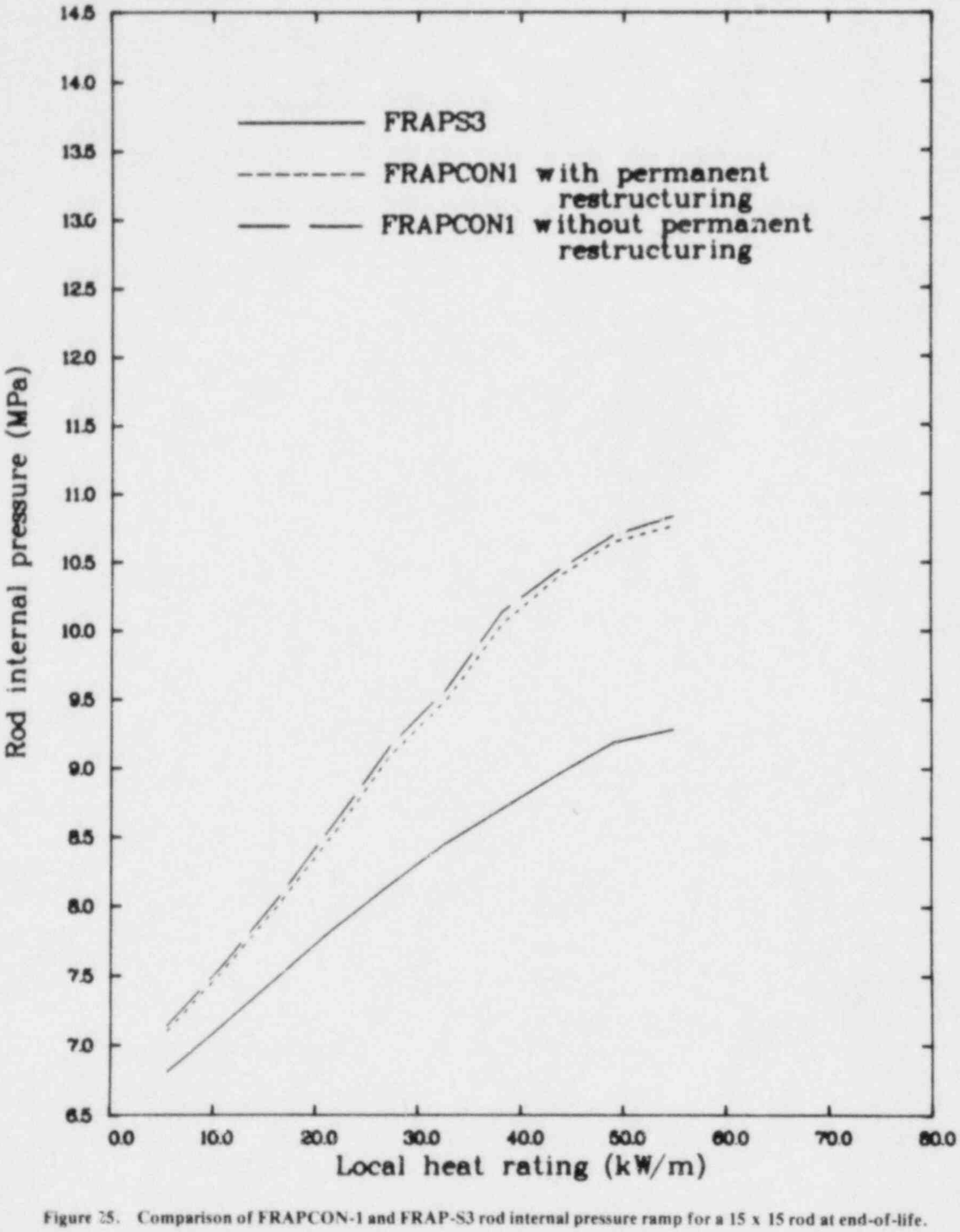

Figure 25. Comparison of FRAPCON-1 and FRAP-S3 rod internal pressure ramp for a 15 x 15 rod at end-of-life.

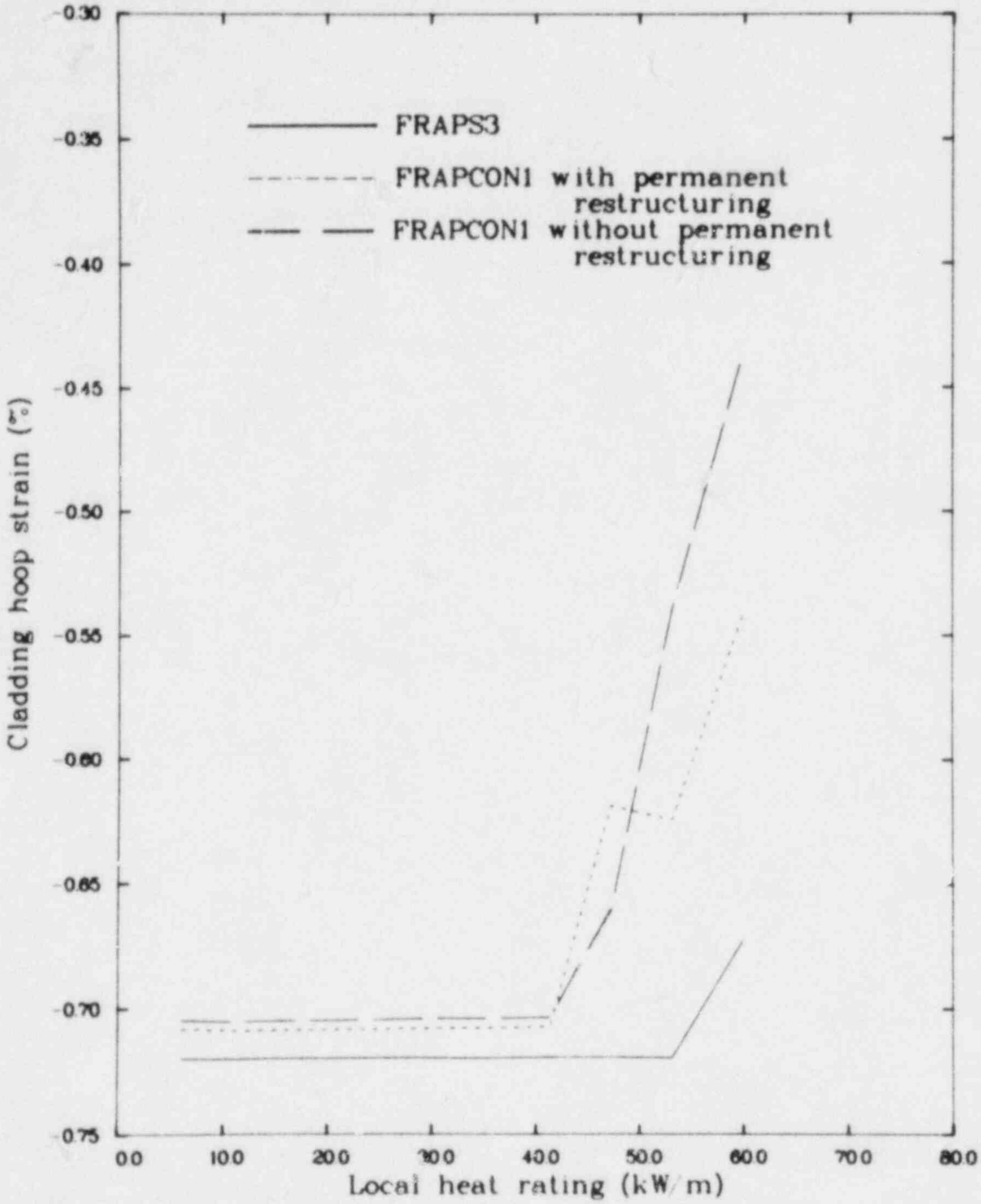

Figure 26. Comparison of FRAPCON-1 and FRAP-S3 cladding hoop strain for a 7 x 7 rod at end-of-life.

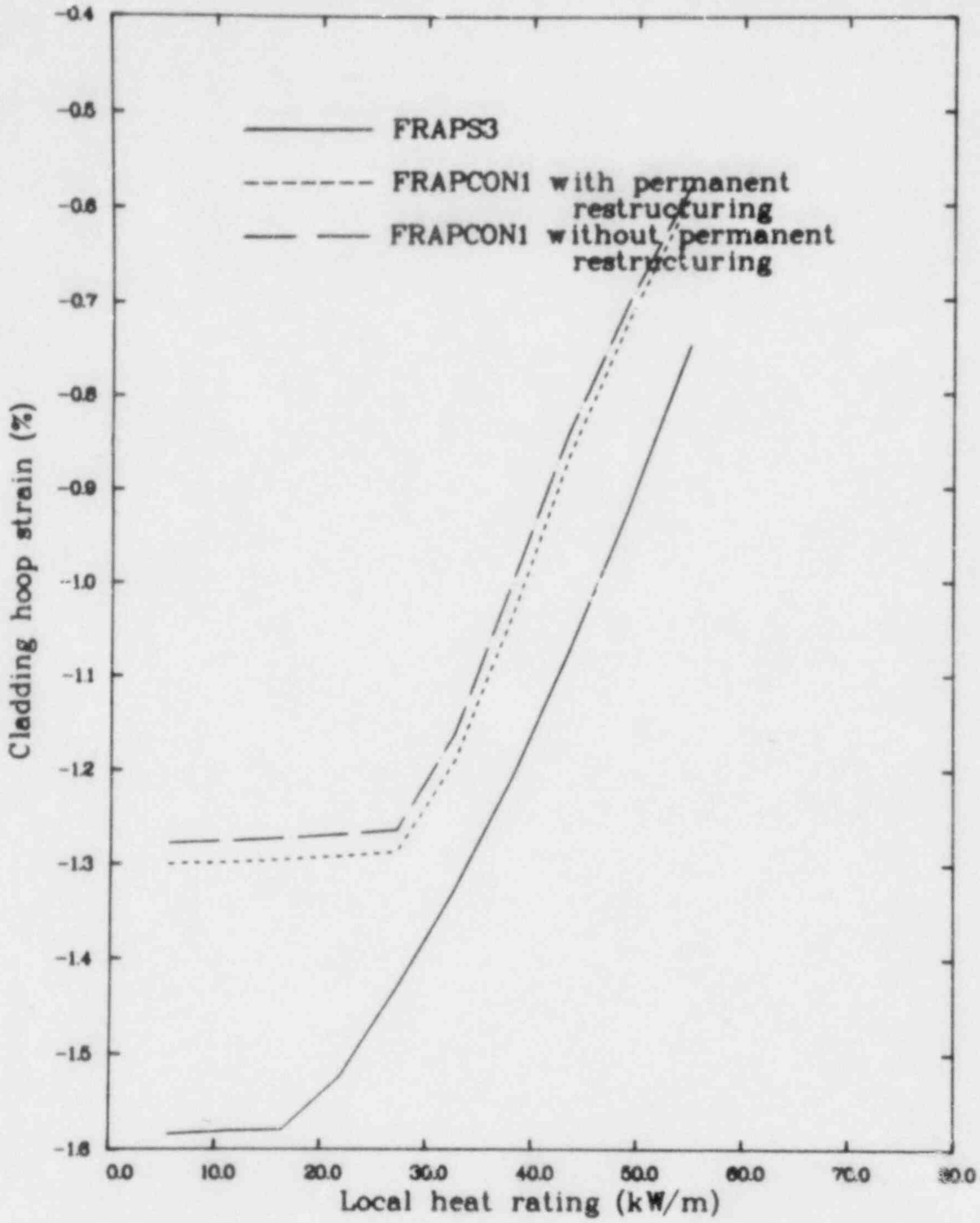

Figure 27. Comparison of FRAPCON-1 and FRAP-S3 cladding hoop strain for a 15 x 15 rod at end-of-life.

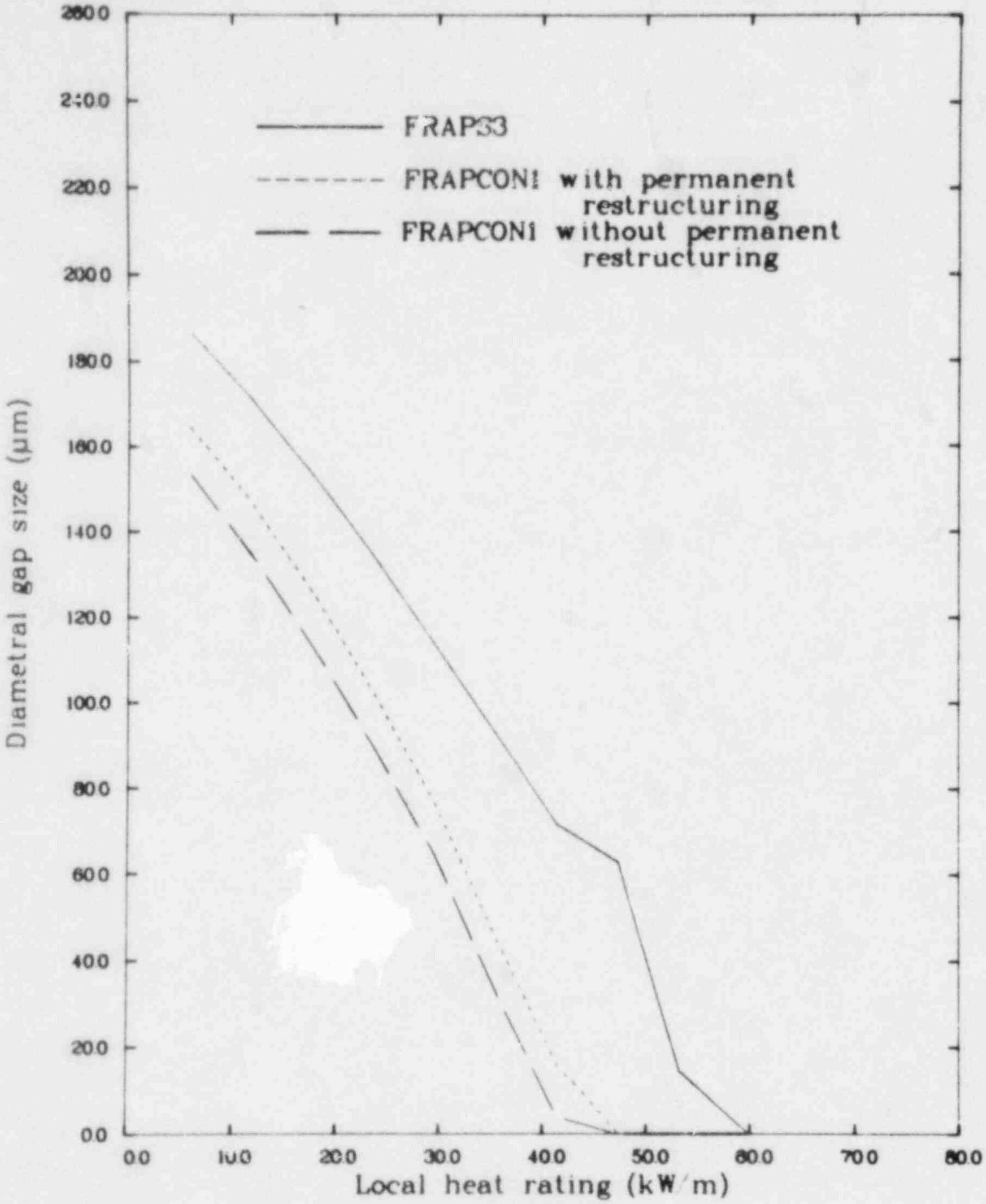

Figure 28. Comparison of FRAPCON-1 and FRAP-S3 diametral gap size for a 7 x 7 rod at end-of-life.

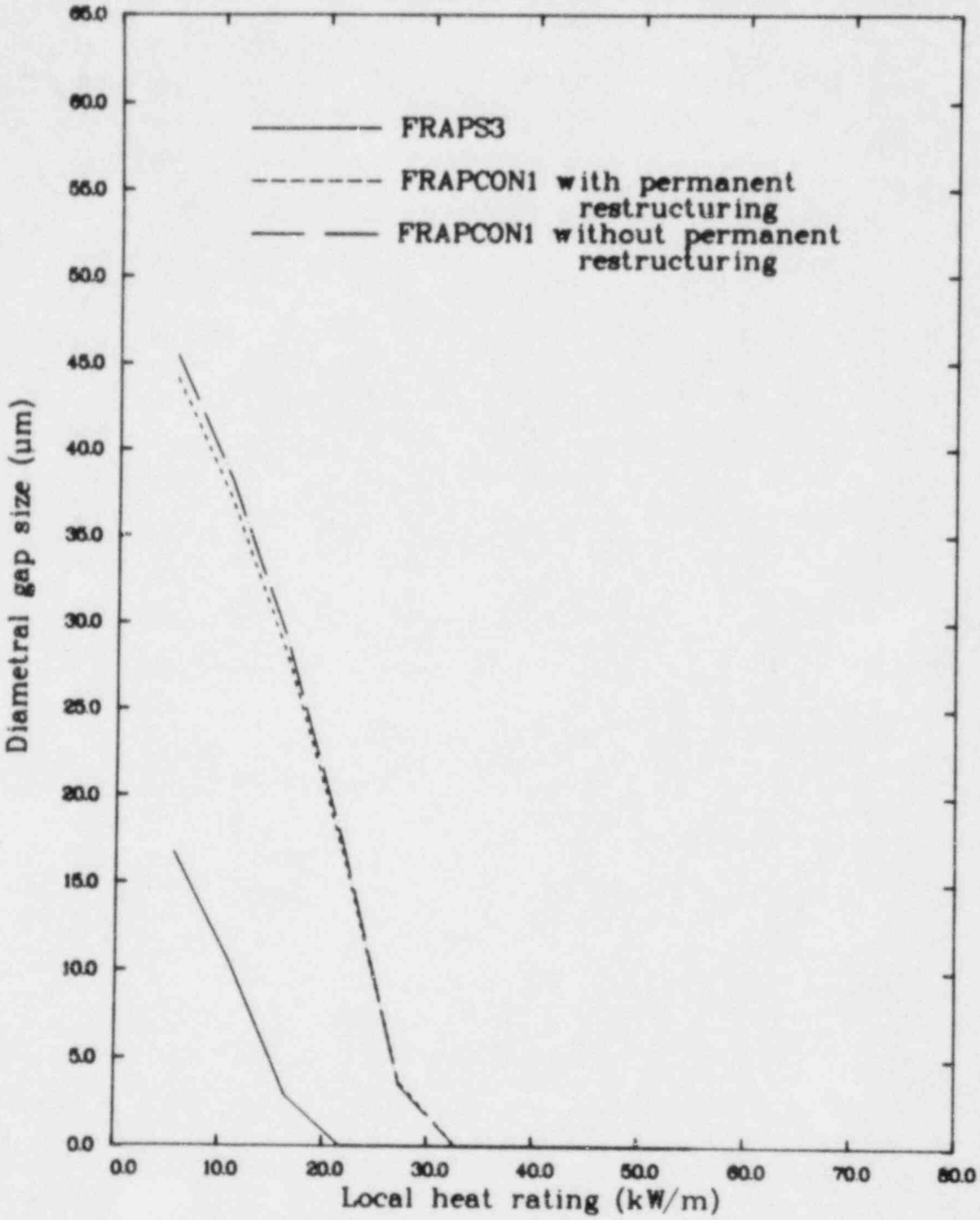

Figure 29. Comparison of FRAPCON-1 and FRAP-S3 diametral gap size for a 15 x 15 rod at end-of-life.

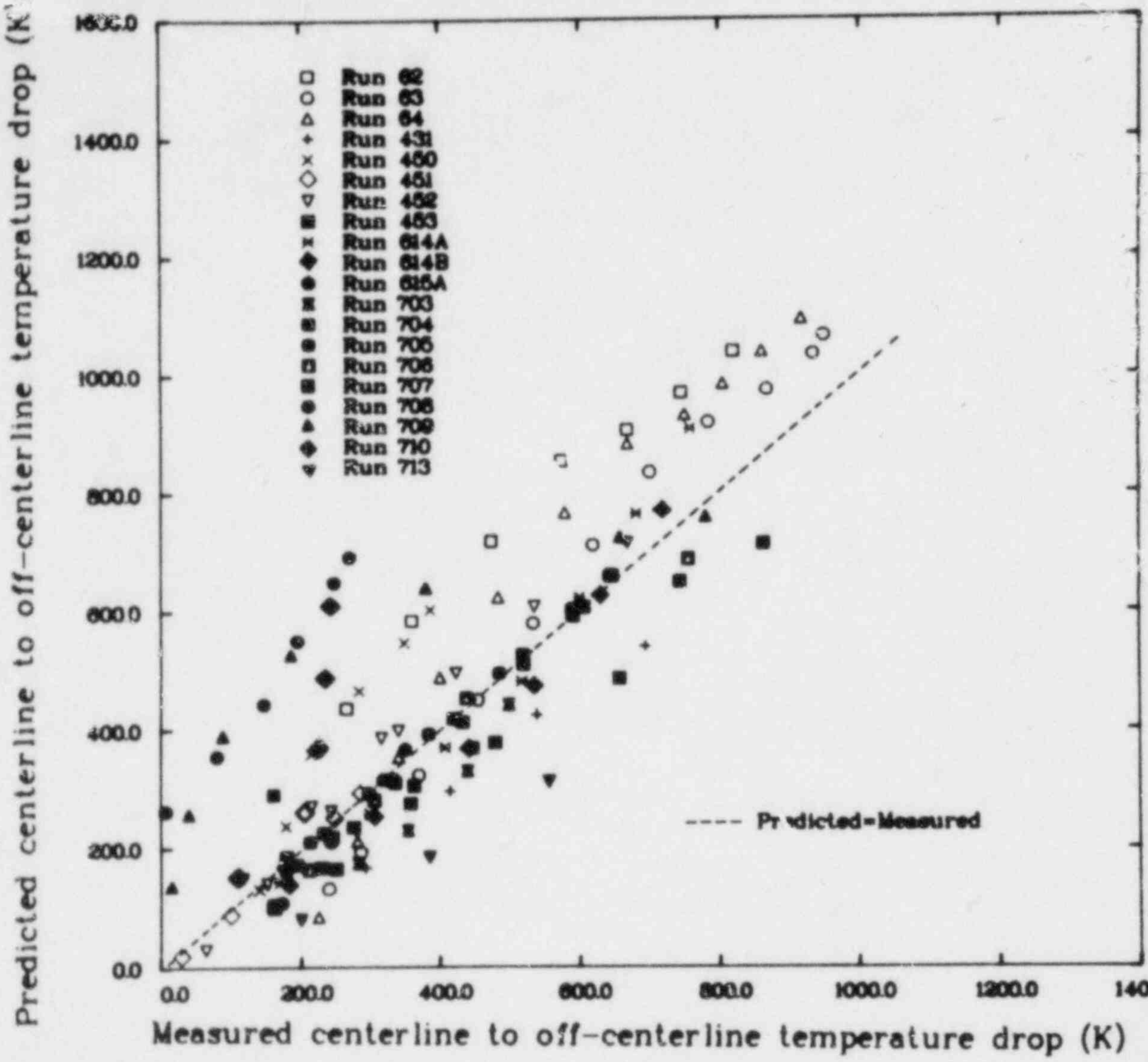

Figure 30. Comparison of FRAPCON-1 predicted and measured temperature difference between fuel centerline and a radially positioned thermocouple.

measured temperature decrease. In addition, the measured temperature decrease from the radially positioned thermocouple to the fuel pellet surface is greater than the predicted decrease, as shown on Figure 31. This conclusion assumes that the predicted fuel surface temperature is equal to a measured fuel surface temperature, because the fuel surface temperature was not measured. However, when allowing for a ± 20% uncertainty in this assumption, the same trend is observed.

The trends observed in Figures 30 and 31 imply that the measured temperature profile in the inner part of the fuel pellet is flat compared to the predicted temperature profile and the measured temperature profile near the pellet surface is steep compared to the predicted temperature profile. Apparently, this trend occurs even though the permanent fuel restructuring model restores the cracked fuel pellet conductivity to the laboratory value in the inner regions of the fuel where the fuel temperature exceeds 0.9 times the fuel sintering temperature. The fact that the measured temperature profile near the pellet surface is steep compared to the predicted temperature profile may be due to the following; (a) the effective fuel conductivity model assumes that the cracks are uniformly distributed (the comparison indicates that the cracks are not uniformly distributed but are concentrated more toward the pellet surface), or (b) the multiplier of 0.9 on the sintering temperature may be too high.

5.2.1.2 Summary Of Fuel Temperature Results—Presented herein are the fuel centerline temperature results for a data sample of 93 rods, representing over 740 FRAPCON-1 code-to-data, and FRAP-S3 code-to-FRAPCON-1 code, comparison points. Figures 32 and 33 compare measured and predicted (FRAPCON-1) centerline temperatures for unpressurized and pressurized rods, respectively. The standard deviation between measured and predicted values is 170 K for the unpressurized rods, and 294 K for the pressurized rods. Results for the unpressurized rods are more representative of different fabrication, design, and operating conditions than in the case of the pressurized rods, due to the availability of a larger data sample for the unpressurized rods. As a result, code-to-data comparisons are probably less affected by systematic data errors in the case of the unpressurized rods than in the case of the pressurized rods. Consequently, the code-to-data comparisons might be expected to result in smaller standard deviations for the unpressurized rods than for the pressurized rods, as observed. In both cases, however, the general trend is that FRAPCON-1 overpredicts the measured values.

Figures 34 through 39 relate fractional model error for all centerline thermocouple data points to the expected first order design and operating effects; namely, fuel density, local burnup, gap size, and local power. Underestimating gap conductance, which would tend to increase predicted fuel centerline temperatures, is not considered a significant source of systemmatic error, as specified in the Gap Conductance section. Fractional model error is defined as the difference between the prediction and the measurement, divided by the measurement. For example, a fractional error of 0.2 means that the measurement was overpredicted by 20%.

Figure 34 shows the fractional model error in predicted fuel centerline temperature versus density for all rods considered in this study. In this case, the fractional error decreases with increasing fuel density, probably due to a decrease in the effect of pellet cracks on conductivity for the higher density fuels. The data points shown on Figure 34 were separated into 2 groups representing results of the pressurized rods and the unpressurized rods, shown on Figures 35 and 36, respectively. Apparently, the trend to overpredict centerline temperature with decreasing fuel density is dominant for the pressurized rods. This discrepancy is probably not attributable to a deficiency in the gap conductance model because soft (thermal) gap closure is attained at low power levels for the pressurized rods. At higher power levels, the gap conductance model becomes very insensitive to changes in power. Therefore, this overprediction trend is probably due to improper treatment of crack gas behavior such as conductivity and temperature, by the effective fuel conductivity model. This model does not account for varying crack gas pressures, which may be important when simulating small crack widths in the Knudsen domain.

Even though relatively few fuel centerline temperature measurements are available over extended operating periods, the fractional model error trend is to overpredict fuel centerline

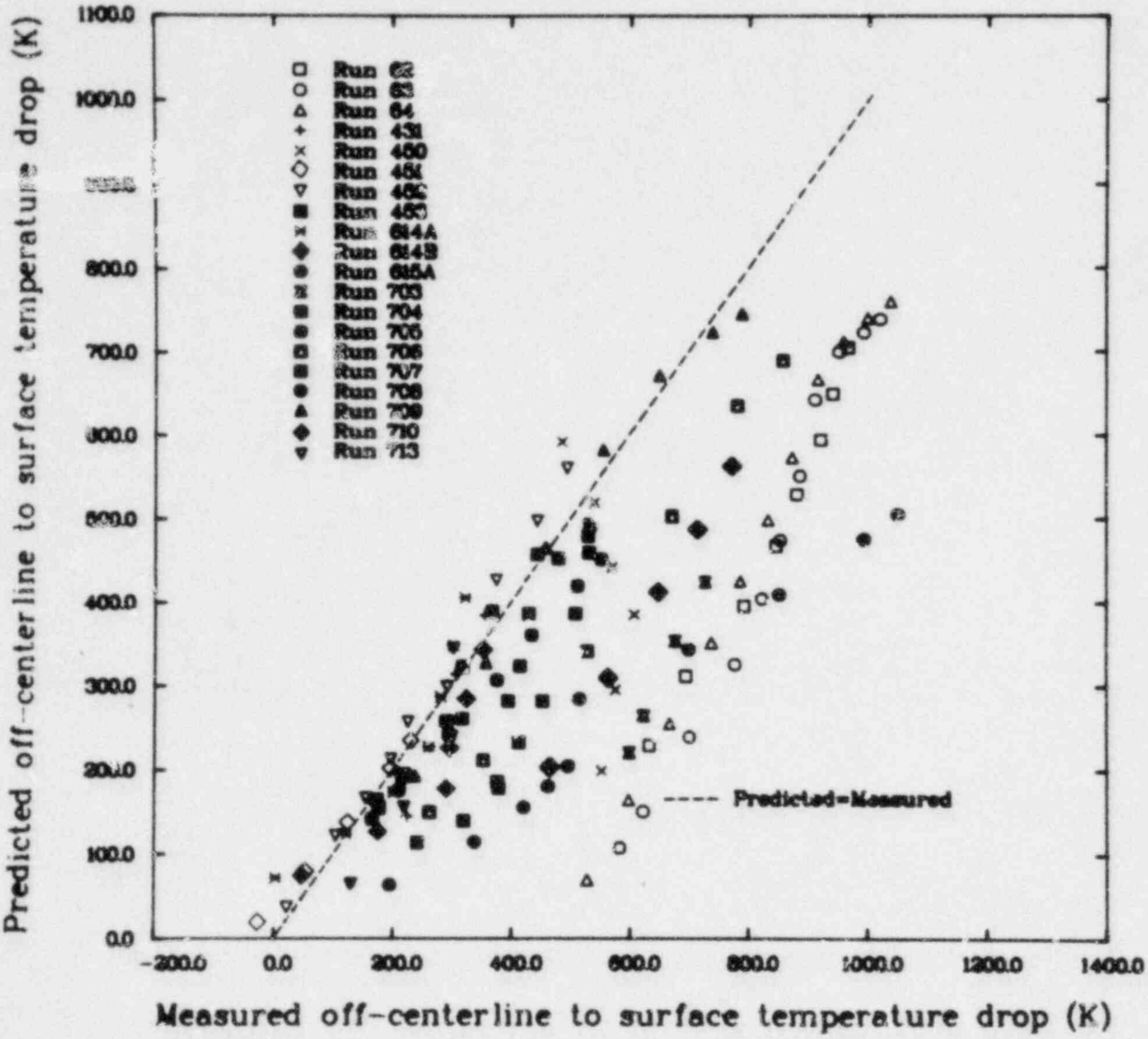

Figure 31. Comparison of FRAPCON-1 predicted and measured temperature difference between a radially positioned thermocouple and the pellet surface.

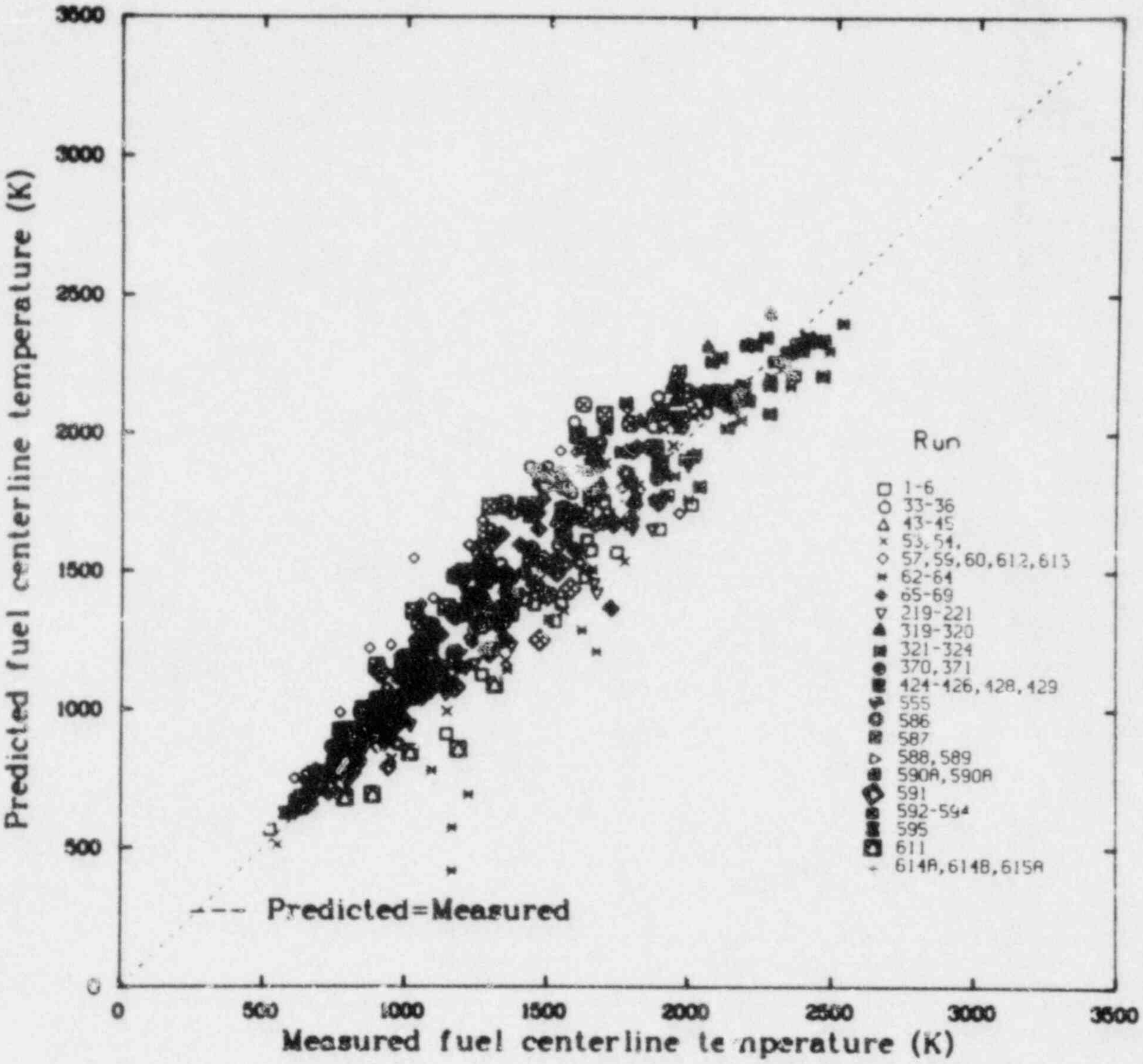

Figure 32. Comparison of FRAPCON-1 predicted and measured centerline temperatures for unpressurized rods.

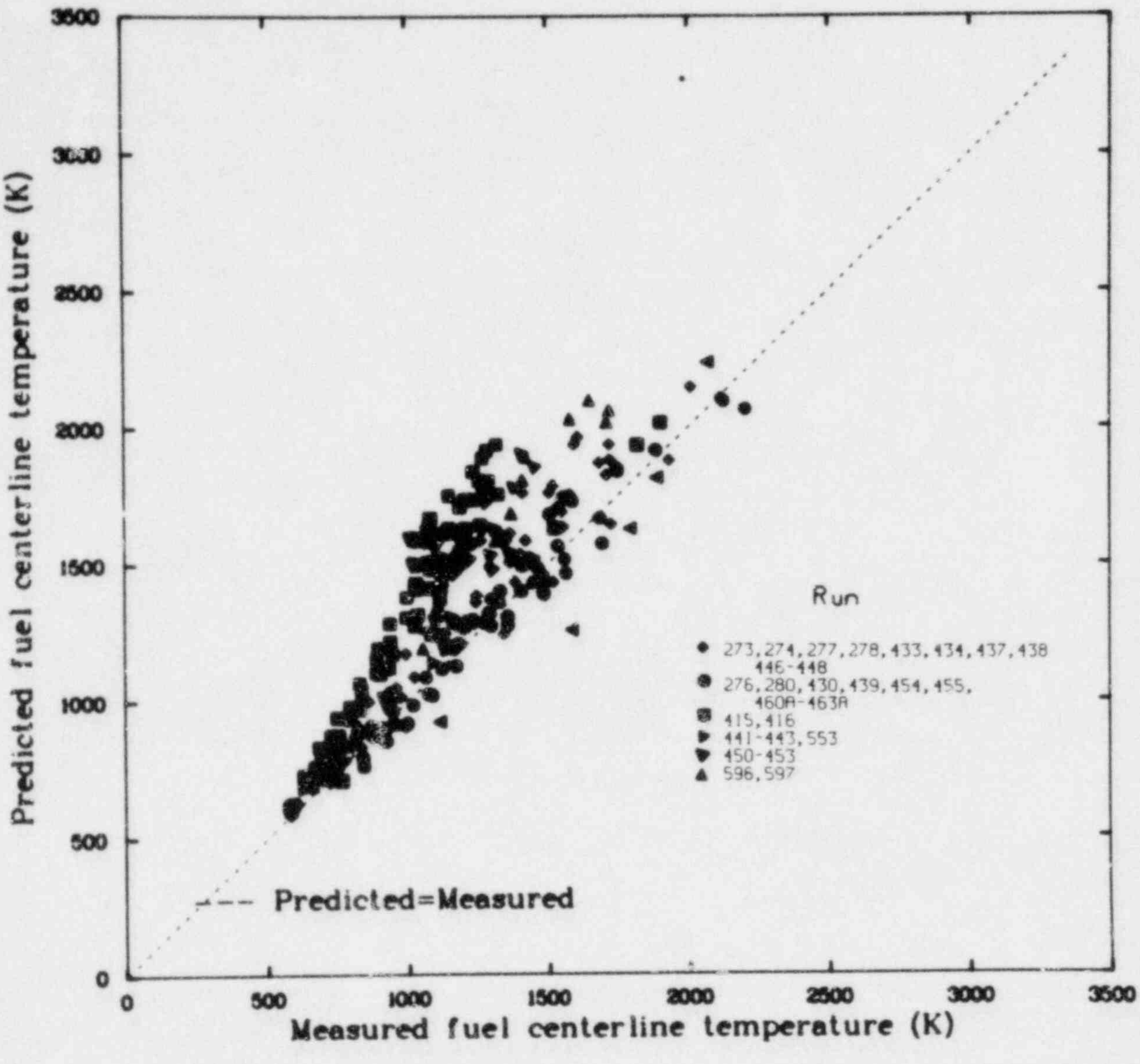

Figure 33. Comparison of FRAPCON-1 predicted and measured centerline temperatures for pressurized rods.

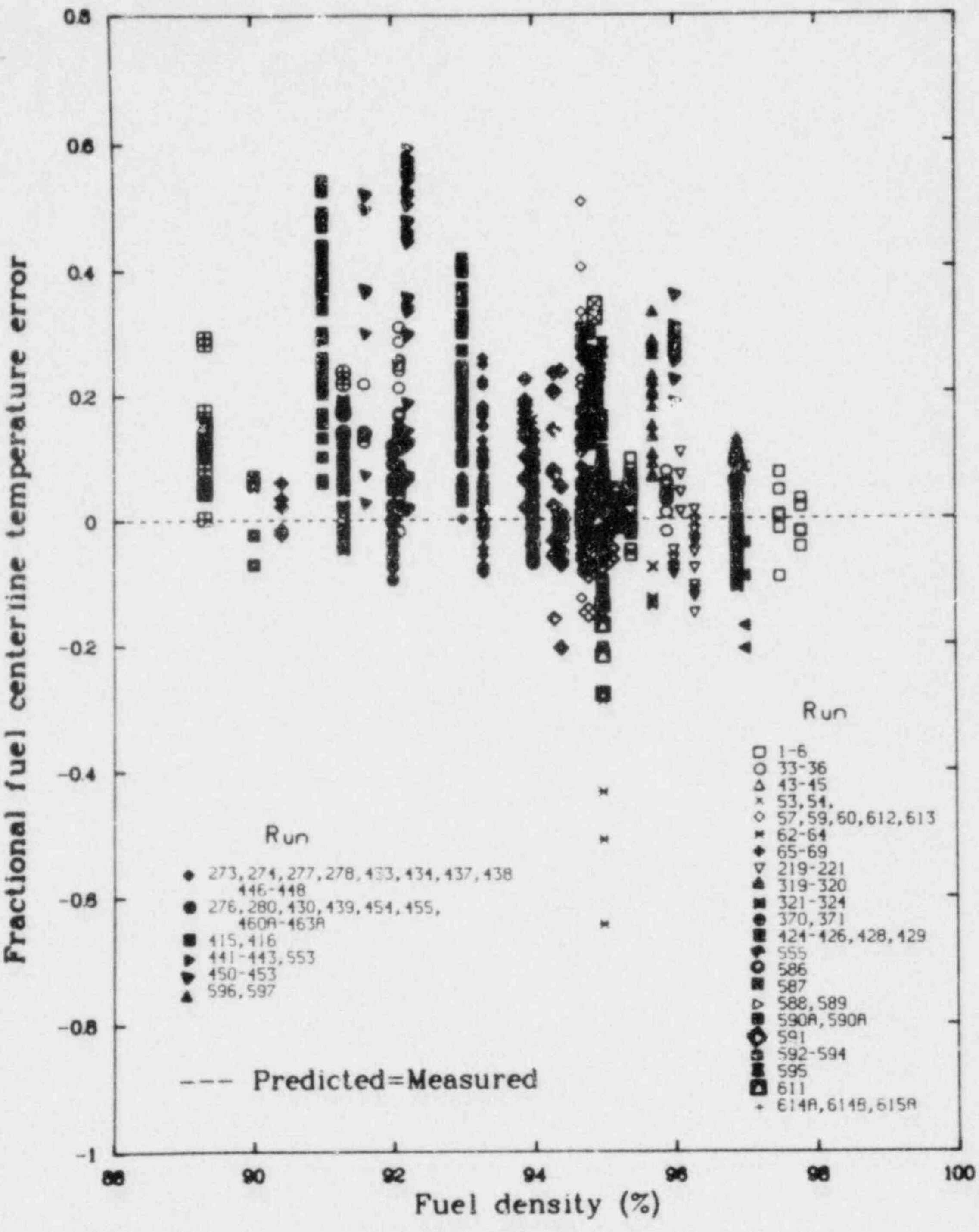

Figure 34. Effect of fuel density on FRAPCON-1 centerline temperature error (all rods).

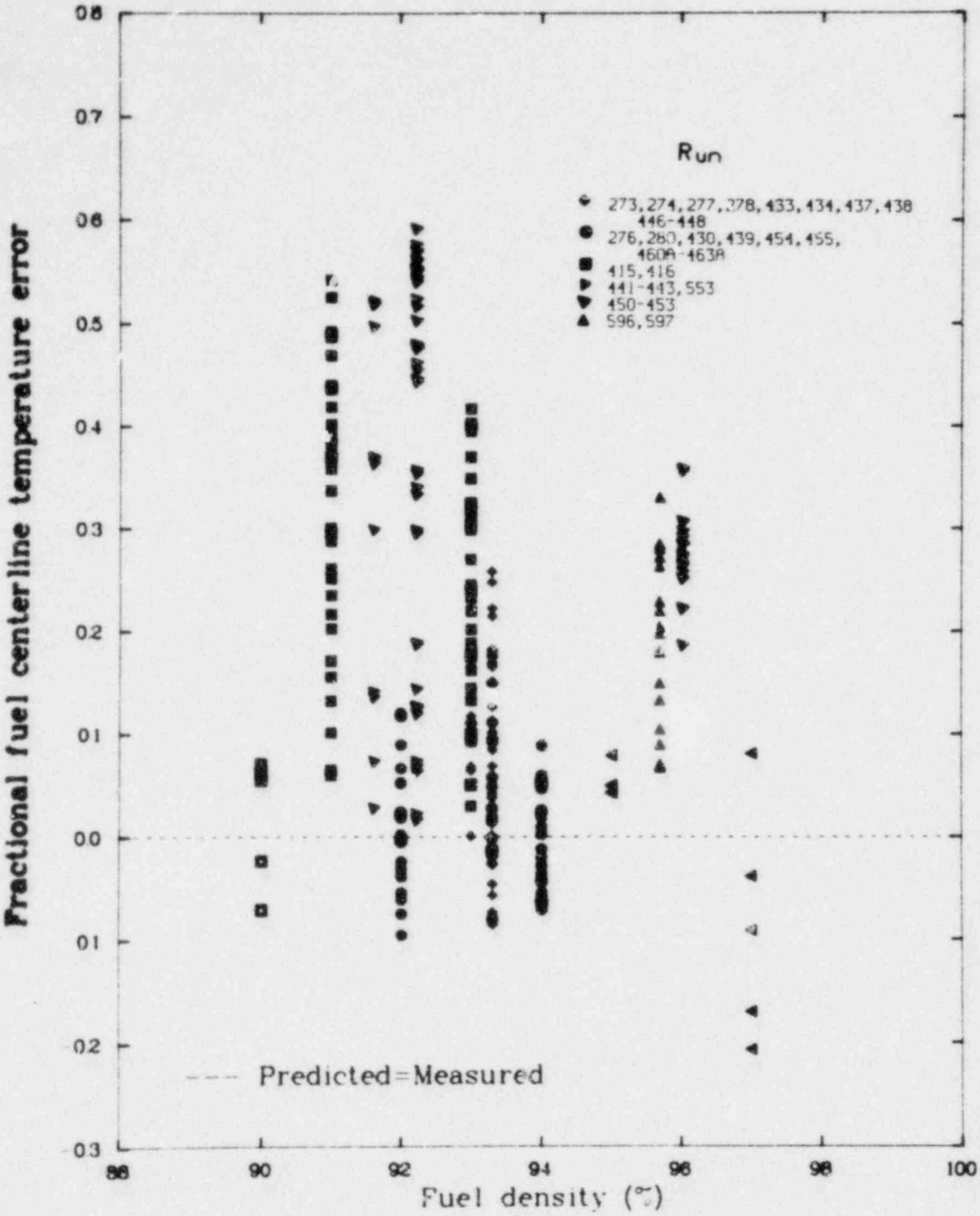

Figure 35. Effect of fuel density on FRAPCON-1 centerline temperature error (pressurized rods).

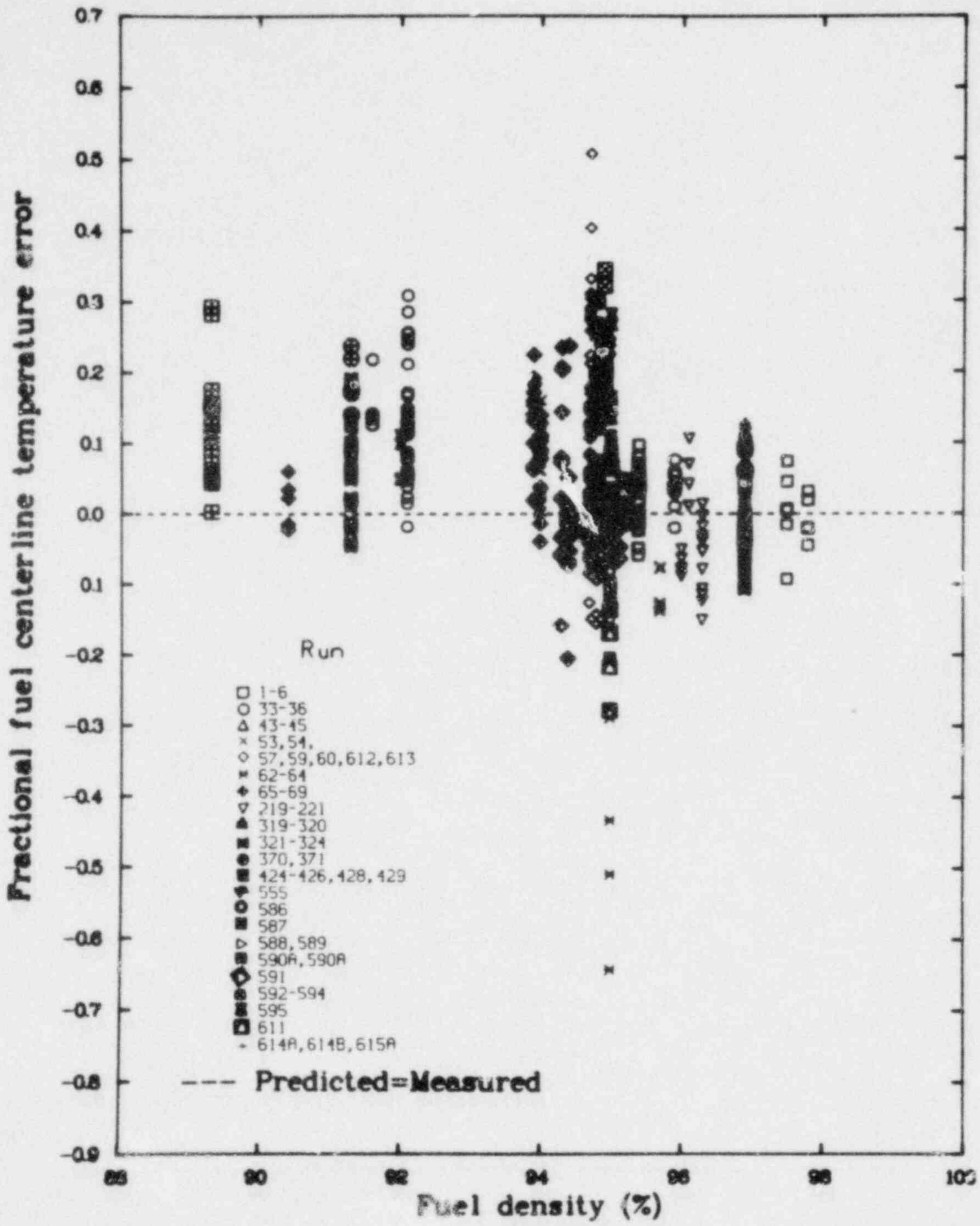

Figure 36. Effect of fuel density on FRAPCON-1 centerline temperature error (unpressurized rods).

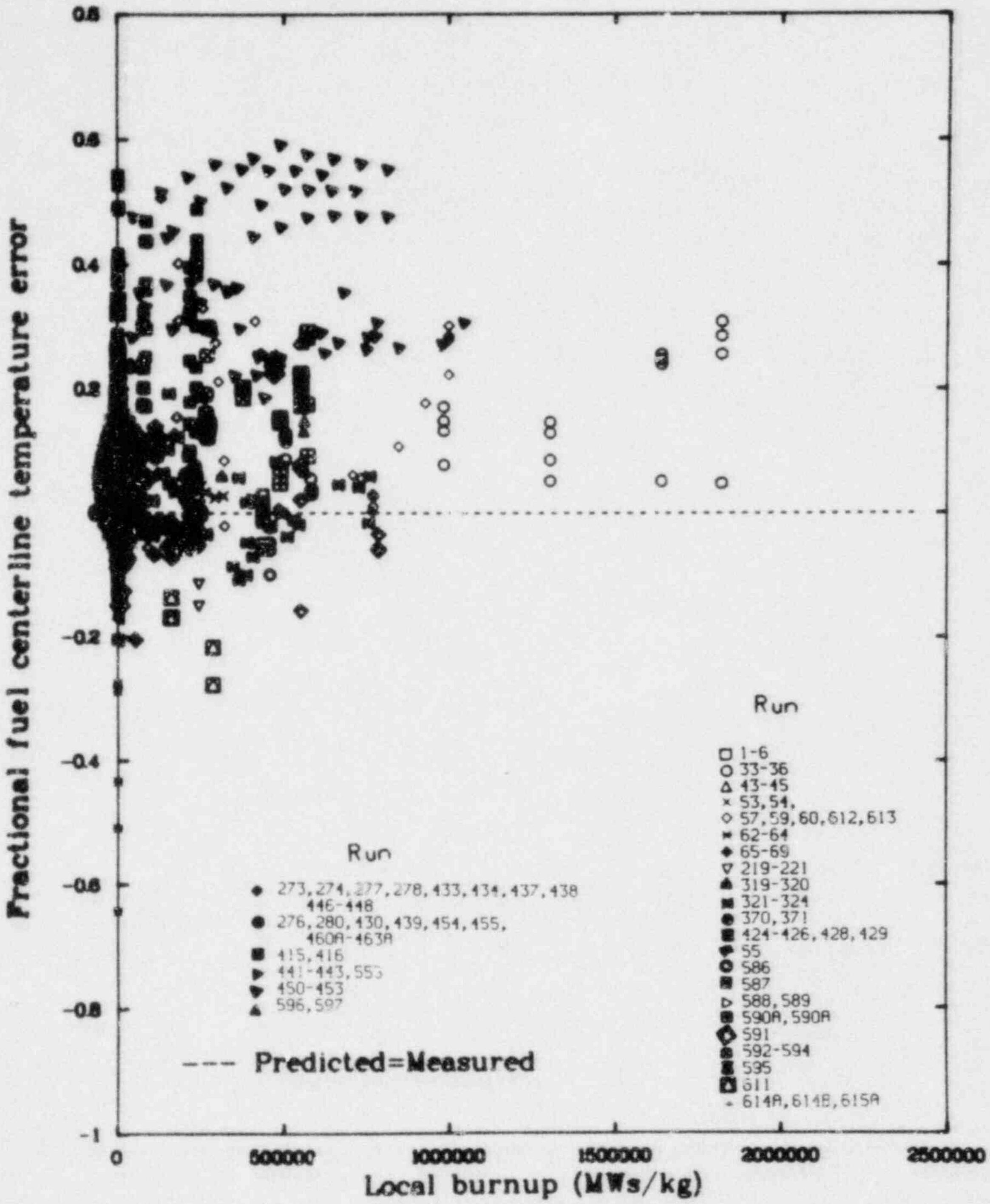

Figure 37. Effect of local burnup on FRAPCON-1 centerline temperature error.

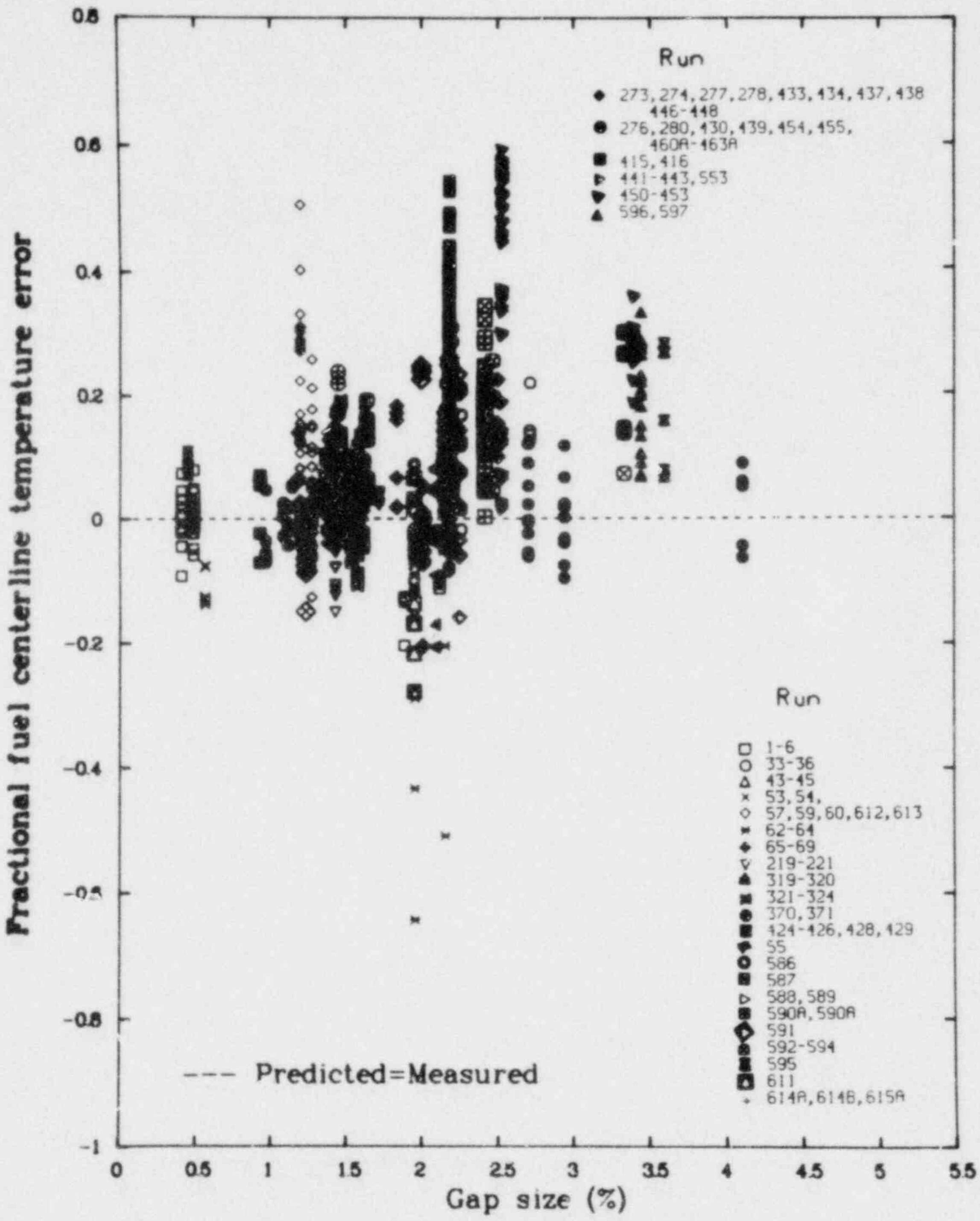

Figure 38. Effect of gap size on FRAPCON-1 centerline temperature error.

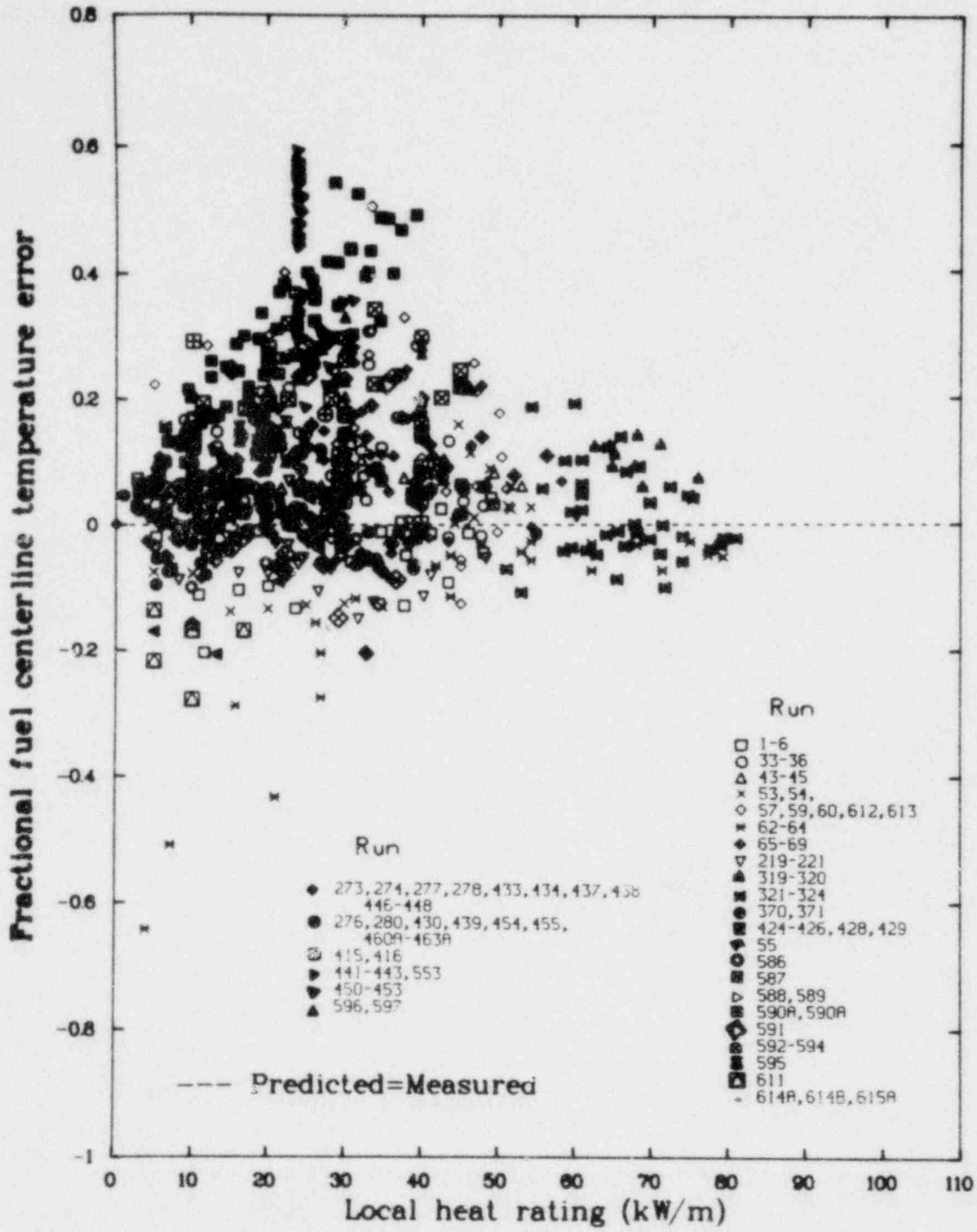

Figure 39. Effect of local heat rating on FRAPCON-1 centerline temperature error.

temperatures at low or moderate burnups, more so than at high burnup conditions, as shown on Figure 37. This same trend was previously observed and is probably due to the higher burnup data base being biased toward unpressurized rods.

The fractional model error in FRAPCON-1 predictions of fuel centerline temperature versus cold gap size showed an increased tendency to overpredict fuel centerline temperatures for radial gaps greater than 2% of the cold pellet radius, as shown on Figure 38. This trend indicates that relocation effects may be limited for gaps greater than 2%. The current model does not limit the effects of relocation for these gap sizes.

Figure 39 relates fractional model error in predicted fuel centerline temperature to local linear heat rate. In this case the fractional model error decreases as local linear power increases, probably because nearly all of the fuel rods at high power levels are unpressurized. The fractional model error might be expected to decrease as the local linear heat rate increases, as a result of the fuel restructuring effect on the thermal conductivity.

5.2.1.3 Gap Conductance—Gap conductance values have been analytically derived for various experiments on the basis of thermal model agreement with measured fuel temperatures, or cladding temperature phase lag during programmed power oscillations. Relative agreement between FRAPCON-1 results and derived experimental values is strongly affected by material properties and analytical assumptions. In this case, whether or not the experimental method of determining gap conductance considers relocated pellet geometry and effective conductivity feedbacks, will determine the degree to which FRAPCON-1 results match the gap conductance data.

Figures 40 and 41 compare derived and FRAPCON-1 calculated gap conductance for pressurized and unpressurized rods, respectively. With the exception of a few data points representing rods initially filled with fission gas, the calculated gap heat transfer level is always in excess of 5700 W/m^2 K. Most of the derived values are overpredicted by the model similar to previous assessment results. The relocation model allows high gap conductance to exist under soft (open cracks) as well as hard (closed cracks), gap closure conditions.

The effects of gap size (percentage of cold pellet radius) and power on fractional model error are shown on Figures 42 and 43 for all of the gap conductance data considered. The trends in both cases indicate more consistency between measured and calculated values for operating conditions promoting hard gap closure, that is, small initial gap sizes or high heat ratings. This observation is not unexpected since the effects of differences between FRAPCON-1 and the experimental method of determining gap conductance are minimized when FRAPCON-1 calculates hard gap closure. Under open or soft gap closure conditions, the inferred experimental values are overpredicted by factors of 2 to 10. For code-to-data consistency, it is worthwhile to use experimental gap conductance data reduction techniques where the gap closure assumptions and material properties are identical to those used in FRAPCON-1. Experimental data reduction techniques would then reflect realistic gap geometry conditions that are consistent with assessed code models.

5.2.2 Pressure Models. Backfill pressure, fission gas release, void volumes, and temperatures have a strong influence on operating pressure, effective gap size and gap conductance, and fuel thermal conditions. This section discusses code-to-data comparisons for fission gas release fraction and fuel rod internal pressure.

5.2.2.1 Fission Gas Release Fraction—Analysis of the fission gas release model is based on approximately 150 code-to-data comparisons. The experimental data reflect a wide range of design, operating, and burnup conditions. This section discusses the code-to-data comparison for the fission gas release model, which is primarily temperature dependent. Figure 44 compares the measured and calculated fission gas release fraction for a data sample of approximately 150 unpressurized rods. In general, FRAPCON-1 overpredicts the fission gas release fraction when the measured fraction is less than 20%, and is as likely to overpredict as underpredict when the measured fission gas release fraction is greater than 20%. When all the measured data are considered, the standard deviation between the measured and calculated fission gas release fraction is 16%.

Figure 45 shows the fission gas release fractional model error as a function of fuel temperature. The fuel temperatures are the maximum volume averaged fuel rod temperatures that

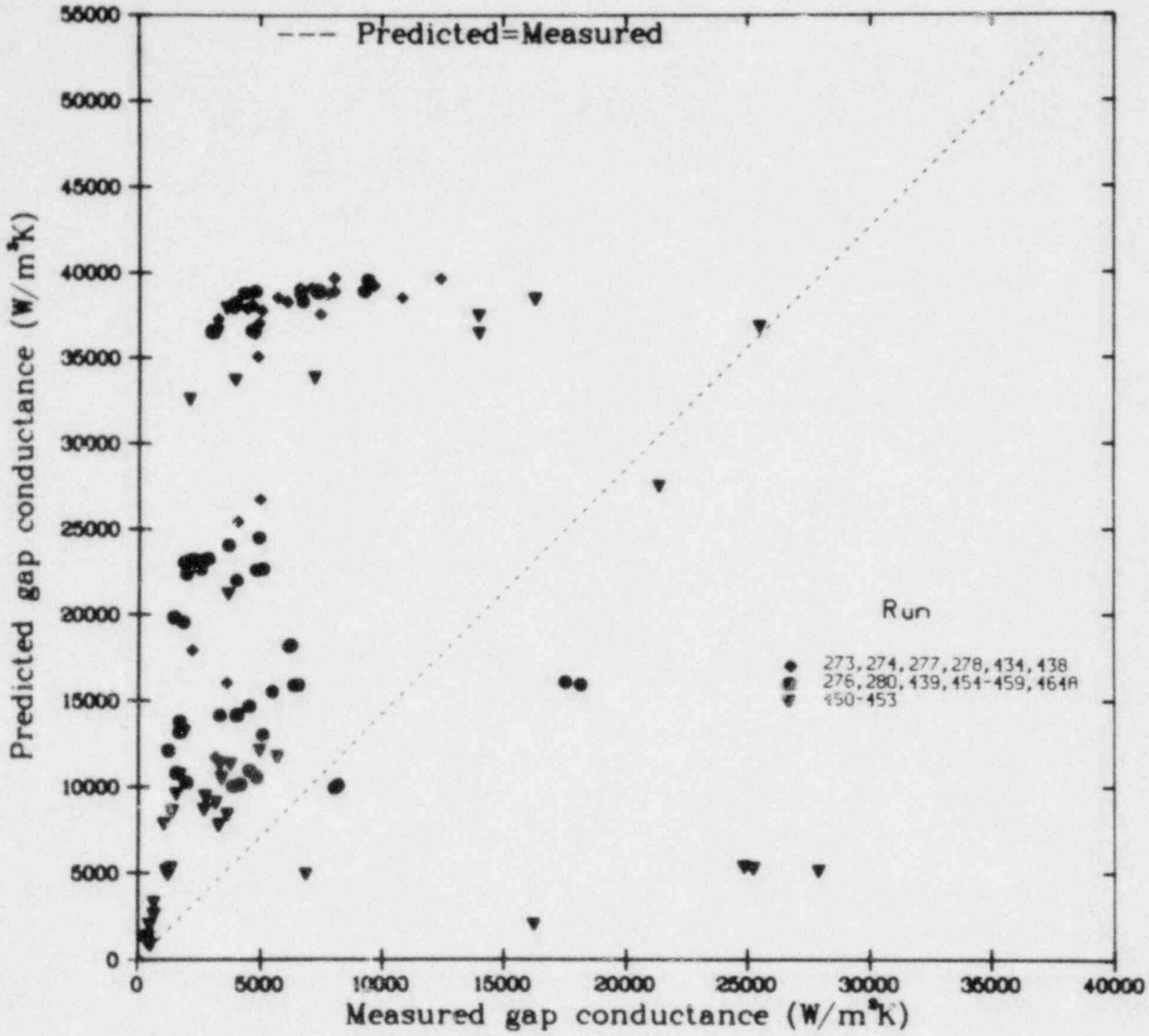

Figure 40. Comparison of FRAPCON-1 predicted and experimentally inferred gap conductance—pressurized rods.

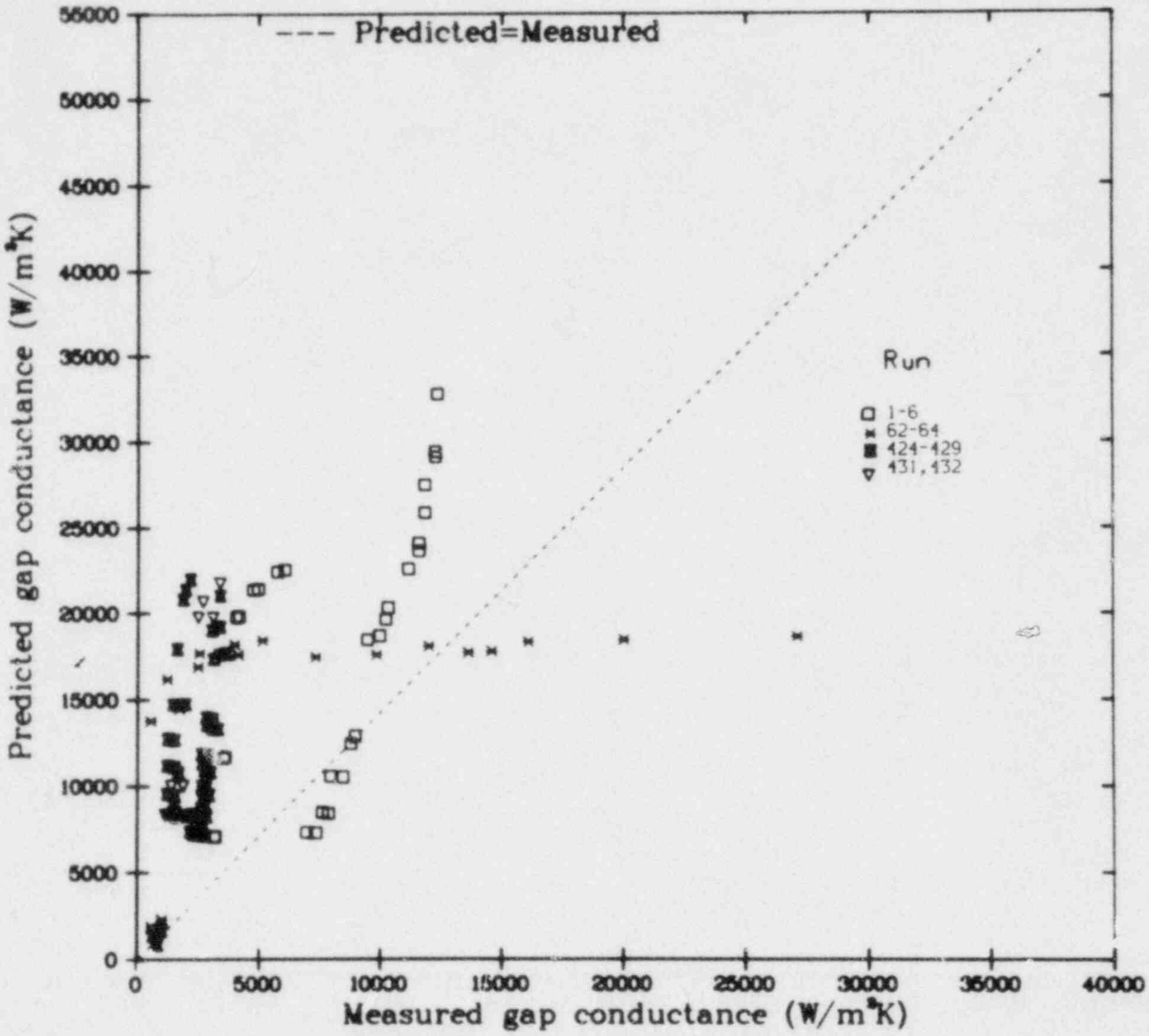

Figure 41. Comparison of FRAPCON-1 predicted and experimentally inferred gap conductance—unpressurized rods.

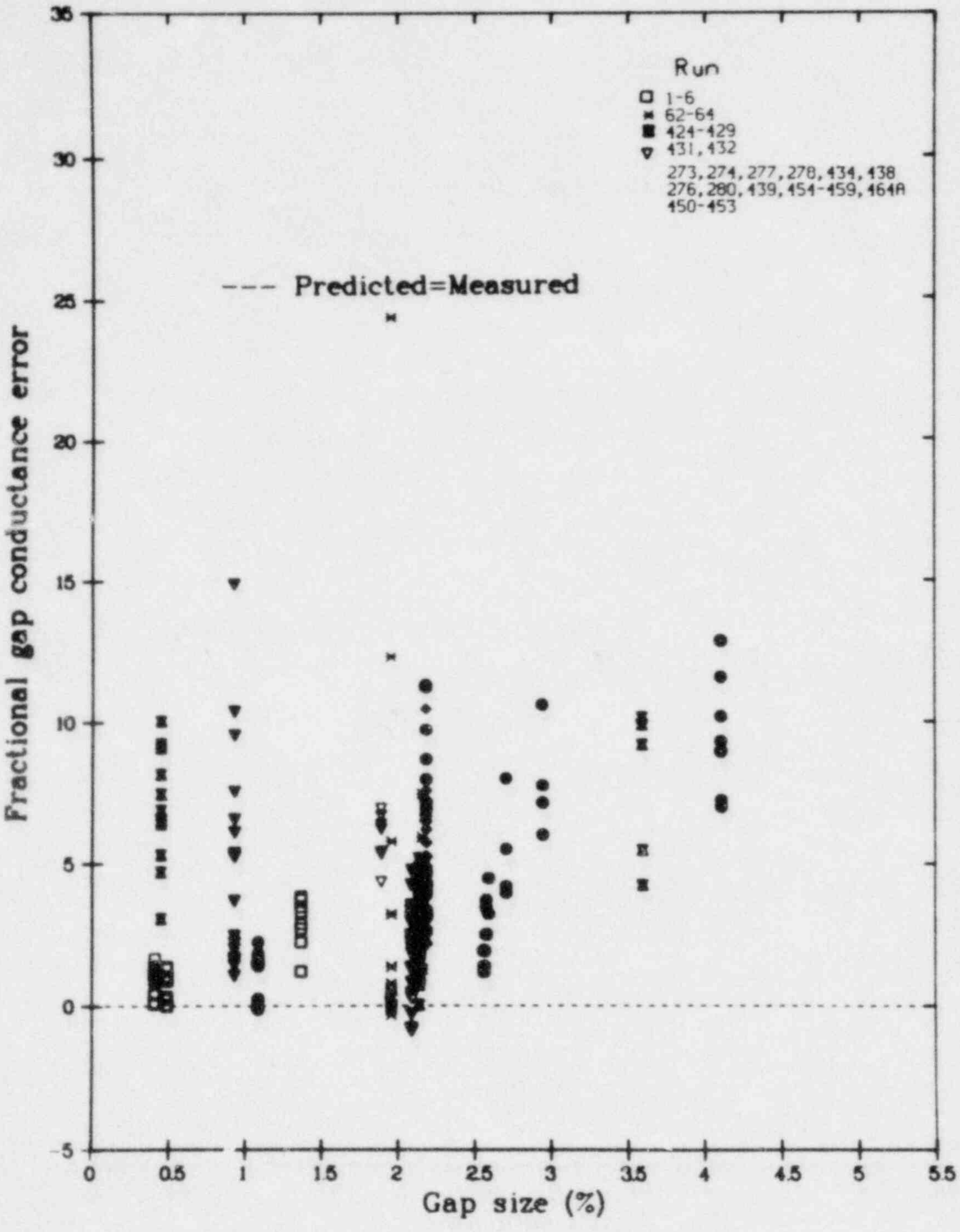

Figure 42. Effect of gap size on FRAPCON-1 gap conductance error.

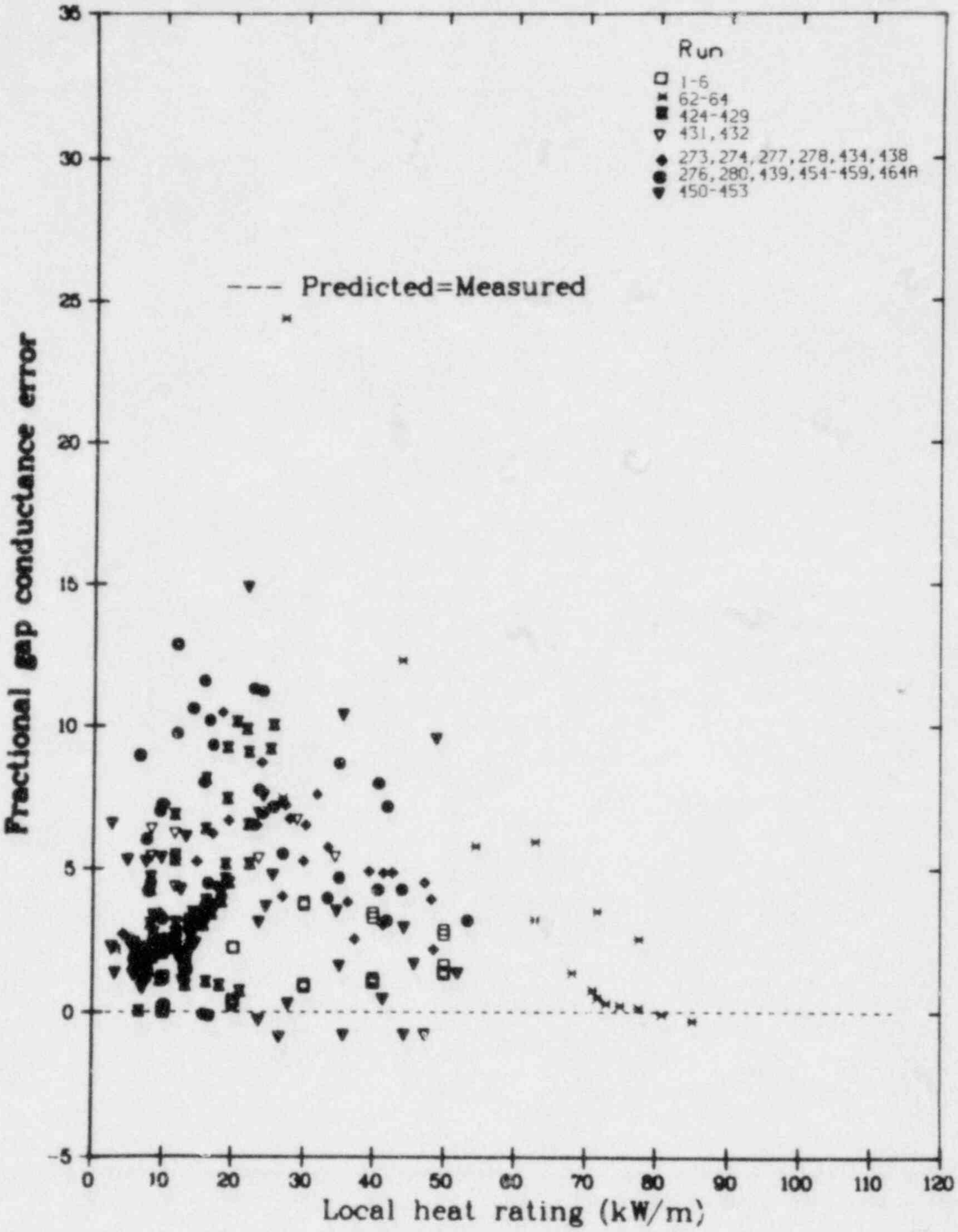

Figure 43. Effect of local heat rating on FRAPCON-1 gap conductance error.

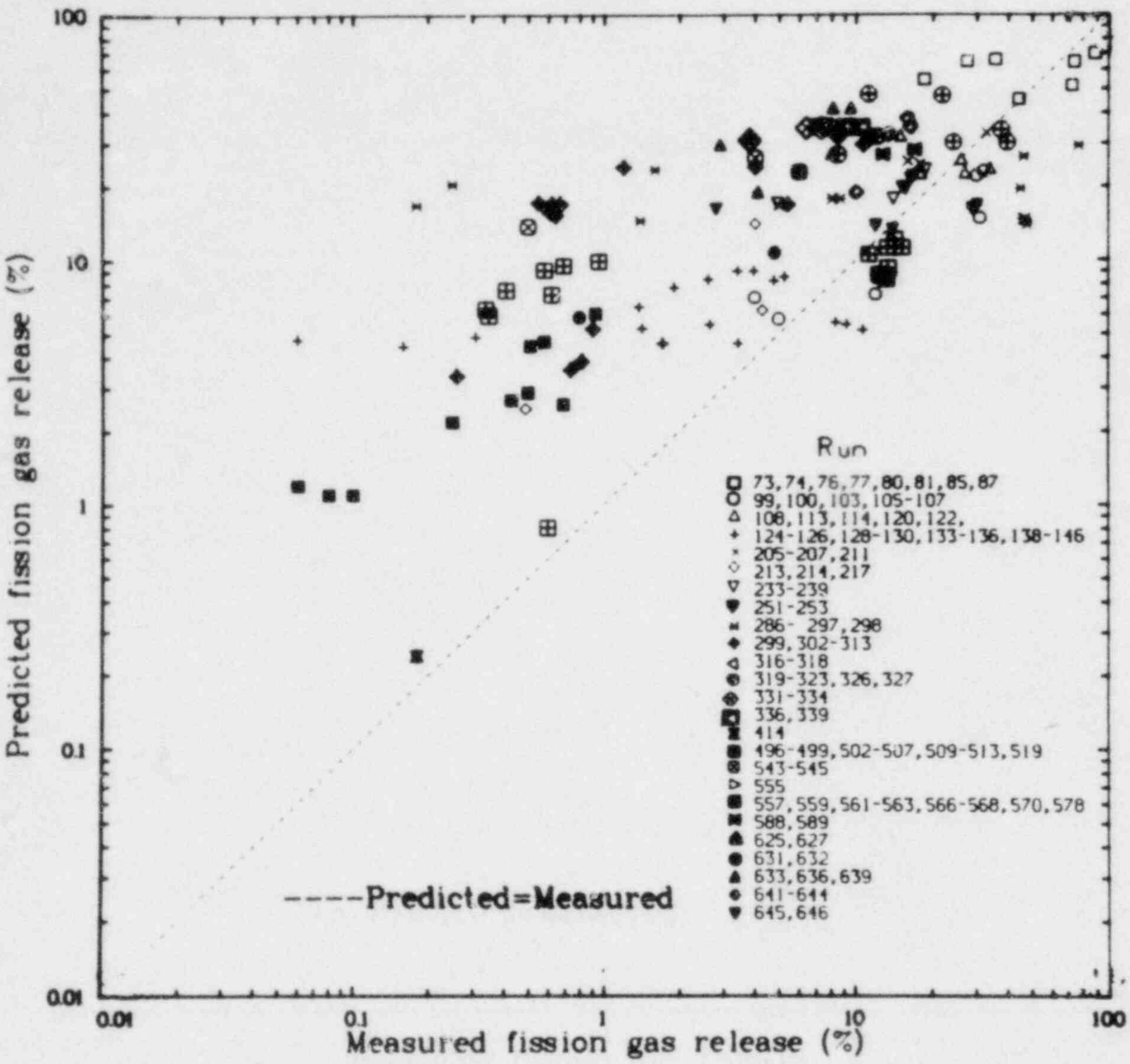

Figure 44. Comparison of FRAPCON-1 predicted and measured fission gas release fraction.

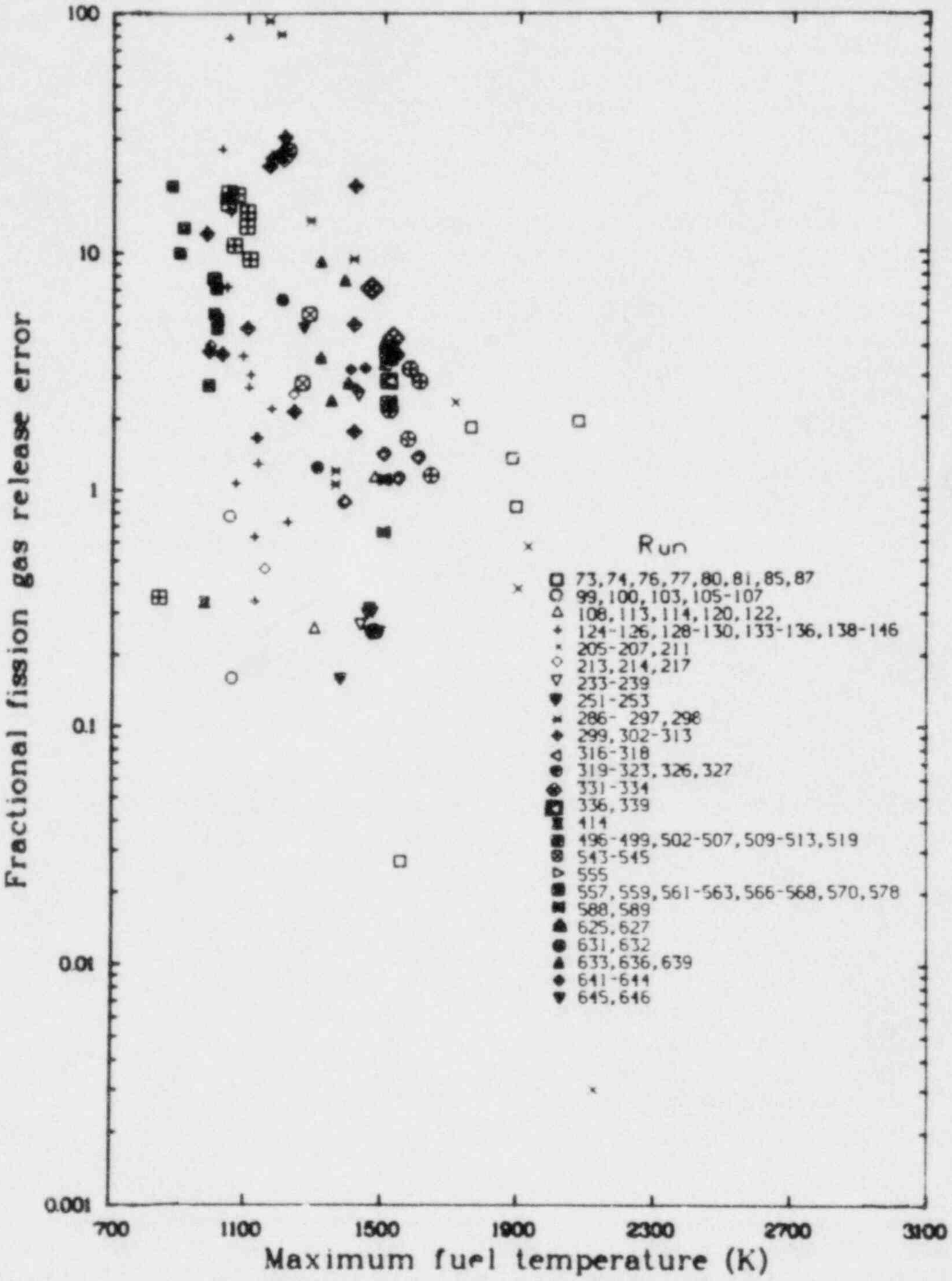

Figure 45. Effect of maximum fuel temperature on FRAPCON-1 fission gas release error.

were predicted to occur during the irradiation. In this case, a general trend of decreasing model error is observed as the maximum temperature increases. A similar trend was observed when the model error was plotted versus the calculated volume-averaged fuel rod temperature at the time-integrated average power level during the irradiation.

The temperature effect on fission gas release corresponds to fission gas bubble mobility, due to the rapid influence of fuel temperature on fuel structure. Figures 46 and 47 show the measured and predicted fission gas release fractions might be expected to saturate, or approach a limiting value as the temperature increases. As a result, the fractional model error would decrease or approach a constant value with increasing gas release fraction, as indicated by the results shown in Figure 44.

Many burnup-dependent mechanisms affect gas release, some of which are influenced by gas bubble location, gradual development of interconnected porosity, and buildup of fission product concentration. To investigate the effect of fuel burnup on fission gas release fraction, the fractional model error in fission gas release fraction was plotted versus fuel rod average burnup, as a function of various temperature intervals. Figures 48, 49, and 50 show the predicted, measured, and fractional model error increases with burnup. Also, at high temperatures (>1300 K), where the temperature effect on fission gas release has begun to saturate, the results shown on Figures 47 and 48 indicate that the gas release fraction increases with burnup. That is, at high temperatures the fission gas release fraction is dominated by changes in the amount of burnup, while at low fuel temperatures, the fission gas release fraction is dominated by changes in temperature.

5.2.2.2 Rod Internal Pressure—The ability of FRAPCON-1 to predict internal pressure is dependent upon model capabilities to predict, for example, fission gas release, plenum volume changes, fuel stack changes resulting from mechanical deformation, and gas absorption by the fuel. In order to separate some of these effects, two sets of comparisons were made. First, code-to-data comparisons at low burnup conditions were performed to reflect the fuel heatup effect on void volumes and gas temperature, and establish an initial operating pressure. Second, code-to-data comparisons at higher burnup conditions were used to assess the performance of the fission gas release and mechanical deformation models.

Figure 51 compares measured and calculated internal pressure for both pressurized and unpressurized rods for low burnup conditions. The standard deviation for the pressurized and unpressurized rods is 1.93 and 1.38 MPa, respectively. Experimental data in excess of 3.4 MPa generally correspond to startup operation for pressurized rods backfilled to either 2.41 or 3.79 MPa. The group of underpredictions at measured pressures between 7.6 and 11.7 MPa corresponds to startup measurements for two rods, which exhibited significant pressure transducer drift. In general, the predicted pressure for the pressurized rods exceeds the measured pressure. For the unpressurized rods, the measured pressure is as likely to be overpredicted as underpredicted.

Figure 52 compares the fractional model error versus the fuel rod average linear heat rating for low burnup conditions. An overall trend of increasing error with increasing local linear heat rating is seen. Experimental results[65] have indicated a reduction in gas communication to the plenum with increasing fuel rod power or cladding collapse onto the fuel stack. Consequently, the measurements essentially saturate as power increases, whereas the calculated values do not reflect this trend. As a result, the predictions would tend to exceed the measurements. A similar trend was noted when the relative model error was plotted versus fuel rod average temperature.

The fractional model error for the code-to-data comparisons for both pressurized and unpressurized rods at low burnup conditions is shown on Figure 53 versus fuel rod plenum void volume. In this case, the relative model error decreases as the more easily characterized plenum void volume increases, indicating that changes in the calculation of crack volumes, gap volumes, and dish volumes are required. However, additional analyses indicated that the fractional model error, with respect to the cold fuel-cladding gap size, showed little trend.

Figure 54 compares measured and predicted internal pressures for both pressurized and unpressurized rods at high burnup conditions. In

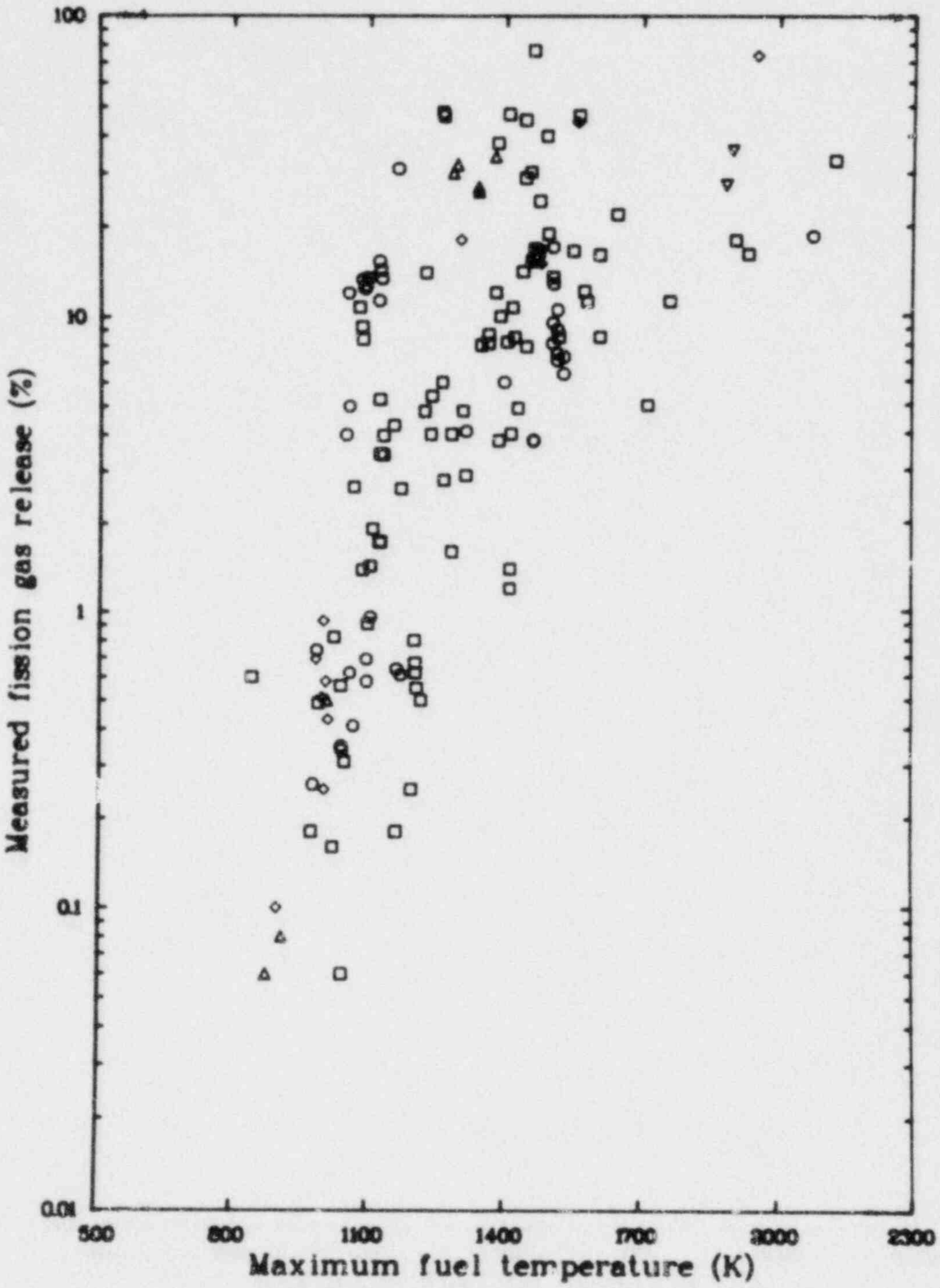

Figure 46. Effect of maximum fuel temperature on measured fission gas release fraction.

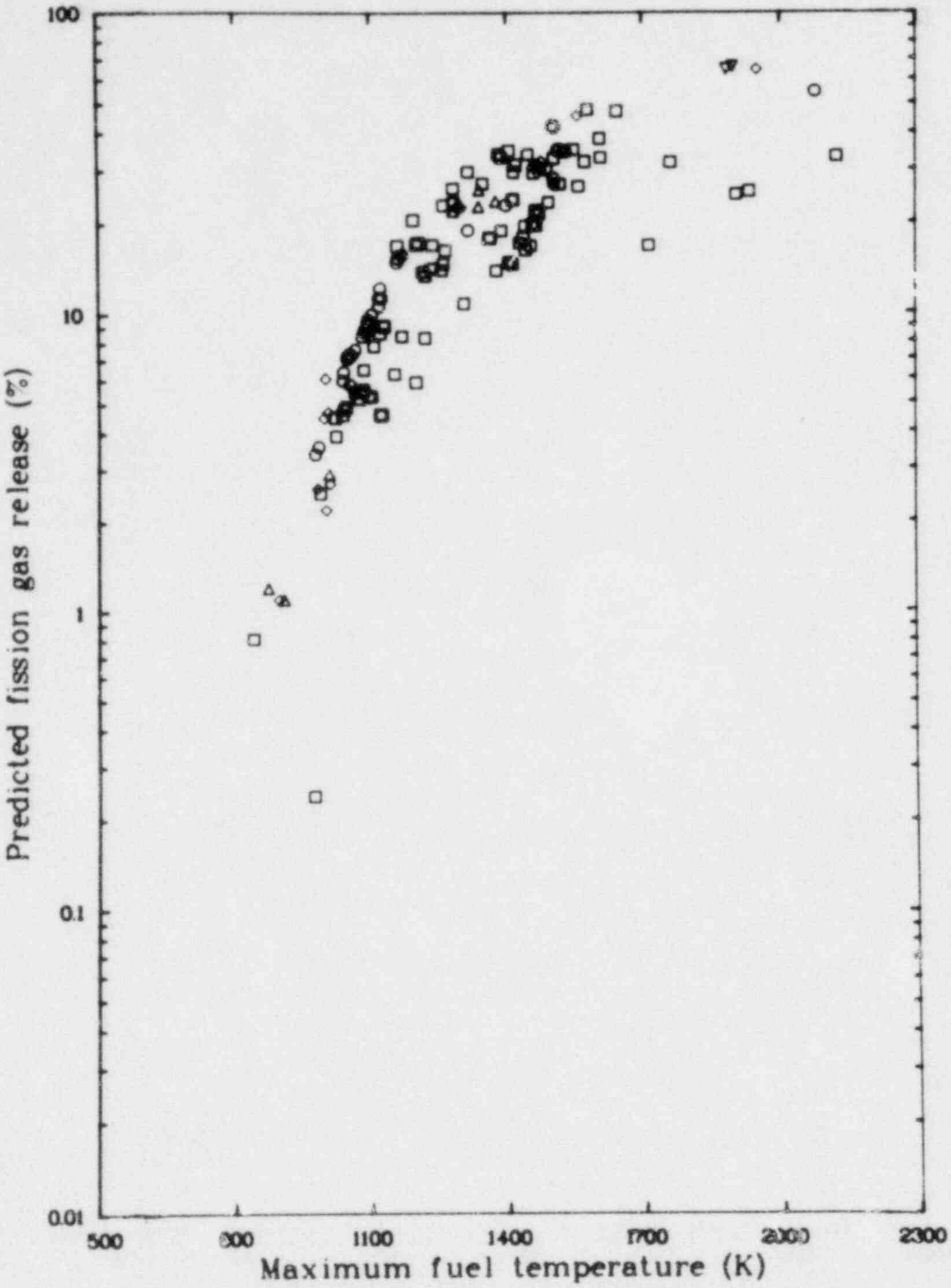

Figure 47. Effect of maximum fuel temperature on FRAPCON-1 predicted fission gas release fraction.

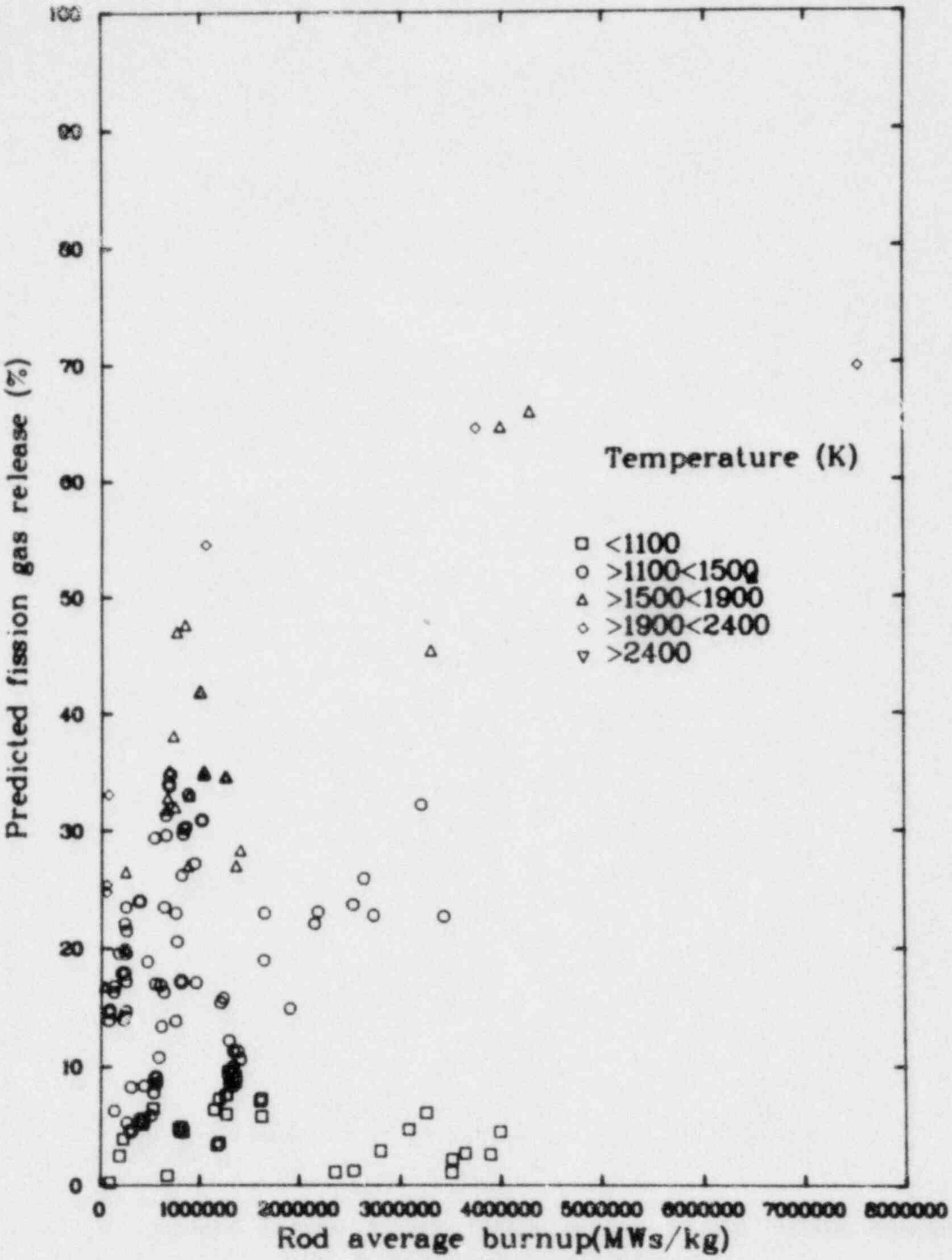

Figure 48. Effect of rod average burnup on FRAPCON-1 predicted fission gas release fraction.

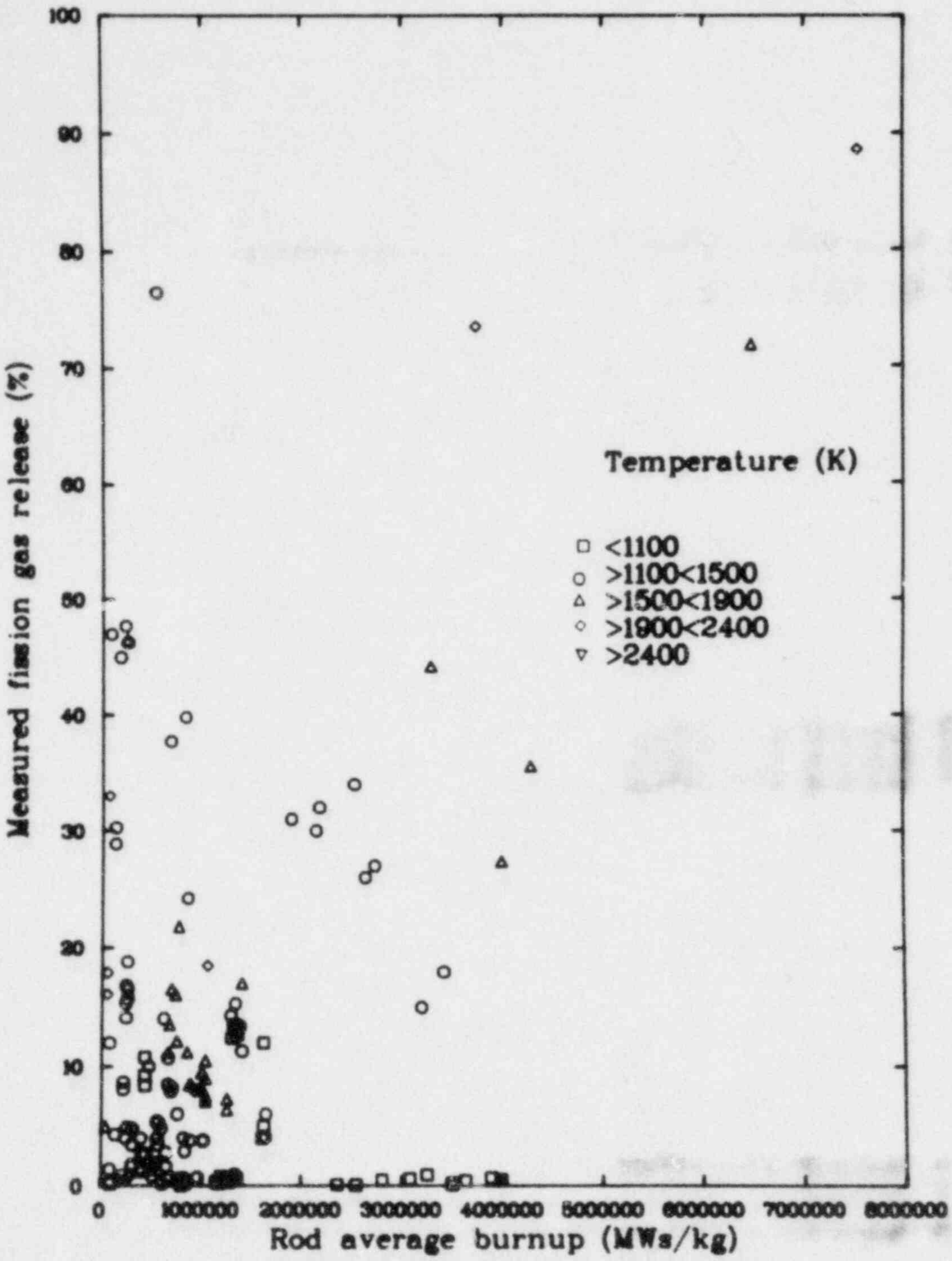

Figure 49. Effect of rod average burnup on FRAPCON-1 measured fission gas release fraction.

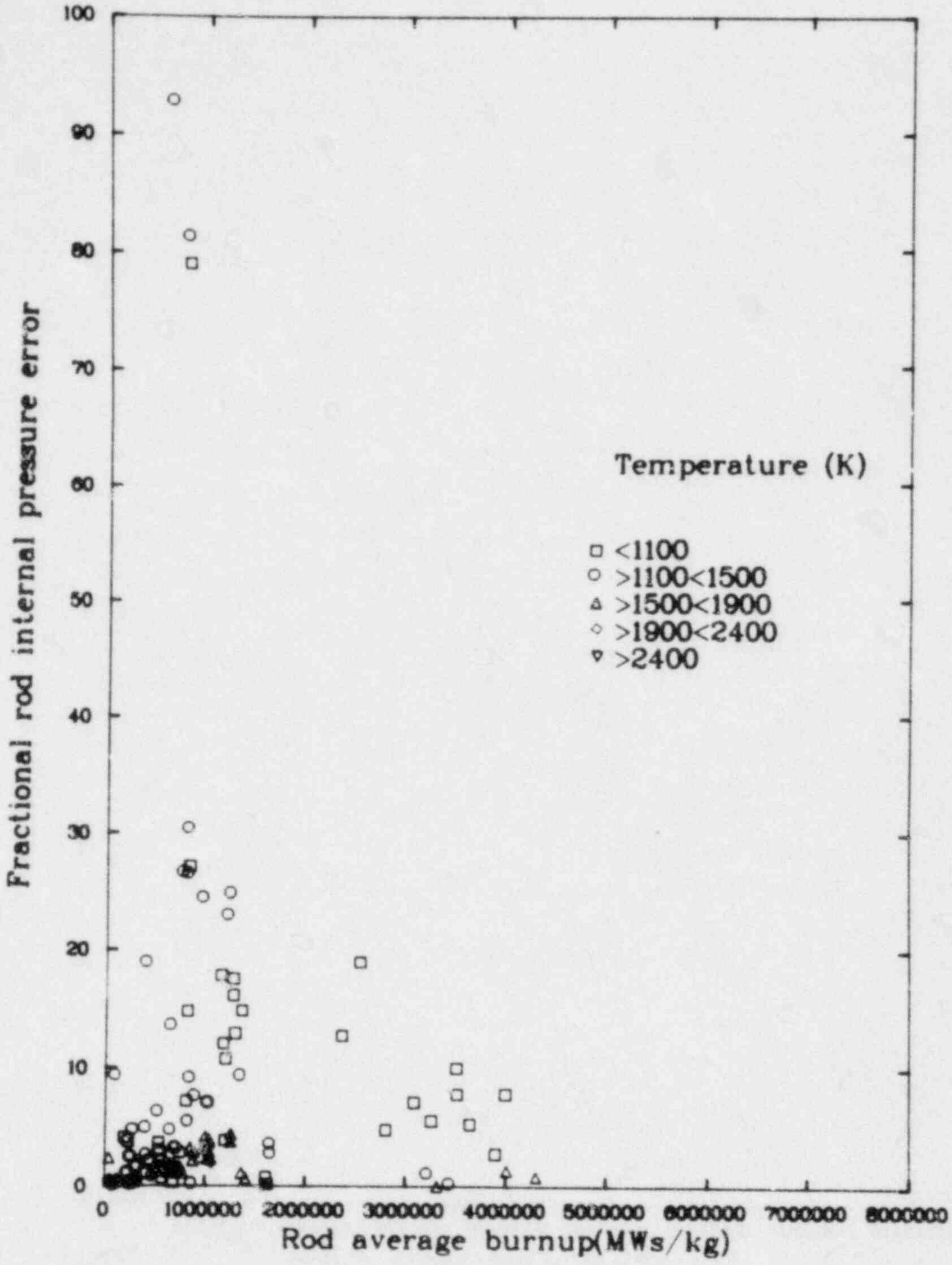

Figure 50. Effect of burnup on FRAPCON-1 fission gas release error.

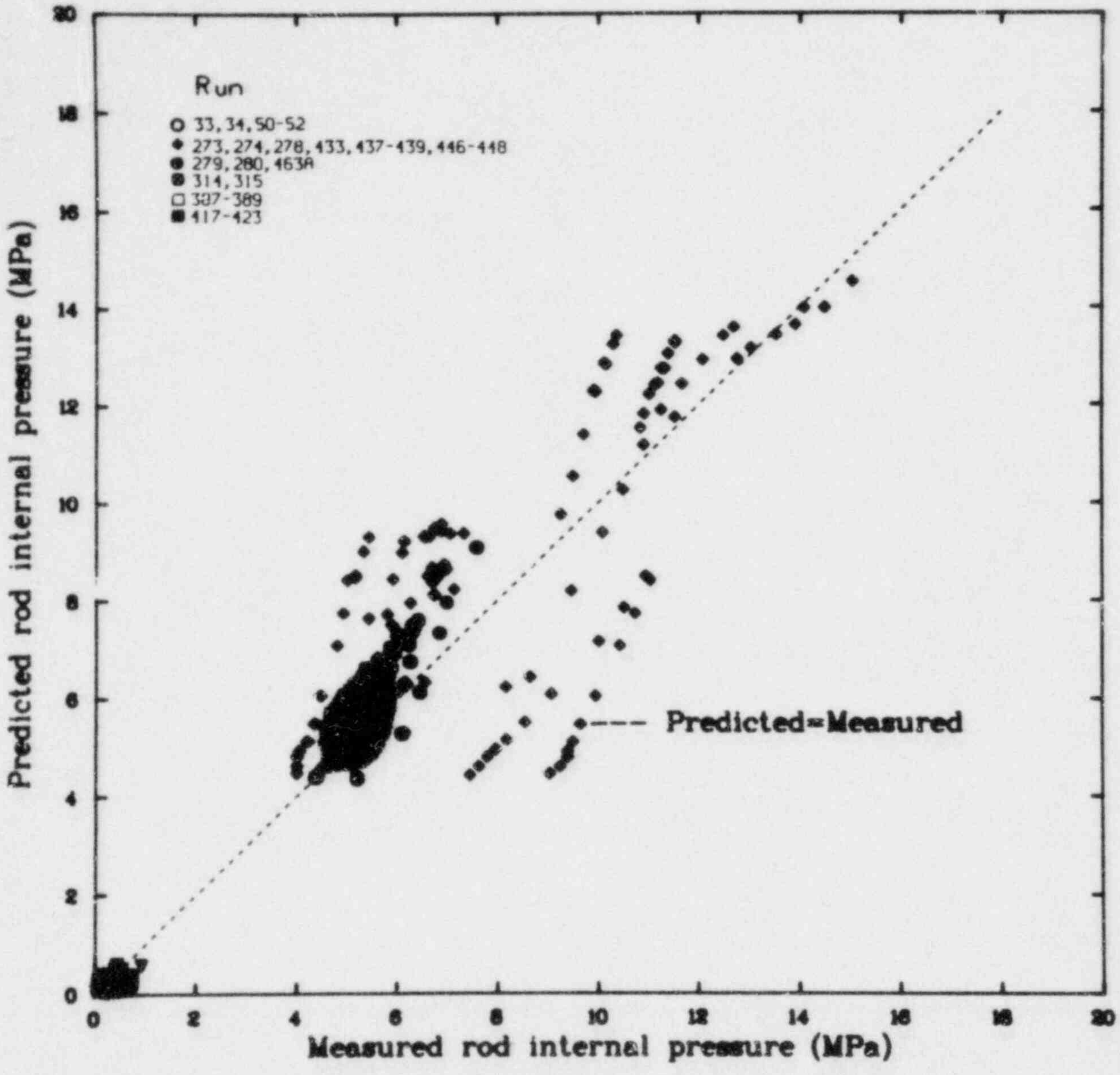

Figure 51. Comparison of FRAPCON-1 predicted and measured rod internal pressure.

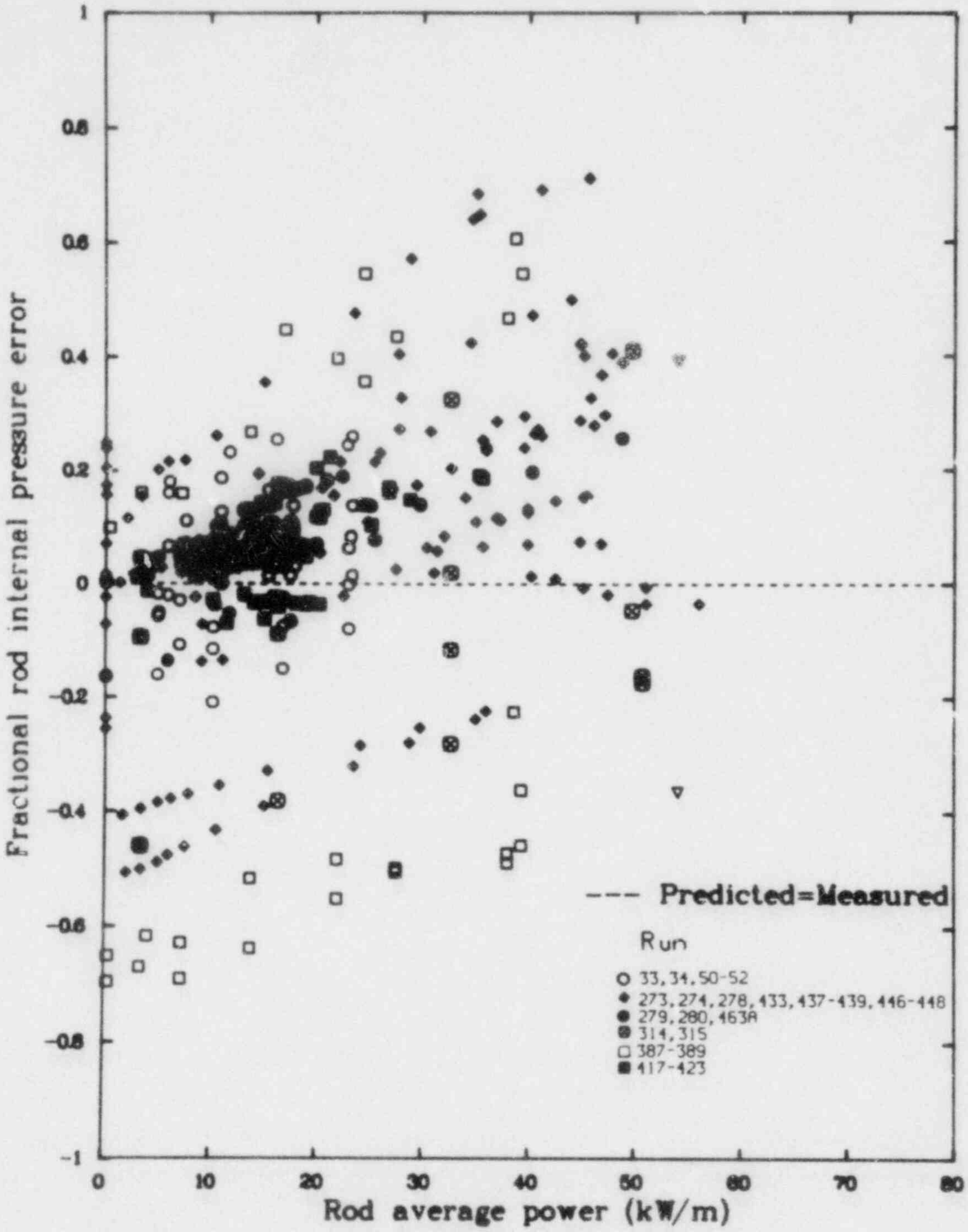

Figure 52. Effect of average heat rating on FRAPCON-1 internal pressure error.

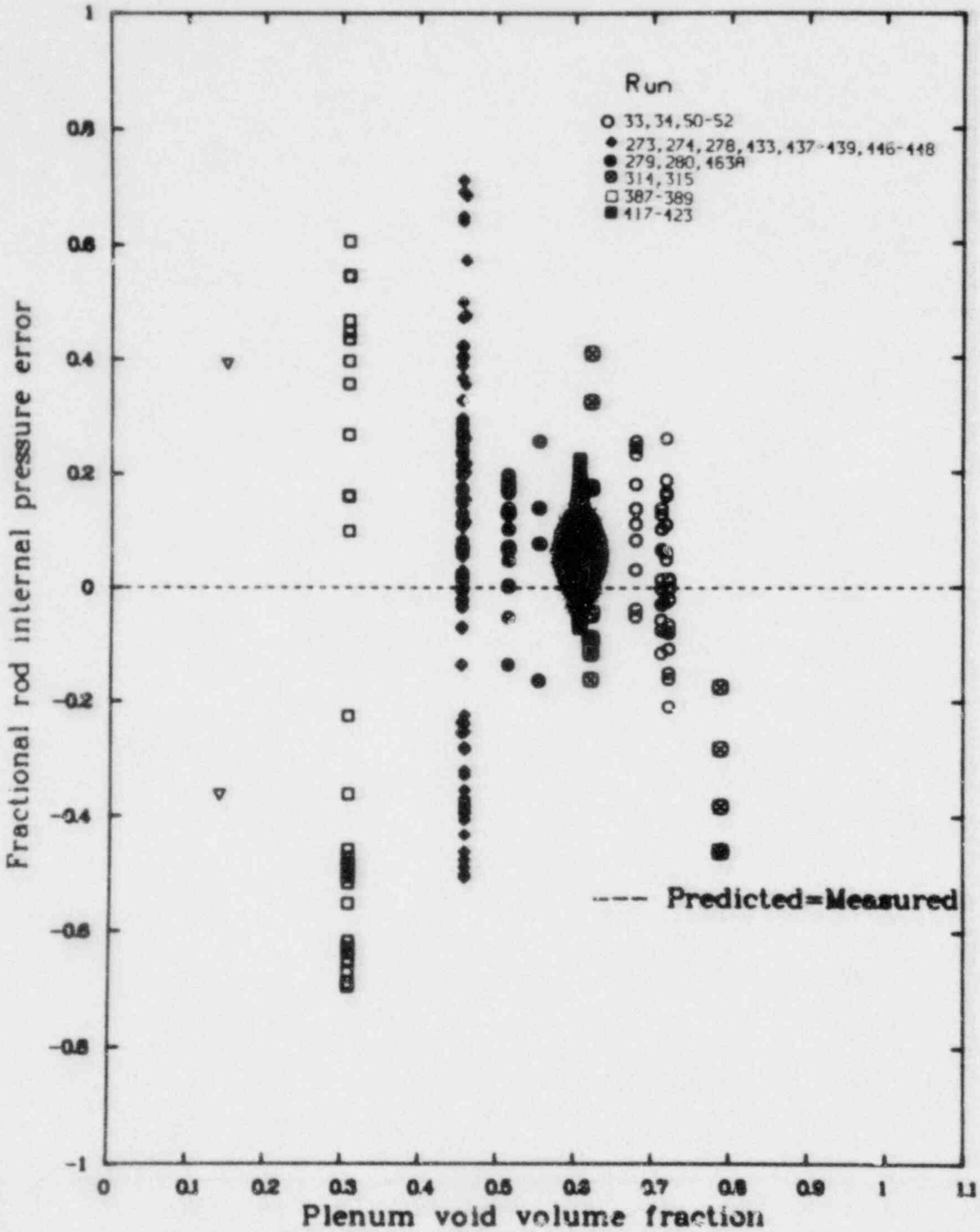

Figure 53. Effect of plenum void volume fraction on FRAPCON-1 internal pressure error.

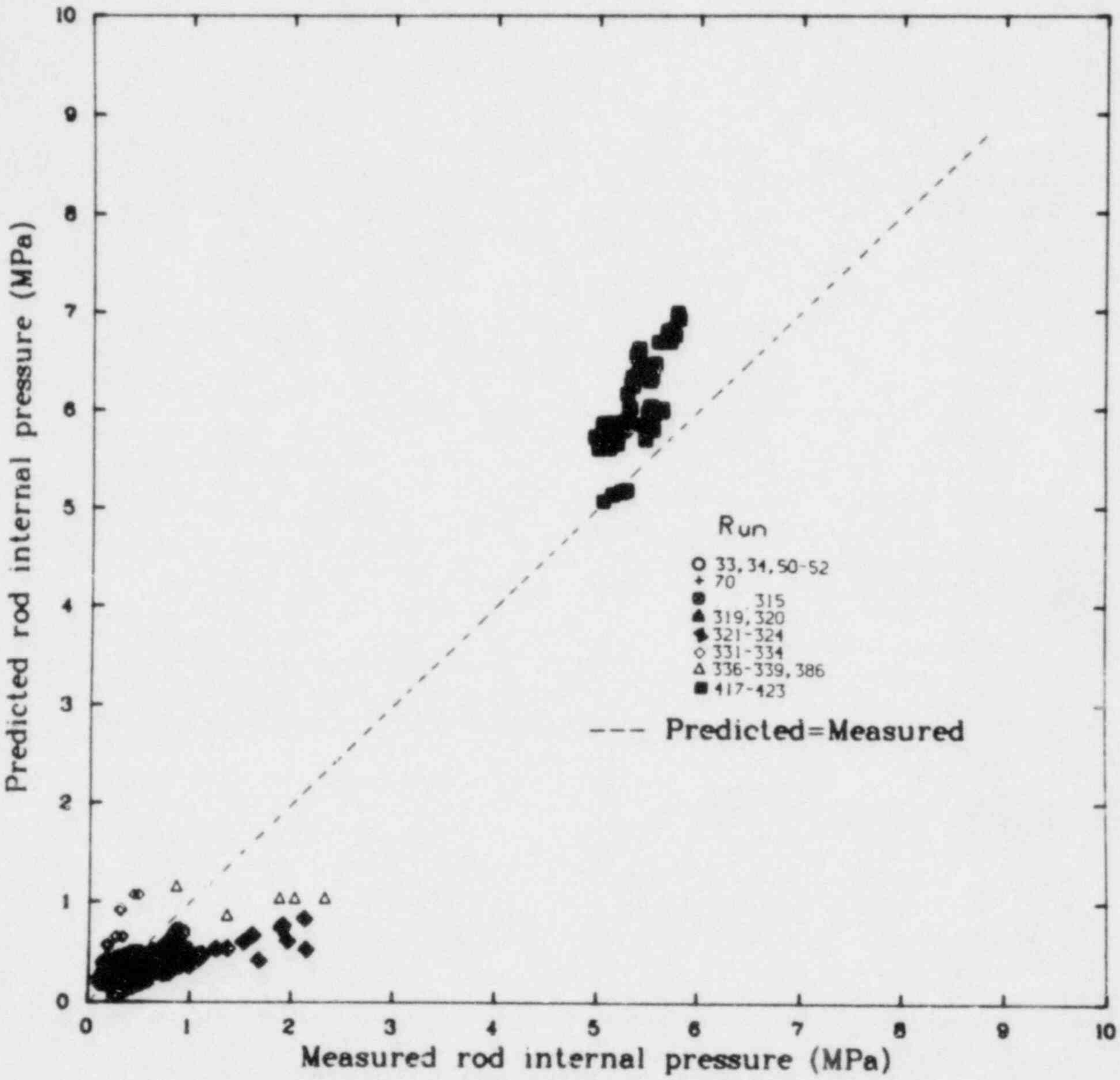

Figure 54. Comparison of FRAPCON-1 predicted and measured rod internal pressure at high burnup conditions.

this case, the internal pressure is consistently underpredicted for the unpressurized rods. For the pressurized rods the predicted internal pressure consistently exceeds the measured value similar to the trend for low burnup conditions. On Figure 55, the fractional model error is plotted versus fuel rod average linear heat rating. In this case, the relative error decreases with increasing average linear heat rate.

The results shown on Figures 54 and 55, indicate that the internal pressure behavior for the unpressurized rods as a function of burnup is different from that of the pressurized rods. In any case, the apparent reduction in gas communication shown in Figure 52 does not appear to occur for high burnup conditions. This finding further indicates that changes in the calculation of crack volumes, gap volumes, dish volumes, and fission gas release are required to produce similar trends for both pressurized and unpressurized rods as a function of burnup.

At high burnup conditions, trends similar to the low burnup trends were observed when fractional model error was plotted versus plenum void volume and cold gap width.

5.2.3 Deformation Models. The capability of FRAPCON-1 to predict the thermal conditions of the fuel rod is strongly influenced by the predicted pellet-cladding gap. Whether the fuel rod is experiencing open, soft, or hard gap closure conditions directly affects the gap conductance model. Assessment of the deformation models was performed in three parts. First, code-to-data comparisons were used to determine how well FRAPCON-1 predicts the onset of pellet-cladding gap closure. Only beginning of life data were used to eliminate the effects of fuel densification and swelling, cladding irradiation growth, pellet-cladding interaction (PCI), and creep cladding collapse. Second, and third, fuel and cladding deformation predictions were compared with experimental data obtained throughout the rod lifetime. The following section discusses the results from these three studies.

5.2.3.1 Gap Closure Conditions—Figure 56 shows measured versus predicted heat rating corresponding to the onset of pellet-cladding gap closure for about 90 instrumented test rods. The data sample represents a wide range in geometry, design, and instrumentation. The measurement values correspond to an observed departure of the cladding strain response from linear thermal expansion during startup power ramps. The predicted values represent closure of the thermal, as opposed to the structural gap. Physically, the onset of thermal gap closure corresponds to initial, soft contact between the cladding and the cracked fuel pellet, prior to hard (structural) gap closure, which is attained at higher power levels.

Generally, the onset of thermal gap closure is predicted to occur within the range of the measured values. Predicted gap closure heat rating ranges from 11 to 41 kW/m and measured heat rating ranges from about 0 to 52 kW/m. The standard deviation between the measured and calculated values is 11.4 kW/m. The best agreement between the code calculation and the data appears between 20 and 25 kW/m. This range brackets typical commercial reactor operating power levels.

The fractional model error in predicted gap closure heat rating is plotted against gap size in Figure 57. (Gap sizes are reported as percentages of the cold pellet radius.) A general tendency to overpredict gap closure heat rating is seen for gap sizes less than 1% and a general tendency to underpredict when greater than 2%. Also, the average overprediction at approximately 0.5% is much greater than at other gap sizes. By coincidence, the fuel pellet relocation model has a transition point at 0.5% gap size. Above 0.5%, the pellet geometry is adjusted outward to account for fuel cracking. Below 0.5%, no adjustment is made. Figure 57 indicates the relocation model needs adjustment for modeling rods with gap sizes less than 0.5%.

No trend in fractional model error was observed regarding fuel density and temperature. These same bulk fuel parameters did not exhibit an identifiable influence previously.[66]

5.2.3.2 Fuel Deformation—Performance of the fuel deformation model was evaluated from results of fuel thermal expansion and permanent fuel stack deformation code-to-data comparisons.

5.2.3.2.1 Fuel Thermal Expansion—The measured versus predicted fuel stack axial expansion relative to cladding length at hot steady conditions is shown on Figure 58. These data were obtained during startup power ranges from 20 rods representing both dished and flat pellet design.

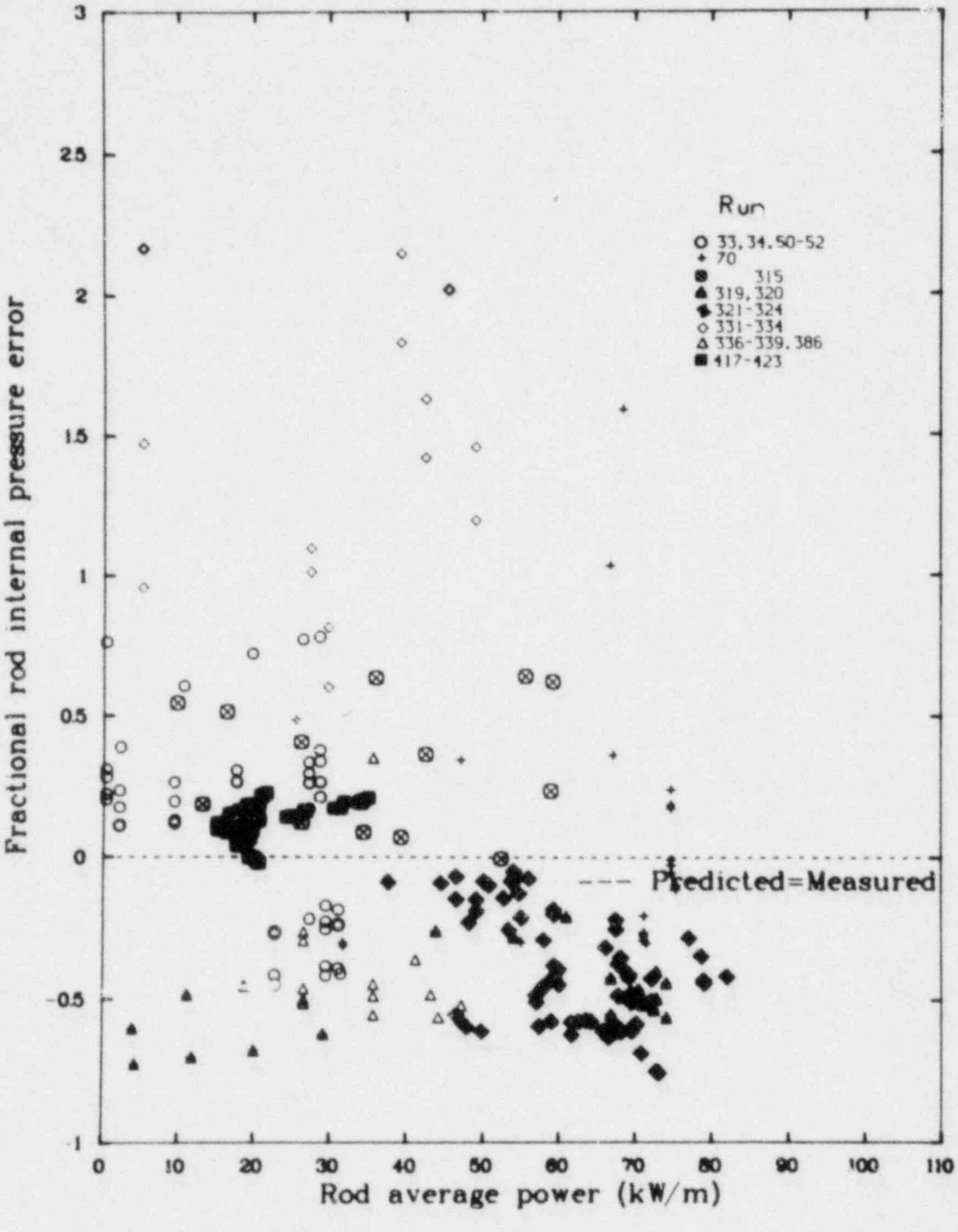

Figure 55. Effect of average heat rating on FRAPCON-1 internal pressure error at high burnup conditions.

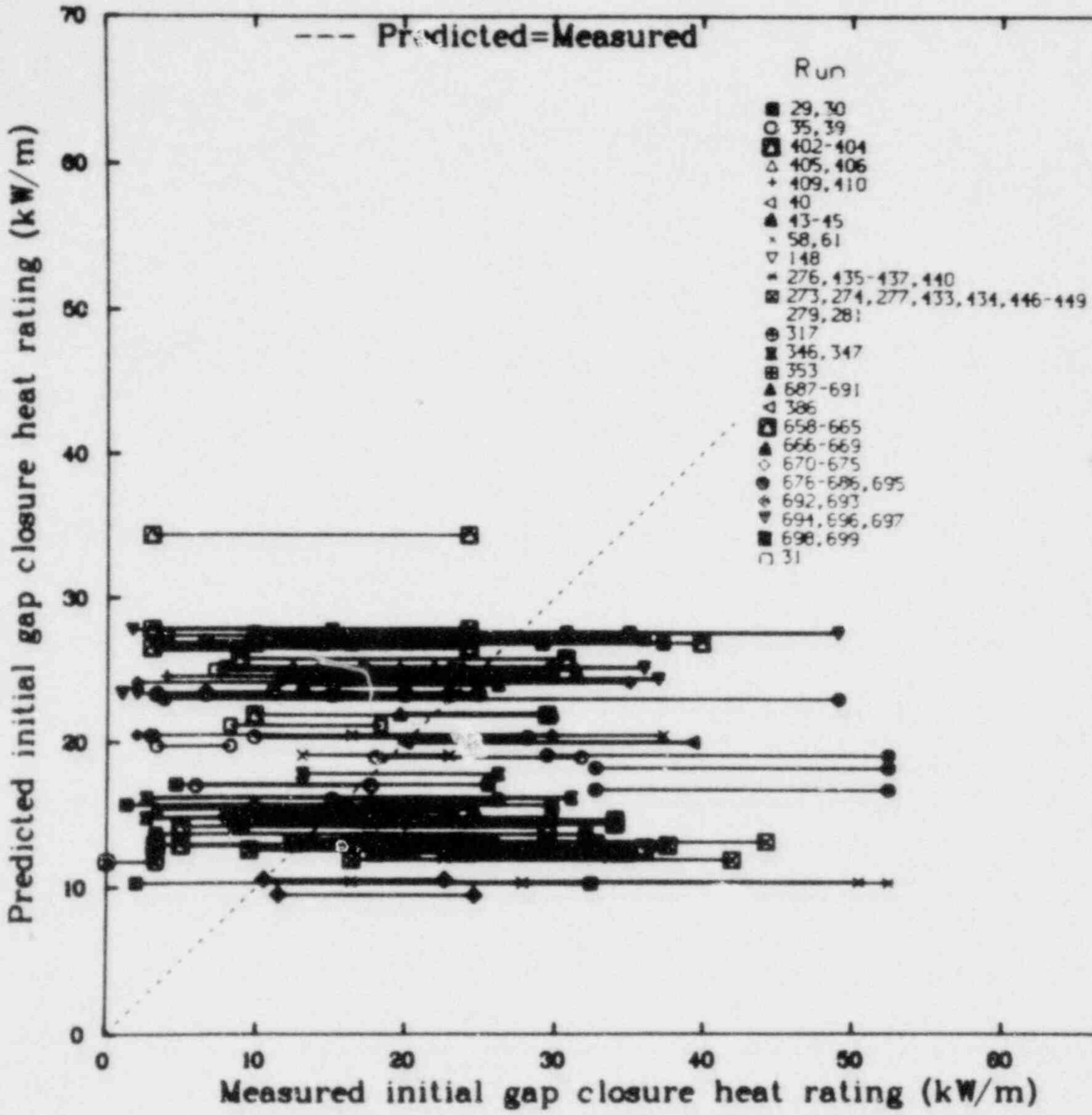

Figure 56. Comparison of FRAPCON-1 predicted and measured gap closure heat rating.

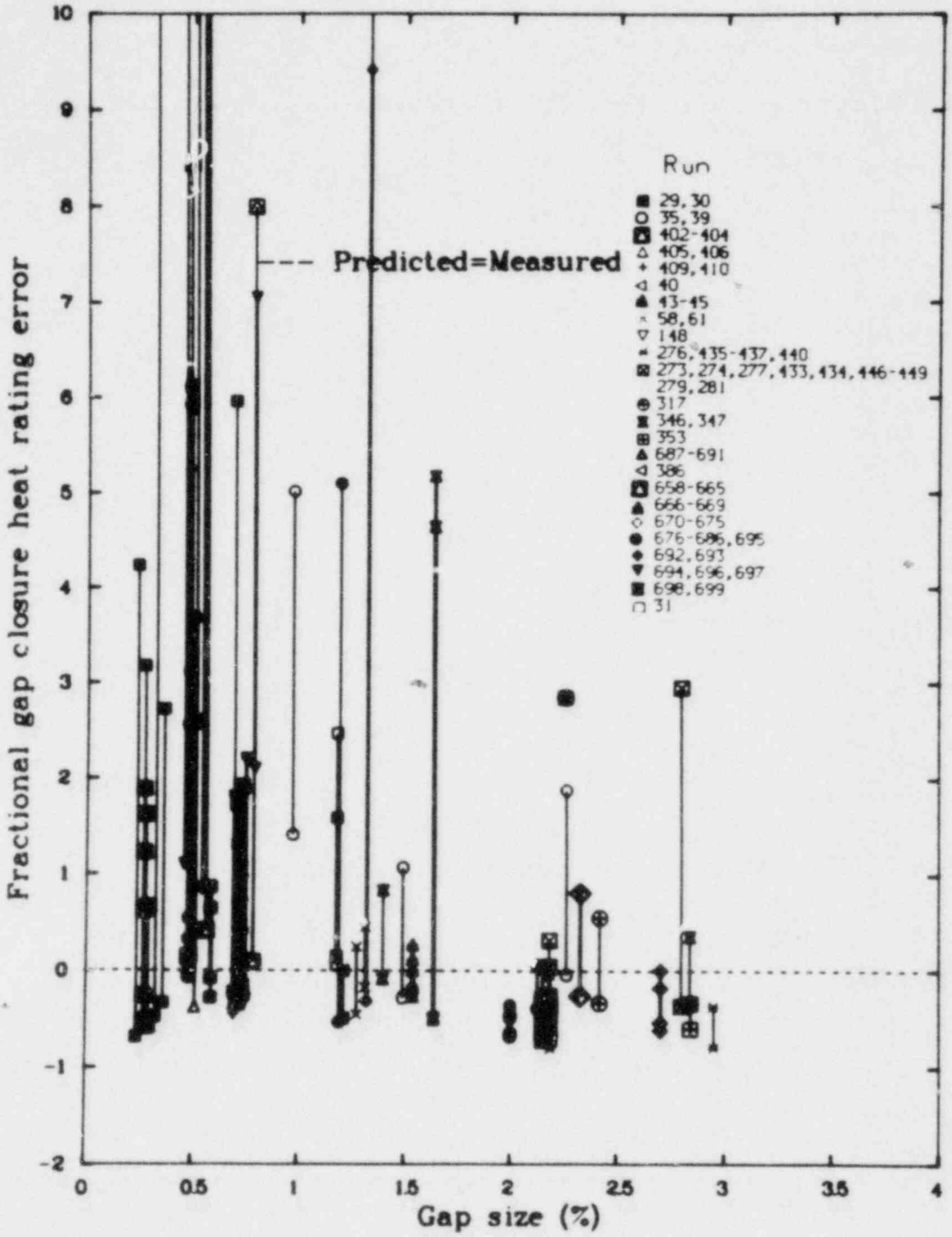

Figure 57. Effect of gap size on FRAPCON-1 gap closure heat rating error.

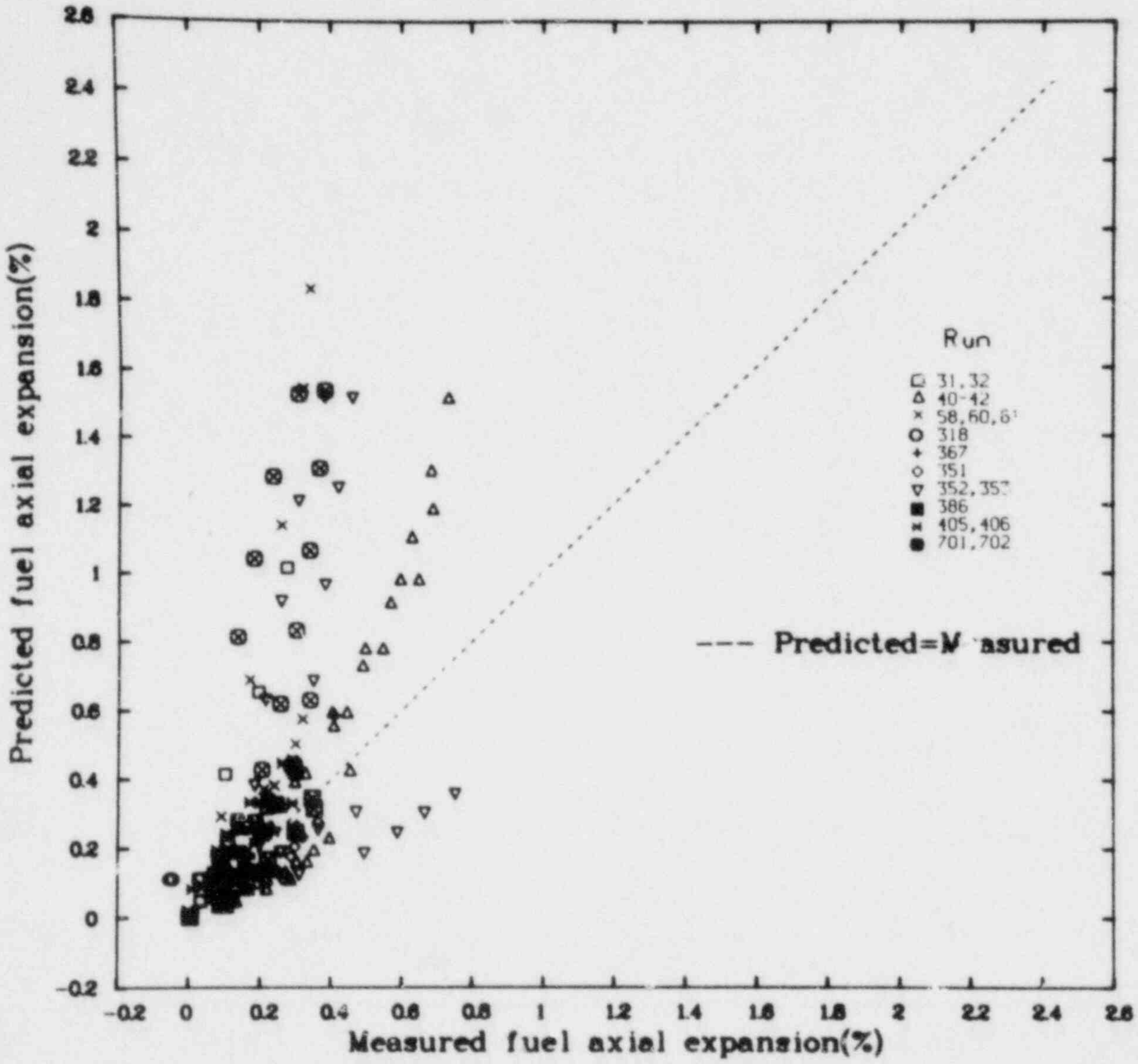

Figure 58. Comparison of FRAPCON-1 predicted and measured fuel axial expansion during heatup.

The measurements and predictions are in close agreement for strains less than 0.3%, when the pellet-cladding gap is usually open. Above 0.3% strain, when pellet-cladding interaction (PCI) occurs, FRAPCON-1 overpredicts the measured axial expansion. This trend indicates that the fuel and cladding are in solid contact and the cladding is restraining axial fuel stack deformation, or the fuel pellets are slipping over the cladding inner surface thereby reducing the measured fuel stack strain measurements. Neither of these mechanisms is modeled in FRAPCON-1. The standard deviation between measurement and prediction is 0.23% of the stack length for measured strain less than 0.3% and 0.56% of the fuel stack length for measured strain greater than 0.3%.

Figures 59 and 60 show the fractional model error for predicted fuel thermal expansion against average stack temperature and as-built gap size, respectively. These results indicate that relative error is not a function of temperature. However, Figure 60 indicates that overpredictions correspond mainly to rods with small gap sizes and the fractional model error decreases with increasing gap size. This overprediction trend complements the results shown in Figure 58. That is, at low strain levels before PCI is attained, the agreement is good. Figure 60 shows that better code-to-data agreement is observed for rods with large gap. For large gaps PCI onset is not attained until a higher rod power level is achieved.

5.2.3.2.2 Fuel Stack Permanent Deformation—The principal mechanisms affecting fuel stack permanent deformation include densification, swelling, and compression. FRAPCON-1 only accounts for the first two mechanisms. Present code modeling first allows fuel pellet dimension reductions resulting from densification. When maximum densification has been attained at about 2.5×10^5 MWs/kg, FRAPCON-1 then increases the pellet dimensions resulting from fuel swelling. The data base used to assess the fuel stack permanent deformation represents about 100 rods. Most of the data were obtained when fuel burnup was less than 2.5×10^5 MWs/kg. Therefore, predicted fuel stack permanent deformations usually reflect only densification effects.

Figure 61 presents the measured and predicted permanent fuel stack length changes. FRAPCON-1 generally underpredicts the amount of permanent deformation, probably due to not modeling fuel compression and slippage effects. As expected, very few rods exhibited a net positive length change. The majority of the changes were negative, with the greatest negative changes being observed for rods with unstable fuel types. Overall, the standard deviation between the measured and calculated deformation values is 0.45% of the fuel stack length.

The fractional model error of the permanent deformation prediction is shown on Figures 62 and 63 as functions of fuel density and burnup. In both figures, the relative error is randomly distributed over the measured ranges for density and burnup.

5.2.3.3 Cladding Deformation—The capability to accurately predict cladding mechanical behavior is important because (a) cladding integrity is the first line of defense toward maintaining reactor integrity, and (b) changes in cladding hoop strain directly influence the pellet-cladding gap size, thereby providing feedback to the thermal model calculation (that is, fuel temperature and stored energy predictions).

Figure 64 compares the measured and predicted permanent cladding hoop strain for 130 fuel rods. The data set is dominated by negative strain values, indicating that hard gap closure was not prevalent. The few rods which have small gap sizes, extended burnup, or both, did exhibit a net positive strain. FRAPCON-1 generally predicts the negative strain trend well, but overestimates the extent of creepdown even though gas release, internal pressure, and fuel temperatures are generally overestimated. The overpredicted creep rate may result from two sources. First, the fast flux level is often undocumented and a default value is used. The default value may be too high, or the influence of the fast flux term itself may be too high, or both. Second, the operating power level of these rods is usually low enough to avoid hard gap closure but high enough to attain soft gap closure. For this case, FRAPCON-1 does not consider PCI-induced stress upon the cladding, even though instrumented rod data suggest the contrary. For the few cases where positive strain was measured, FRAPCON-1 did not predict the observed cladding behavior trends. The permanent deformation was underpredicted, indicating again the lack of modeling pellet-cladding interaction during soft gap closure. Overall, the standard

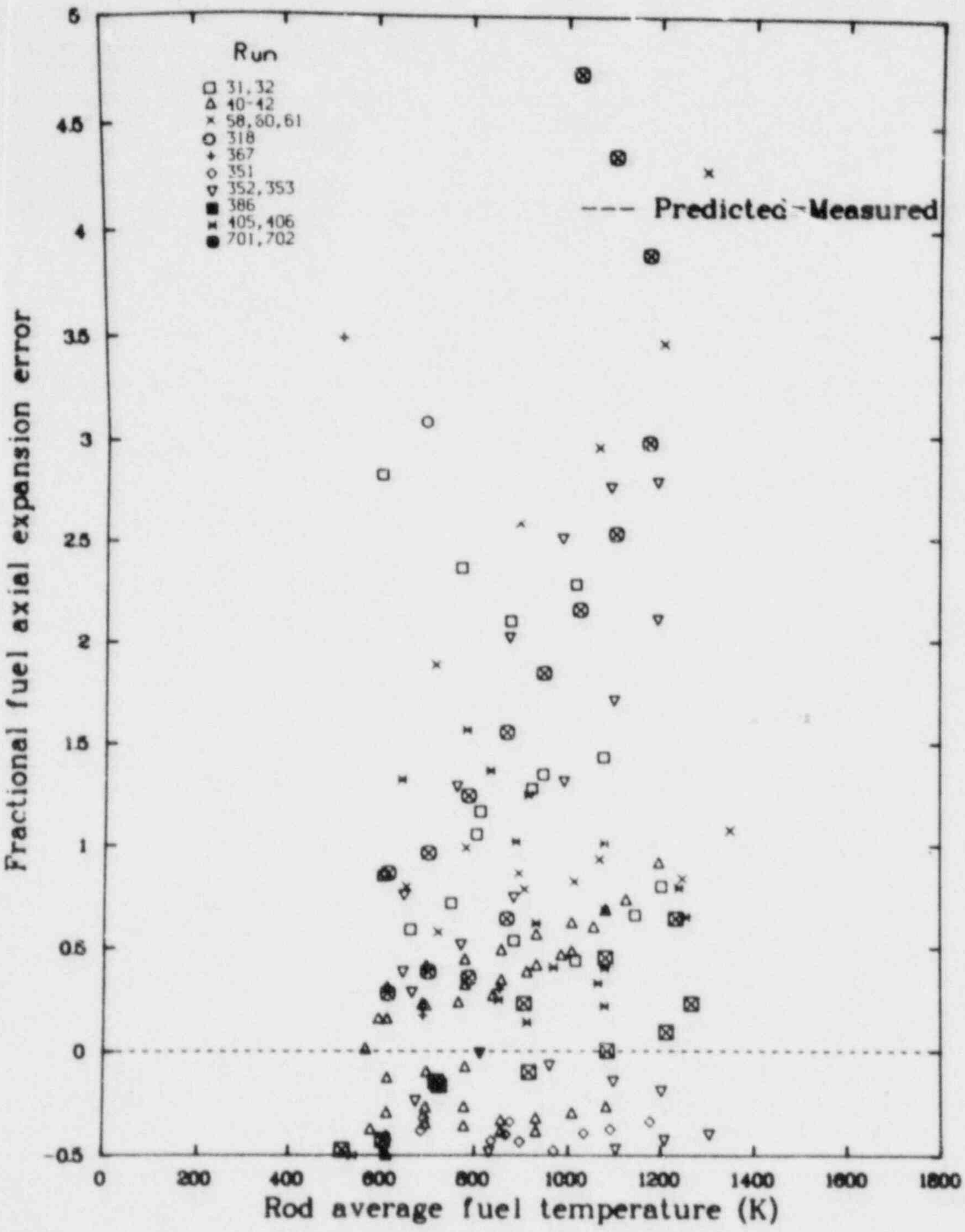

Figure 59. Effect of average fuel temperature on FRAPCON-1 fuel axial expansion error during heatup.

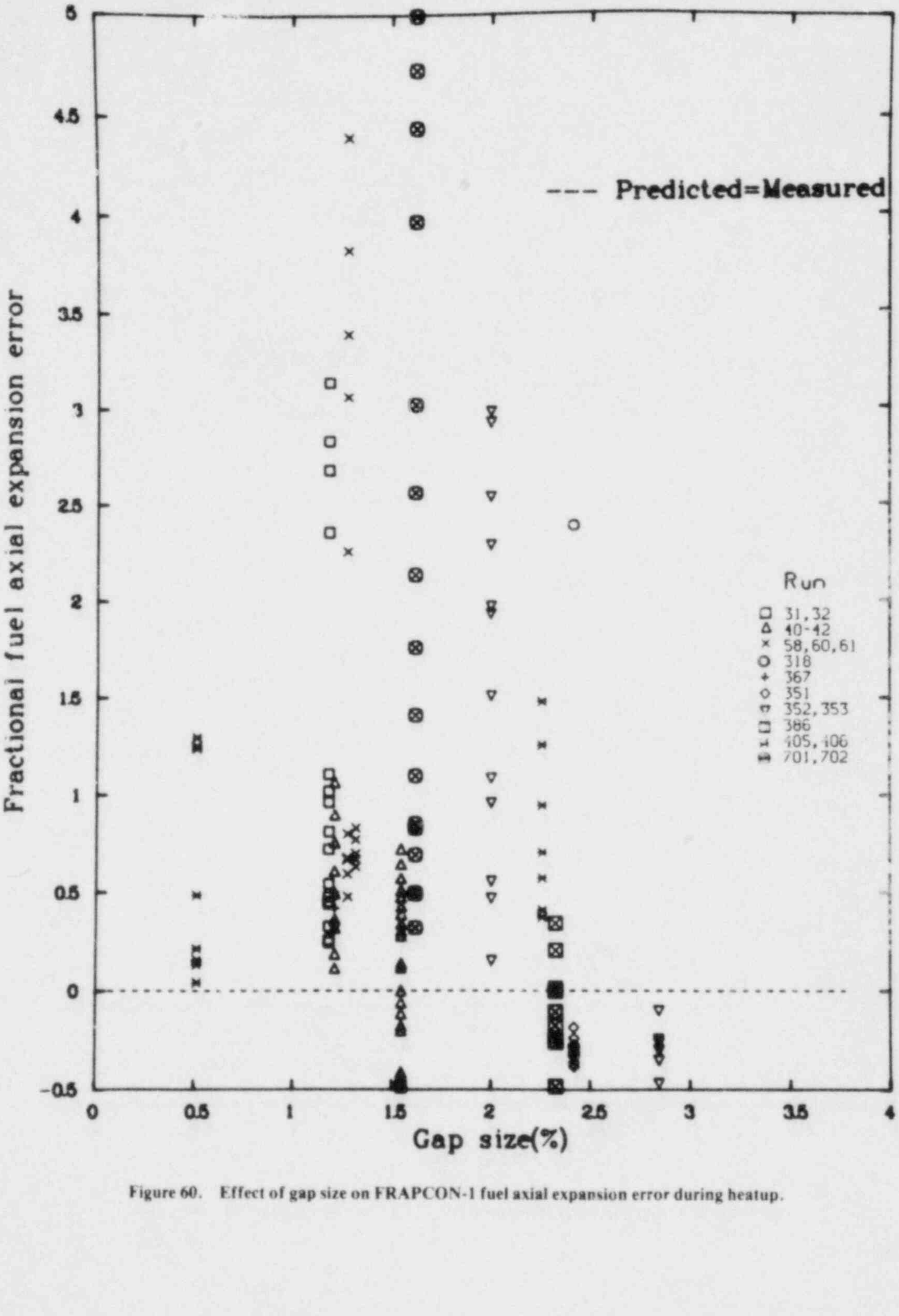

Figure 60. Effect of gap size on FRAPCON-1 fuel axial expansion error during heatup.

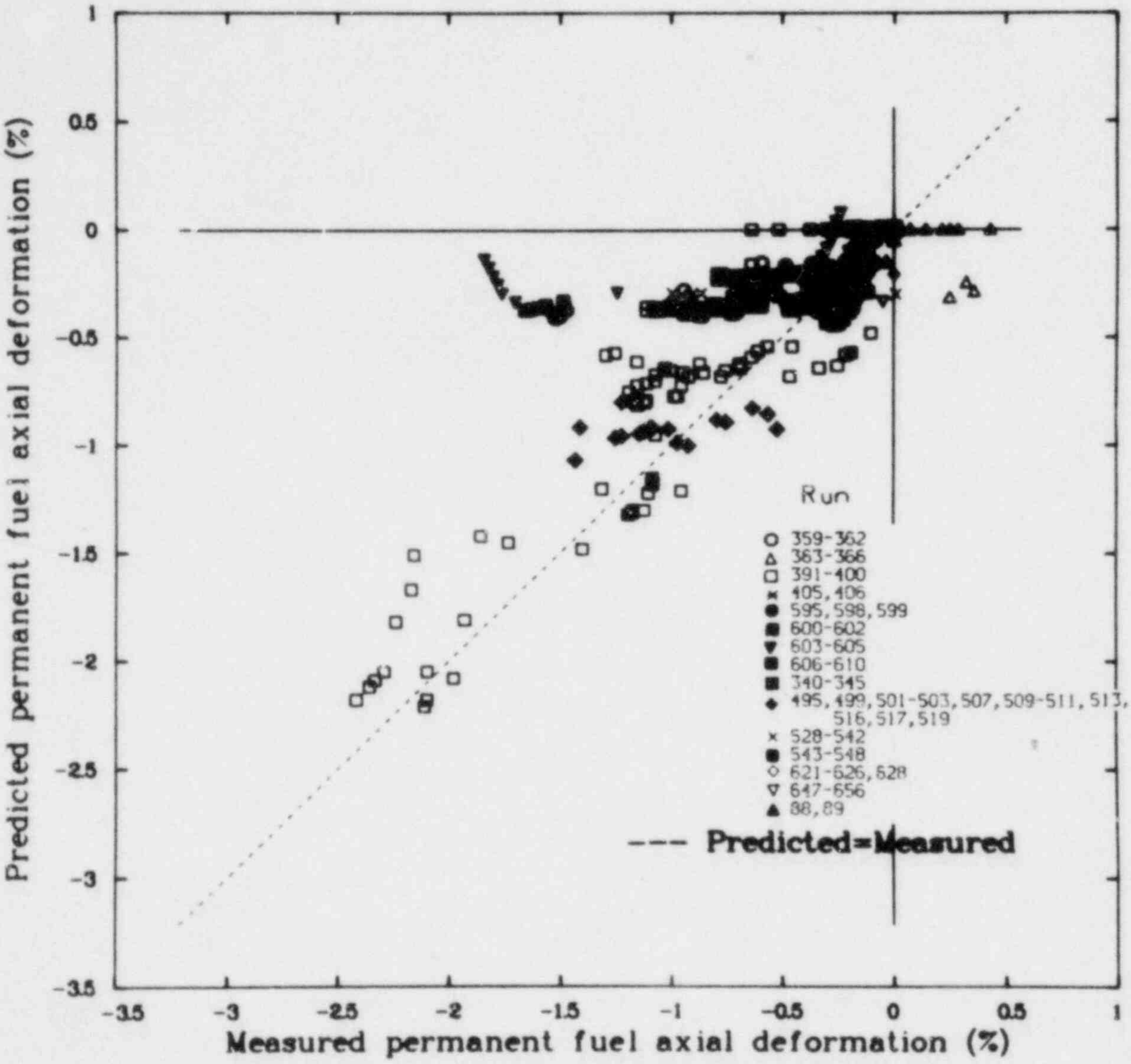

Figure 61. Comparison of FRAPCON-1 predicted and measured permanent fuel axial deformation.

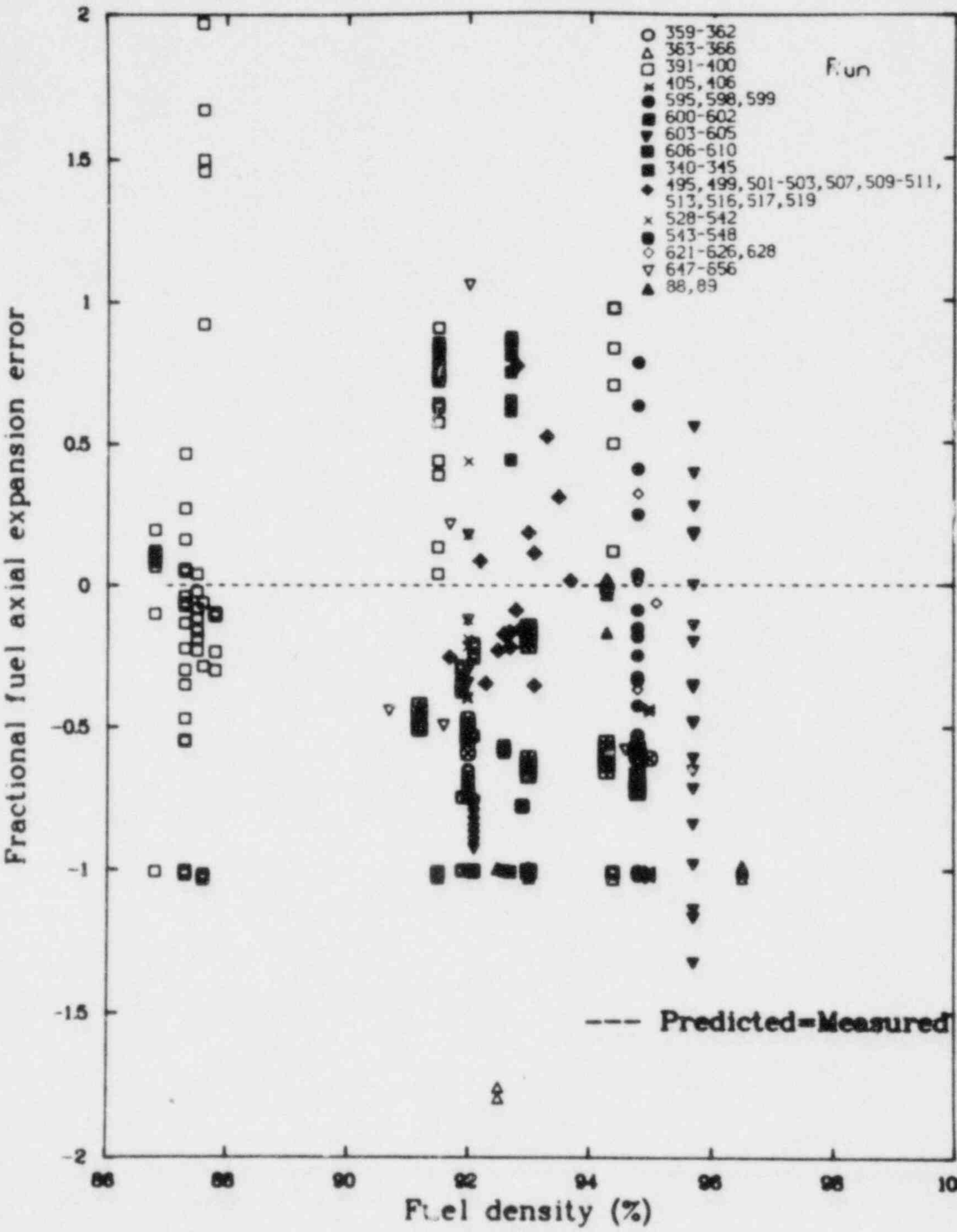

Figure 62. Effect of density on FRAPCON-1 permanent fuel axial deformation error.

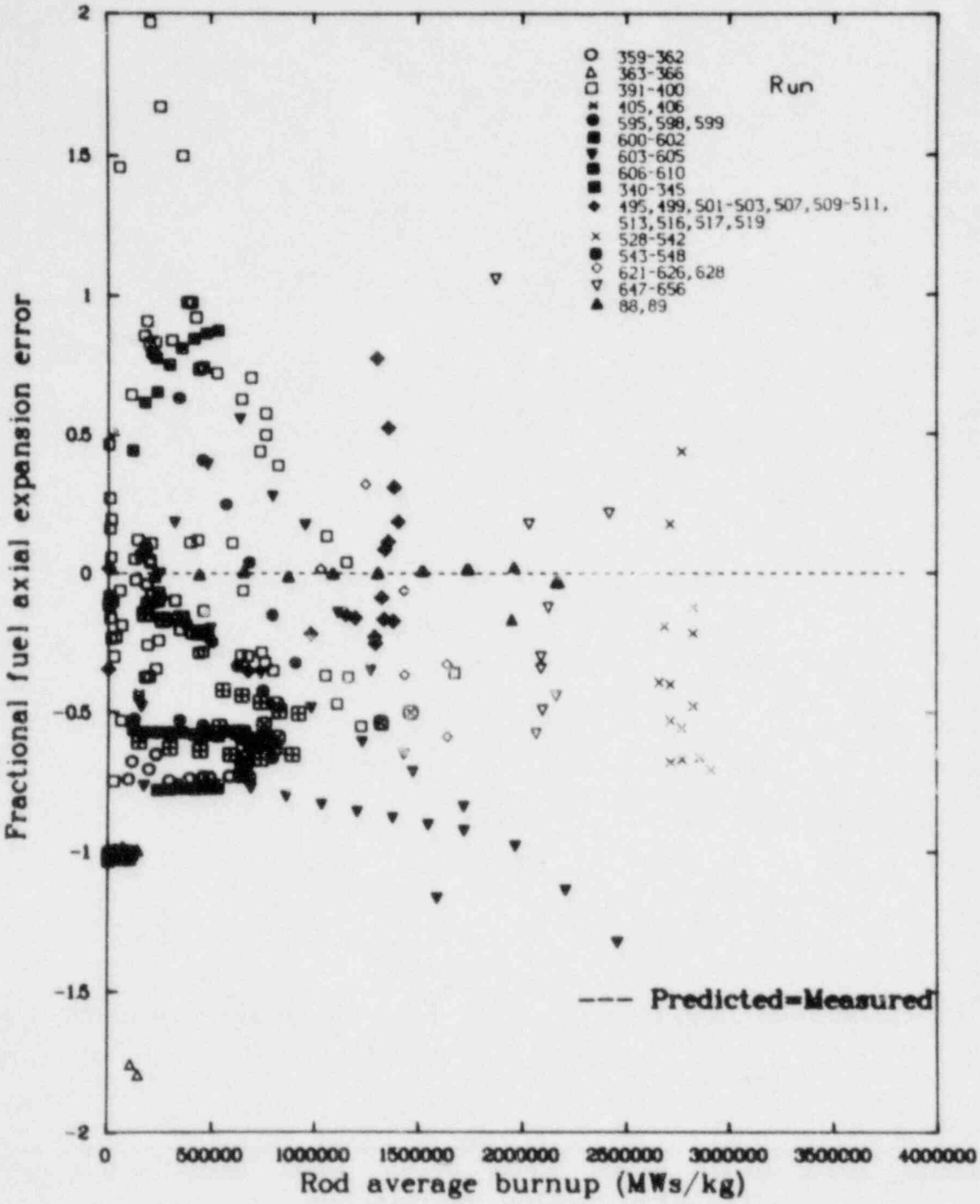

Figure 63. Effect of burnup on FRAPCON-1 permanent fuel axial deformation error.

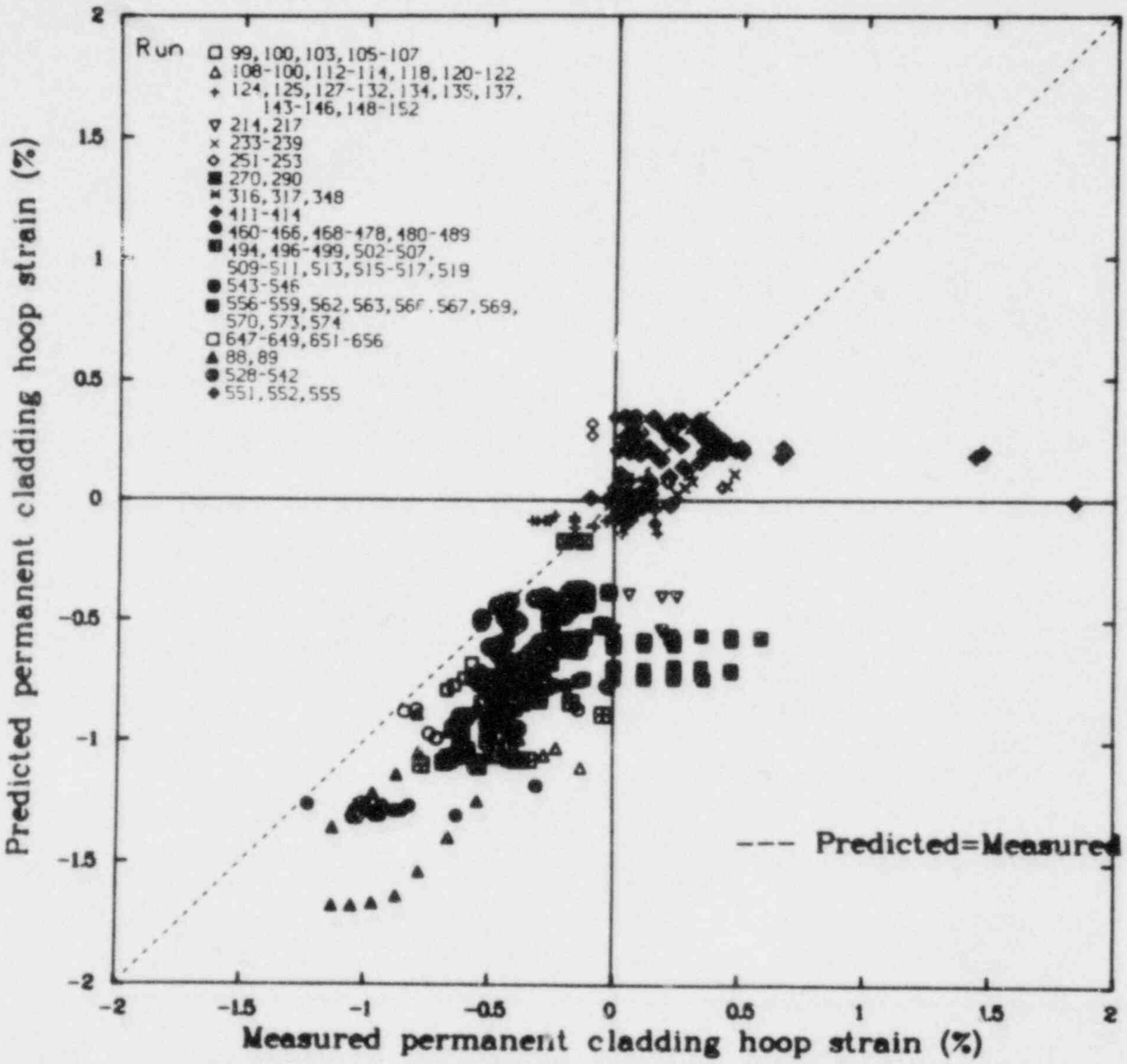

Figure 64. Comparison of FRAPCON-1 predicted and measured permanent cladding hoop strain.

deviation between measured and predicted permanent hoop strain is about 0.5% of the cladding diameter.

The overprediction of cladding permanent hoop strain is shown on Figure 65, which presents fractional deformation model error against as-built gap size. Hoop strain is consistently overestimated when gap size is greater than about 2%. These particular rods are not predicted to experience hard gap closure at heat ratings below 50 to 60 kW/m. The underpredictions correspond to smaller gap rods. Hard gap closure is generally not predicted for these cases either, but the data reflect some PCI during soft gap closure. Overpredictions for the very small gap sizes correspond to cases where hard gap closure was predicted. The influence of PCI was overestimated because the fuel pellet was not allowed to deform when experiencing compression.

The measured and predicted permanent cladding axial strain is shown on Figure 66. The calculations are clearly divided into two groups—underpredictions and overpredictions. The underpredictions represent the larger gap rods which do not attain hard gap closure, but are affected by PCI stress during soft gap closure. The overpredictions represent the smaller gap rods which do attain hard gap closure; FRAPCON-1 neglects the moderating effects of pellet compression. These trends are consistent with those observed in the hoop strain comparisons. The standard deviation between measured and predicted permanent axial strain is about 0.2% of the rod active length.

5.2.4 Cladding Corrosion Models. Two types of data comparisons were made to assess FRAPCON-1 cladding corrosion models; cladding surface corrosion and hydrogen pickup.

5.2.4.1 Corrosion—The cladding-water reaction rate correlations currently used at high cladding temperatures typical of departure from nucleate boiling conditions, are sensitive to the initial zirconium oxide layer thickness. Since these correlations are used in transient fuel rod analysis programs, with the initial zirconium oxide layer thickness supplied by a steady state code, assessment of the ability of FRAPCON-1 to predict the initial zirconium oxide layer thickness is important.

The FRAPCON-1 corrosion model is dependent on coolant conditions and cladding surface temperature. The effect on corrosion rates due to differences in system temperature and oxygen availability is controlled by internal code logic for calculation of in-pile corrosion rates. Figure 67 shows measured versus predicted cladding surface corrosion thickness for several experiments representing both BWR and PWR system conditions. The uncertainty in the predictions accounts for preirradiation surface treatment effects which typically result in as-built corrosion layer thicknesses between 0 and 2.5 μm. In general, the zirconium oxide layer thicknesses are underpredicted and the standard deviation in characterizing the corrosion layer thickness is 5.8 μm. This underprediction trend may be due to grid-induced flow patterns or programmed changes in system chemistry which would affect the measurements and are not considered by the model. Also, since postirradiation examination measurements are more frequently made at locations exhibiting some departure from an expected effect, some of the available measurements are probably not indicative of the uniform corrosion mechanisms considered by the model. This lack of corrosion consistency is further demonstrated on Figures 68 and 69, where the model error shows no clear relationship to either time at temperature or system inlet temperature.

5.2.4.2 Hydrogen Pickup—Pickup of hydrogen by the cladding normally occurs as a result of both the external oxidation process and the internal outgassing of small amounts of moisture from the fuel. Experimental results indicate that a fuel rod hydrogen concentration below about 200 ppm (typical for commercial rods) has very little effect on cladding mechanical properties. However, fuel rods with initial internal hydrogen contamination that have been operated under normal conditions, show areas of high hydrogen concentration (∿600 ppm) and low ductility near failure locations.

Figure 70 shows measured versus predicted cladding hydrogen concentration for essentially the same fuel rods used in the corrosion model assessment. In this case, the uncertainty in the predictions accounts for up to 30 ppm hydrogen content in the as-built condition. In general, the hydrogen concentration is underpredicted and the standard deviation in characterizing the hydrogen

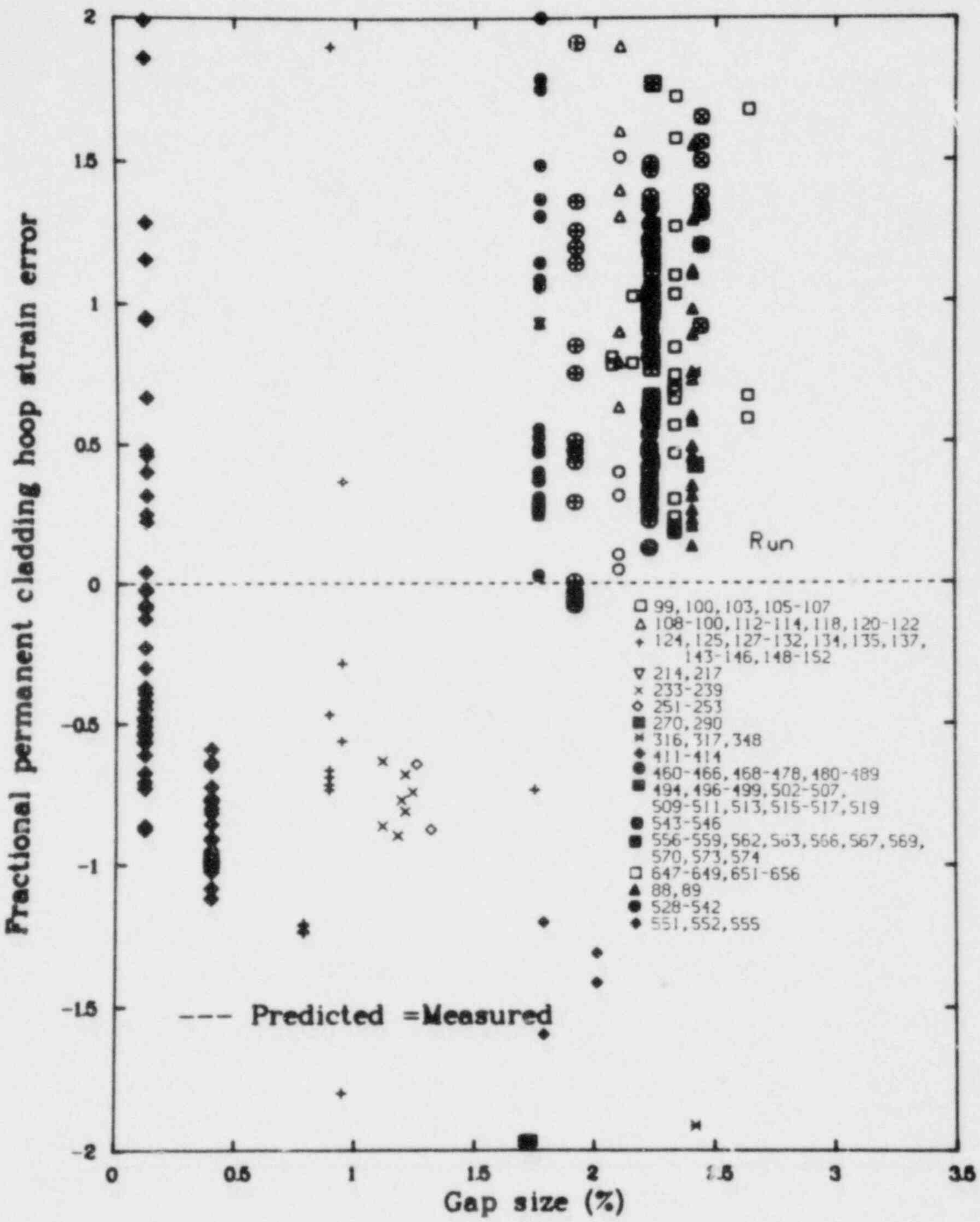

Figure 65. Effect of gap size on FRAPCON-1 permanent cladding hoop strain error.

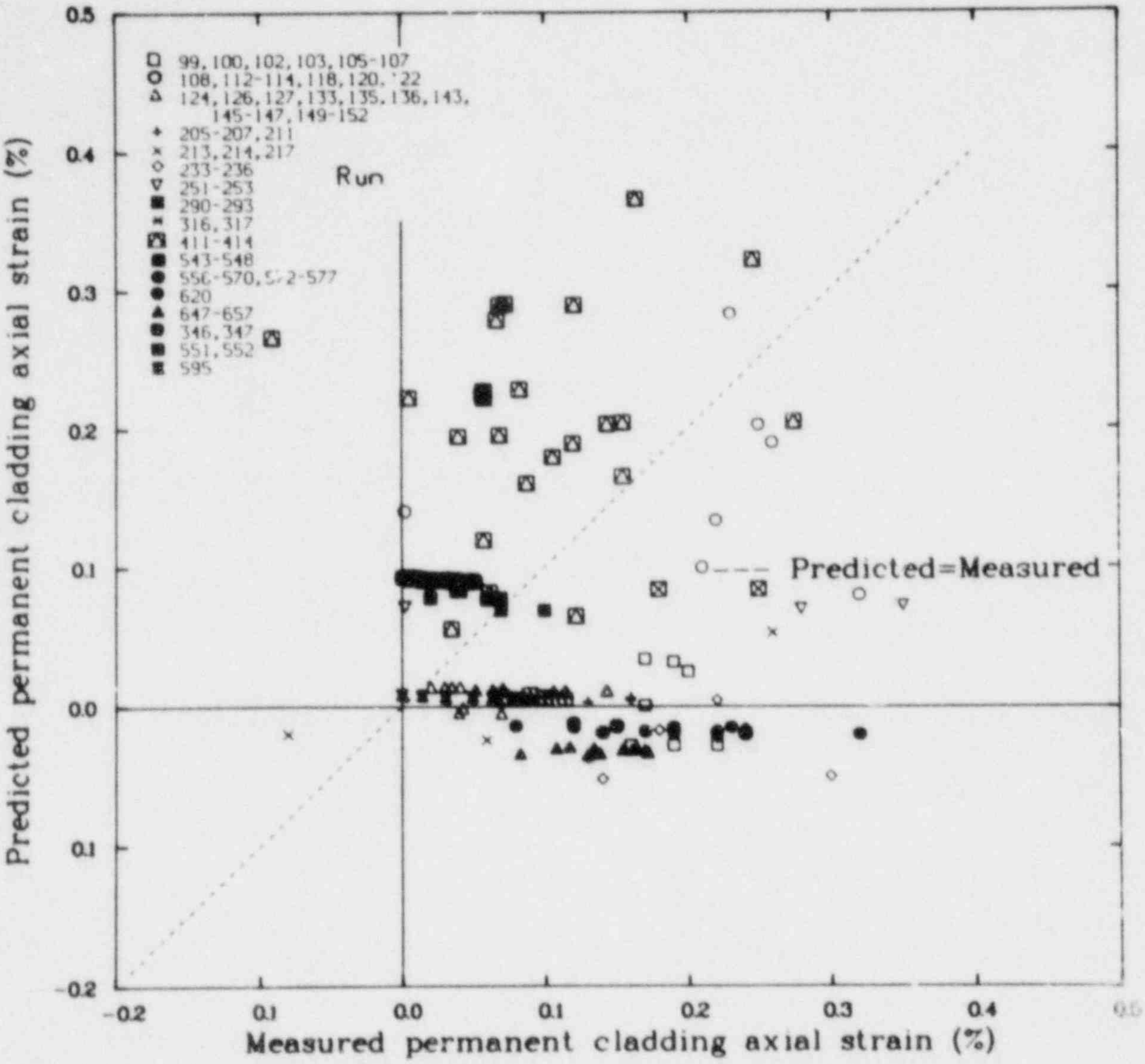

Figure 66. Comparison of FRAPCON-1 predicted and measured permanent cladding axial strain.

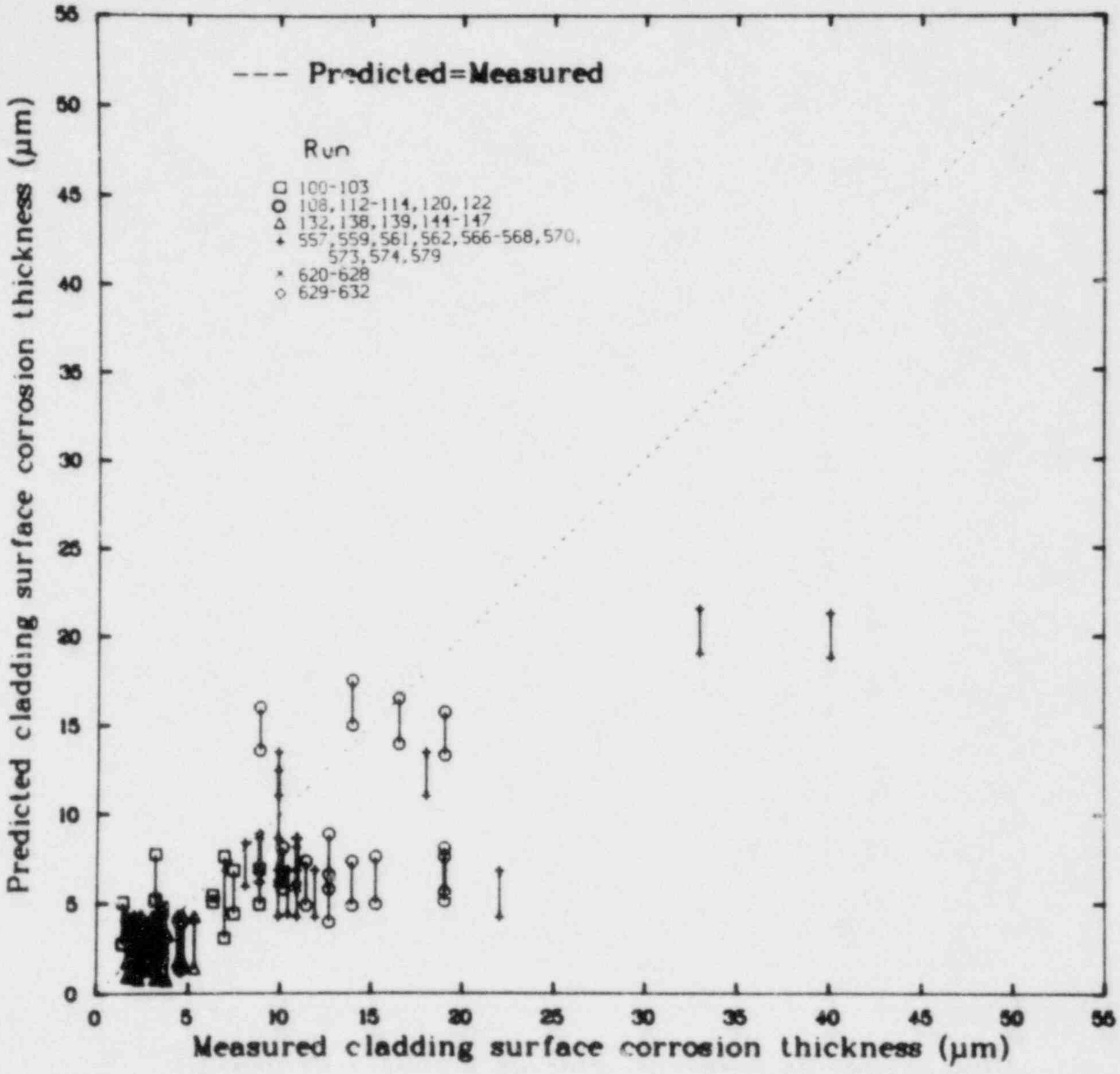

Figure 67. Comparison of FRAPCON-1 predicted and measured rod surface corrosion buildup.

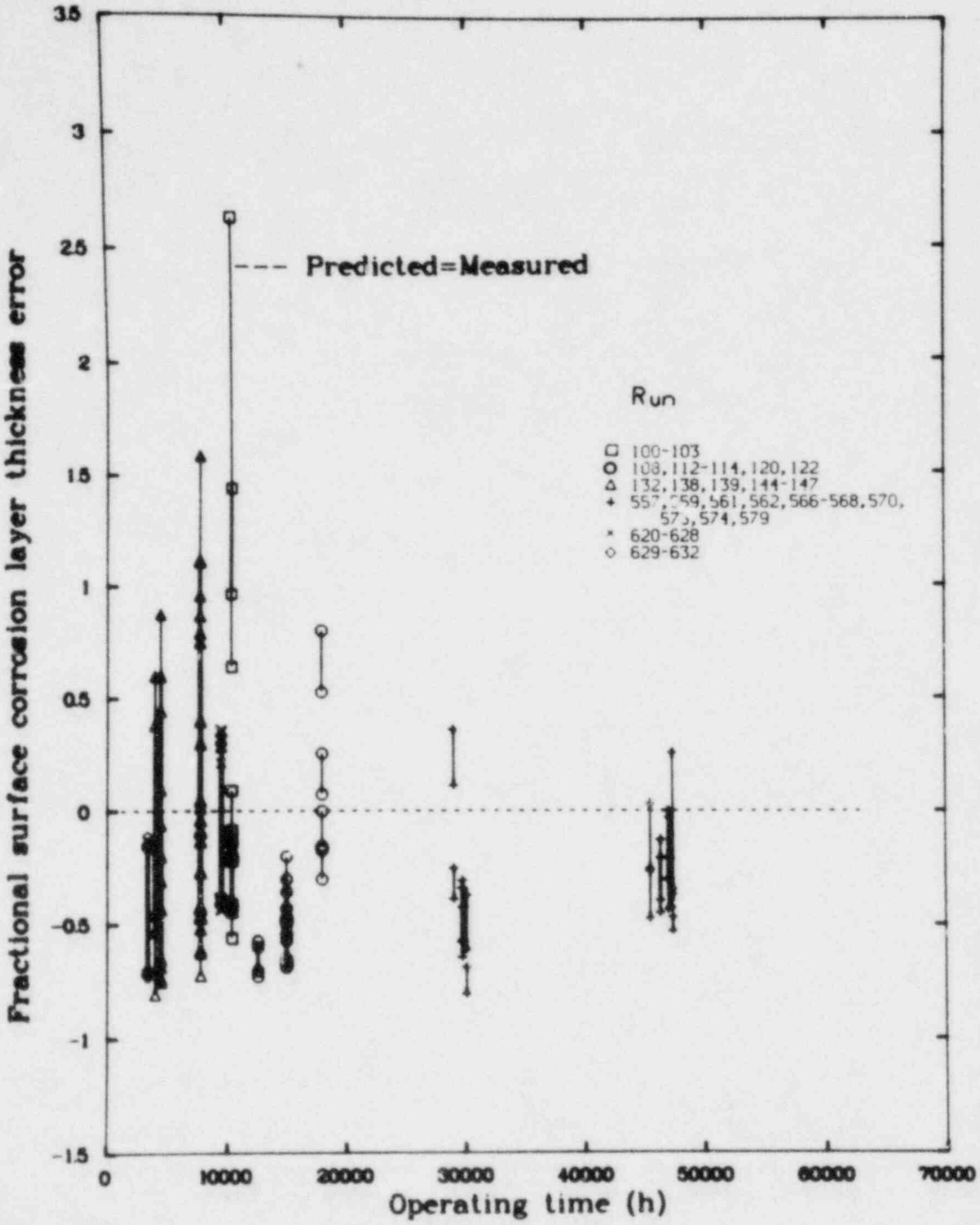

Figure 68. Effect of operating time on FRAPCON-2 error in rod surface corrosion buildup.

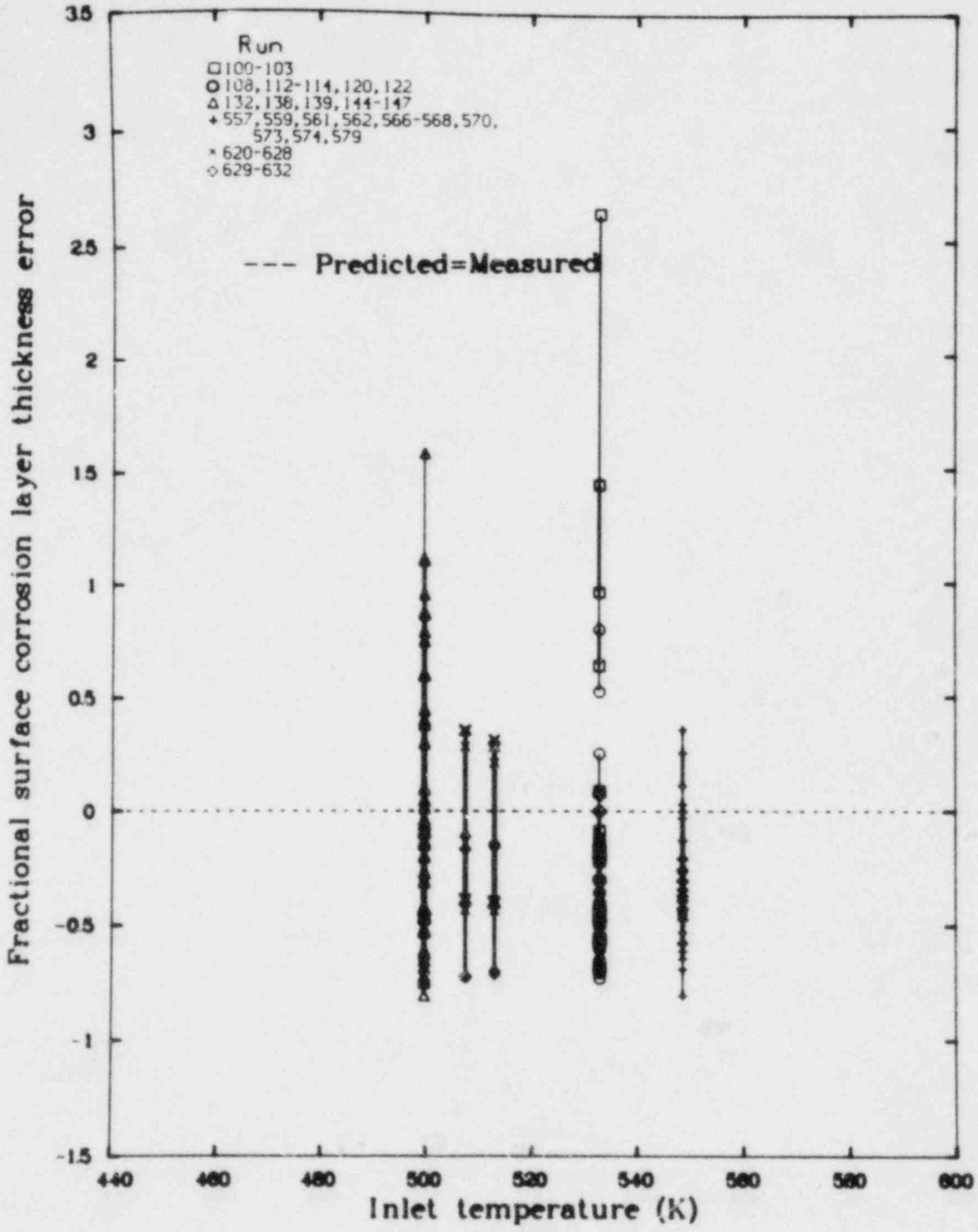

Figure 69. Effect of system inlet temperature on FRAPCON-1 error in rod surface corrosion buildup.

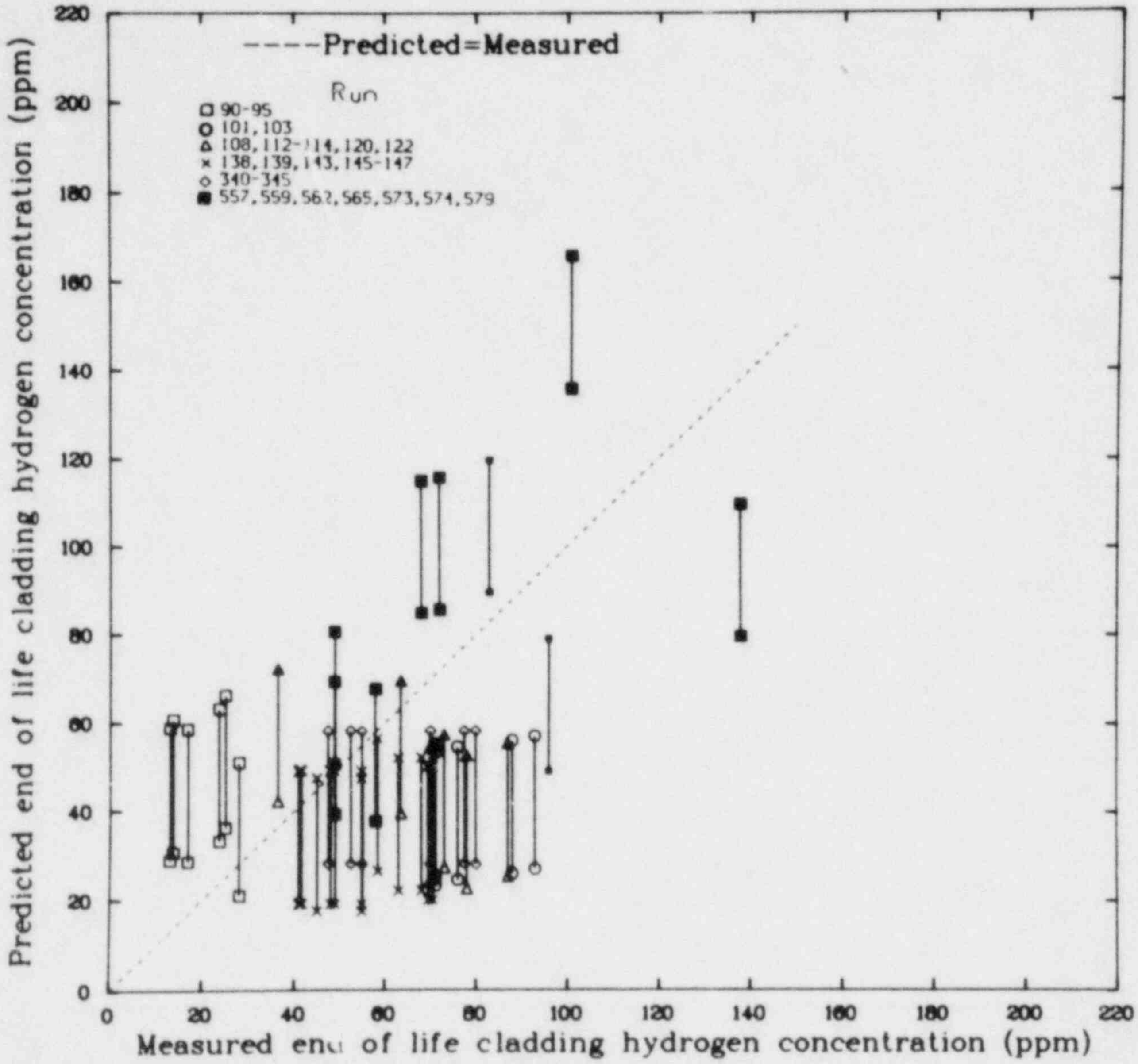

Figure 70. Comparison of FRAPCON-1 predicted and measured cladding hydrogen concentration.

concentration is 37 ppm. Figures 71 and 72 show the model error versus time at temperature and initial fuel moisture content, respectively. The highest overpredictions reflect a combination of relatively high initial internal moisture content and relatively low irradiation time. This overprediction trend is expected since the hydrogen pickup model is based on the assumption that the internal hydrogen concentration is essentially instantaneously available to the cladding interior. Lack of fabrication details required the use of a default initial hydrogen concentration of 5 ppm. Nonetheless, adequate model capability is indicated for both low and moderate initial hydrogen concentrations up to 15 ppm.

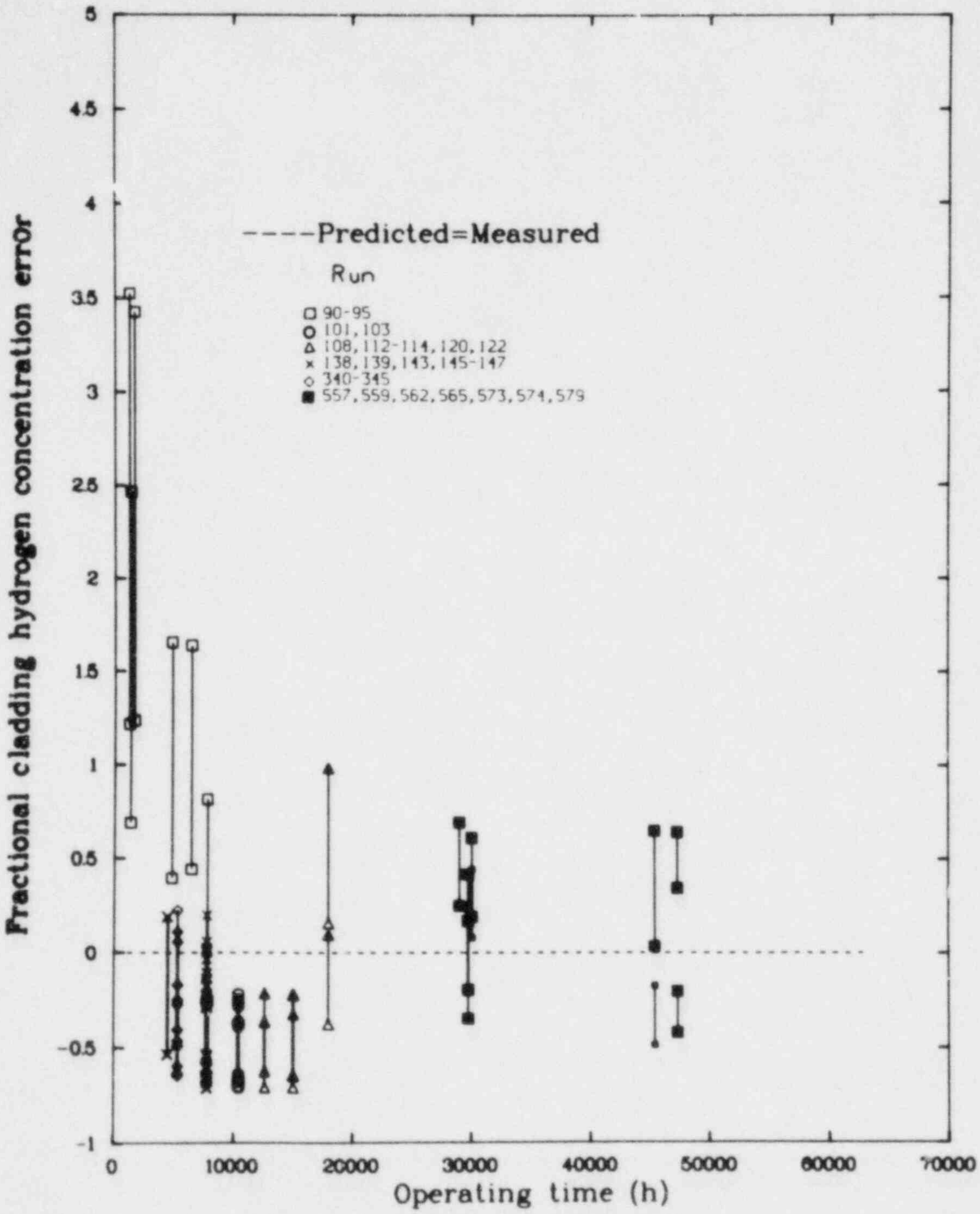

Figure 71. Effect of operating time on FRAPCON-1 cladding hydrogen concentration error.

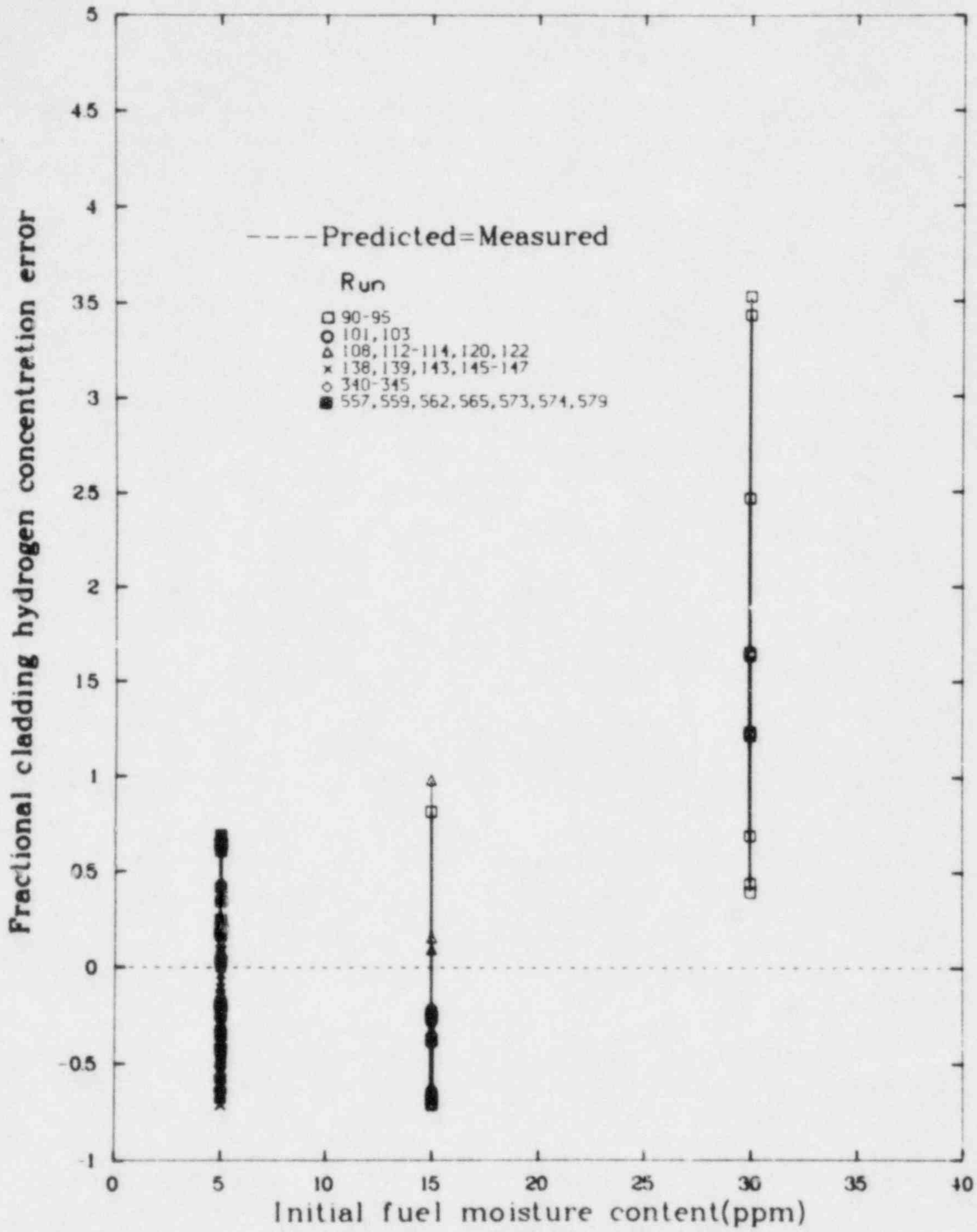

Figure 72. Effect of ... fuel moisture concentration on FRAPCON-1 cladding hydrogen concentration error.

6. CONCLUSIONS

FRAPCON-1 exhibits better calculational accuracy than the previously assessed FRAP-S3 code. The improvement is mainly due to two features, (a) the incorporation of a permanent fuel restructuring model, and (b) an update of the fission gas production model.

Results obtained from this assessment study are summarized as follows.

1. Fuel centerline temperature is generally overpredicted for rods with low density (<95% TD) fuel, and underpredicted for rods with high density (>95% TD) fuel. Better agreement is noted for (a) unpressurized rods rather than pressurized rods, (b) pellet-cladding gap sizes less than 2% of the pellet diameter, and (c) power levels greater than 45 kW/m.

2. The predicted radial temperature profile is too steep in the inner part of the fuel pellet, and too flat near the pellet surface.

3. FRAPCON-1 accurately predicts gap conductance during hard gap closure conditions, but overpredicts the measured value during soft gap closure.

4. Fission gas release fraction is generally overpredicted when the measurement of the fraction is less than about 20%. Although this model includes cumulative burnup effects, a burnup enhancement factor is required.

5. Rod internal pressure is generally overpredicted, especially when the rod power level is high or when cladding collapse onto the fuel stack has occurred.

6. The onset of thermal gap closure is predicted to occur within the range of measured values. Best agreement between FRAPCON-1 and the data appears between 20 and 25 kW/m. FRAPCON-1 overpredicts the amount of relocation for large gap sizes (>2%) and underpredicts for small gap sizes (<2%). An upper limit on the amount of relocation should be imposed.

7. Fuel thermal expansion measurements and predictions are in close agreement for strains less than 0.3%, when the pellet-cladding gap is usually open. Above 0.3% strain, when the pellet-cladding gap is closed, FRAPCON-1 overestimates the measured expansion.

8. For open or soft gap closure conditions, the extent of permanent fuel deformation is underestimated, probably due to the lack of a fuel compression model or fuel stack slippage effects.

9. FRAPCON-1 generally predicts negative cladding strain trends well, but overestimates the extent of creepdown, even though gas release, internal pressure, and temperature are probably overestimated.

10. Cladding corrosion and hydrogen uptake rates are slightly underpredicted.

The standard deviations between the measured and FRAPCON-1 predicted values are summarized on Table 4. For comparison, the FRAP-S3 standard deviations for the same data base are also given.

In general, FRAPCON-1 most accurately predicts the rod behavior when (a) the fuel rods are unpressurized, (b) fuel densities are greater than 94% (TD), (c) gap sizes are less than 2%, and (d) plenum volumes account for more than half of the total void volume.

The predictive capabilities of FRAPCON-1 can be improved by implementing the following recommendations. The sequence of these recommendations is the same order as was used in the Assessment Results section.

1. Thermal models

   (a) The effect of fuel densification on thermal conductivity should be incorporated.

   (b) The threshold temperature multiplication factor used in the fuel restructuring model should be parametrically evaluated.

TABLE 4. FRAPCON-1 VERSUS FRAP-S3 MODEL ASSESSMENT -- SUMMARY OF STANDARD DEVIATIONS BETWEEN MEASUREMENTS AND PREDICTIONS

Output Variable	Sample Size (Number of rods/ number of points)	Standard Deviation FRAPCON-1	Standard Deviation FRAP-S3
Fuel centerline temperature	32/274 (pressurized rods) 61/472 (unpressurized rods)	294 K 170 K	256 K 197 K
Released fission gas	145/145	15.9%	18.7% of generated gas
Rod internal pressure	20/330 (unpressurized rods) 28/285 (pressurized rods)	1.38 MPa 1.93 MPa	1.20 MPa 0.64 MPa
Gap closure heat rating	88/88	11.4 kW/m	12.3 kW/m
Axial fuel thermal expansion	18/160	0.37%	0.35% of stack length
Permanent fuel axial deformation	97/354	0.45%	0.45% of stack length
Permanent cladding hoop strain	154/358	0.47%	0.51%
Permanent cladding axial strain	96/119	0.15%	0.42% of active length
Cladding surface corrosion layer	40/69	5.8μm	5.8μm
Cladding hydrogen concentration	33/46	37.2 ppm	39.0 ppm
Gap conductance	17/112 (unpressurized rods) 20/115 (pressurized rods)	10821 $W/m^2 \cdot K$ 21200 $W/m^2 \cdot K$	9191 $W/m^2 \cdot K$ 21000$W/m^2 \cdot K$
Fuel off-centerline temperature	20/111 11/81	208 K --	-- 253 K

(c) The effective fuel conductivity model should be revised and parametrically evaluated to account for a nonuniform distribution of fuel cracks.

(d) The gas conductivity model should be modified to include pressure feedback effects on effective fuel conductivity and gap conductance.

2. Internal pressure models

(a) The effect of pellet relocation and cracking on void volume and temperature calculations should be improved.

(b) The effect of pellet relocation, cracking, and thermal expansion on gas communication should be investigated.

(c) The fission gas release model should include the effects of burnup and fuel cracking on gas release.

3. Rod deformation models

(a) For cold gap sizes greater than 2%, the amount of fuel pellet relocation should be limited. For gap sizes less than 0.5%, the relocation model needs adjustment.

(b) The pellet relocation model should affect the gap size used in structural response calculations.

(c) The mechanical strength of a cracked pellet during soft gap closure should be greater than the currently used value of zero, but less than that of solid pellets.

(d) Fuel mechanical deformation should be modeled.

(e) The fuel swelling rate at high burnup should be increased or the amount of fuel porosity available for accommodating swelling should be decreased.

7. USER RECOMMENDATIONS

During the assessment of FRAPCON-1, a set of user guidelines was developed which aid in setting up FRAPCON-1 input decks and eliminate the most typical input and nonconvergence problems.

Code input is simple and straightforward. Most of the input variables have reasonable default values. For six of the input variables, caution should be used when selecting values. Table 5 lists and describes these six variables, and presents comments concerning the proper selection of input values. For the remaining variables, best estimate values should be used. If available, default values may be used if best estimate values are unavailable. For analyses where consideration of calculational uncertainty is desired, the user should conduct an uncertainty study, as conducted in Reference 66, in which pertinent design input and correlation factors are systematically varied.

Adhering to the preceding input guidelines does not ensure that convergence problems will not be encountered. However, assessment experience has shown that nonconvergence problems occur very infrequently (in about 5 to 7% of the cases). To aid the user in overcoming nonconvergence problems, Table 6 lists the most commonly encountered problems and some suggestions to remedy the problems.

On the basis of the FRAPCON-1 assessment results, the following qualitative limitations should be noted when interpreting code results:

1. Fuel temperatures are likely to be overestimated at high burnups, if the initial gap size is relatively large (>2%), and if the fuel density is low (< 95% TD).

2. The cladding hoop stress is overestimated under hard gap closure conditions.

3. Cladding strains will be underestimated under soft gap closure conditions.

4. At power levels up to 20 kW/m, measured and predicted internal pressure are in good agreement. For power levels greater than 35 kW/m, the internal pressure will be overpredicted for low burnup conditions, and underpredicted for high burnup conditions.

TABLE 5 FRAPCON-1 INPUT RECOMMENDATIONS

VARIABLE	DESCRIPTION	COMMENTS
1. COLD-WORK	Cladding cold-work	This variable represents the effective cold-work after the mechanical cold-work and stress releaving processes have been completed during manufacturing. The default value of 10% is reasonable for commercial reactor rods of the 1970-75 vintage. However, the 10% may not represent the more recent rods or experimental fuel rods. Care should be taken to select a realistic value for this parameter, especially if pellet-cladding interaction is expected.
2. FLUX	Fast neutron flux	The cladding creepdown model is sensitive to this variable. Excessively high FLUX values will significantly reduce the creepdown rate. Thus, for cases with medium to high burnup and high power levels, accurate FLUX values should be input. The default value of 6×10^{17} n/m^2s produces reasonable results for rods operating at commercial reactor operating levels.
3. IPLANT	Radial power profile	When IPLANT=0, FRAPCON-1 generates the radial power profile across the fuel pellet. Use of this model is limited to fuel pellets with less than 4% enrichment. If enrichment is greater than 4%, IPLANT is set equal to -1 and the radial power profile is input through the RAPOW variable. Also, if a pellet centerline hole exists, use of the RAPOW variable should be considered to input a radial power profile which accounts for the effects of the hole irregardless of the fuel pellet enrichment.
4. NA	Number of axial segments	For commercial rods, a minimum of nine segments should be used. For commercial rods with a highly skewed axial power profile, up to sixteen segments should be used. For test rods up to three feet in length, using three to five segments is sufficient. Again, if the axial power profile is atypical (for example, highly skewed), more segments should be specified.

TABLE 5 (continued)

VARIABLE	DESCRIPTION	COMMENTS
5. TIME	End of time step at power level QMPY	The maximum recommended time step size is 1000 h.
6. TSINT	Fuel fabrication sintering temperature	The fuel densification and effective conductivity models are sensitive to this input variable. The default value of 1873 K is reasonable and typical; however, an exact value should be used, if available.

TABLE 6. FRAPCON-1 TROUBLE SHOOTER'S GUIDE

PROBLEM	POSSIBLE REMEDY
1. Nonconvergence during power up ramp	More power-time pairs might be added to the ramp, to obtain smaller power increases from step to step. See Figure 73.
2. Nonconvergence during long term (>10 h) steady state operation	The nonconverging power-time step might be divided into several parts, in which the power level remains constant but the time step size is 5h. If nonconvergence still occurs, the time step size should be reduced even further.

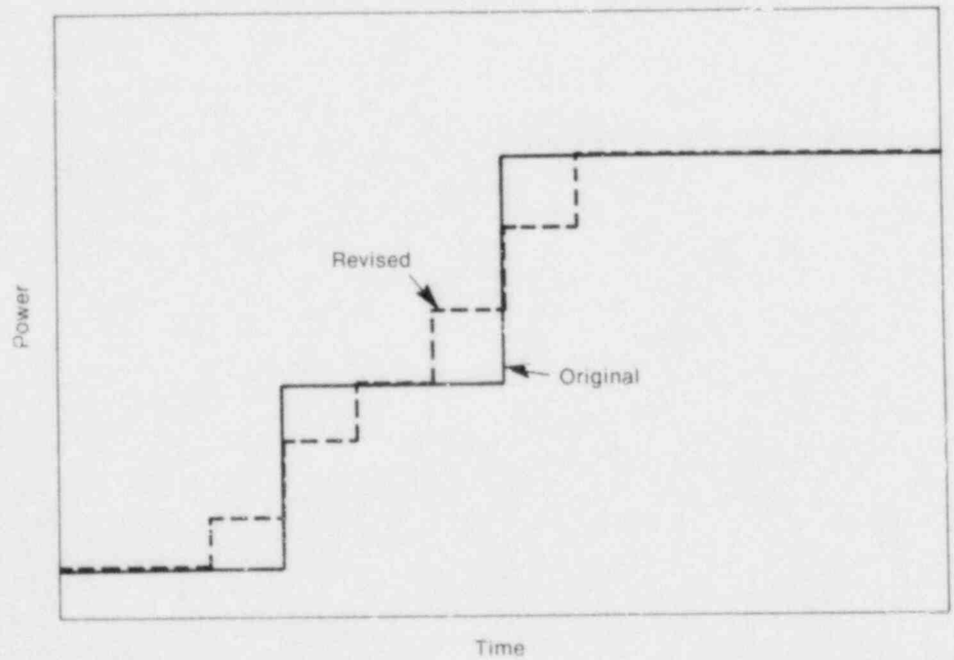

Figure 73. Comparison of original and revised power histories used when eliminating nonconvergence problems during increasing power ramp operation.

8. REFERENCES

1. D. R. Coleman et al., *FRAP-S3: A Computer Code For Steady State Analysis Of Oxide Fuel Rods Model Assessment Report*, NUREG/CR-0786, TREE-1352, April 1979.

2. D. D. Lanning et al., *GAPCON-Thermal-3: A Computer Program for Calculating the Thermal Behavior of Oxide Fuel Rods*, PNL-2434, February 1978.

3. L. J. Siefken et al., *FRAP-T5: A Computer Program For the Transient Analysis of Oxide Fuel Rods*, NUREG/CR-0840, TREE-1281, June 1979.

4. G. A. Berna et al., *FRAPCON-1: A Computer Code for the Steady State Analysis of Oxide Fuel Rods*, NUREG/CR-1463, EGG-2039, June 1980

5. G. A. Reymann (ed.) *MATPRO-Version 10: A Handbook of Materials Properties for Use in the Analysis of Light Water Reactor Fuel Rod Behavior*, TREE-NUREG-1180, February 1978.

6. I. Devold, *A Study of the Temperature Distribution in UO_2 Reactor Fuel Elements*, AE-318, 1968.

7. T. G. Odekirk, *Detailed Test Plan Report for PBF Test Series PCM-20*, ANCR-1095, April 1974.

8. G. Kjaerheim and E. Rolstad, *In-Pile Determination of UO_2 Thermal Conductivity, Density Effects and Gap Conductance*, HPR-80, 1966.

9. M. J. F. Notley et al., *Measurements of the Circumferential Strains of the Sheathing of UO_2 Fuel Elements During Reactor Operation*, AECL-4072, 1972.

10. E. T. Laats et al., *USNRC-OECD Halden Project Fuel Behavior Test Program—Experiment Data Report for Test Assemblies IFA-226 and IFA-239*, ANCR-1270, December 1975.

11. G. Kjaerheim and E. Rolstad, *In-Core Study of Fuel/Clad Interaction and Fuel Centre Temperature*, HPR-107, 1969.

12. M. G. Balfour et al., *Final Report on In-Pile Measurements of UO_2 Thermal Conductivity*, WCAP-2923, March 1, 1966.

13. J. A. Christensen, "Fuel-Cladding Gap Conductance from Large Diameter UO_2 Specimens," *Enlarged Halden Program Meeting, Geilo, Norway, March 16-21, 1975*.

14. G. Testa et al., "In-Pile Fuel Studies for Design Purposes," *Nuclear Applications and Technology*, 7, December 1969.

15. C. J. Baroch and M. A. Rigdon, "Irradiation Behavior of UO_2 at Burnups from 10 to 80 GWd/tonne U," *BNES Conference, 1973*, Paper No. 58, CONF-731004.

16. D. Knodler and H. Stehle, "PWR Fuel Reliability and Quality Assurance KWU Experience," *BNES Conference, 1973*, Paper No. 87, CONF-731004.

17. E. A. Bassler et al., *Saxton Core I Performance Summary*, WCAP-3269-43, 1965.

18. W. R. Smalley, *Saxton Core II Fuel Performance Evaluation*, WCAP-3385-56, September 1971.

19. W. R. Smalley, *Evaluation of Saxton Core III Fuel Materials Performance*, WCAP-2285-57, 1974.

20. D. G. Bridge et al., *UKAEA Fuel Test Assemblies Irradiated in HBWR 1964-1966*, HPR-132, 1970.

21. M. J. F. Notley et al., *Zircaloy Sheathed UO_2 Fuel Elements Irradiated at Values of $\int kd\Theta$ Between 40 and 83 W/cm*, AECL-1676, 1962.

22. R. D. MacDonald and A. S. Bain, *Irradiation of Zircaloy-2 Clad UO_2 to Study Sheath Deformation*, AECL-1685, 1962.

23. M. J. F. Notley and J. R. MacEwan, *The Effect of UO_2 Density on Fission Product Gas Release and Sheath Expansion*, AECL-2230, 1965.

24. M. F. Lyons et al., *UO_2 Fuel Rod Operation with Gross Central Melting*, GEAP-4264, 1963.

25. G. W. Cawood et al., *Power-Cooling-Mismatch Test Series, Test PCM-2A, Test Results Report*, ANCR-NUREG-1347, September 1976.

26. W. J. Quapp et al. *Irradiation Effects Test Series, Scoping Test 1, TREE-NUREG-1066*, September 1977.

27. M. D. Freshly, "Mixed-Oxide Fuel Irradiations in the Plutonium Recycle Test Reactor," *Nuclear Technology, 15*, August 1972, pp. 138, 141, 169, 172, 173.

28. M. Hurme, *Observation of Fuel Pin Internal Pressure*, OECD Halden Reactor Project, HPR-110, June 1969.

29. K. Taketani and M. Ichikawa, "Fuel Irradiation Experiments by JAERI for Light Water Reactors," *Contribution to Crest Specialist Meeting, Sacley, France, October 21-24, 1973.*

30. OECD Halden Reactor Project Quarterly Progress Report, January - March 1968, HPR-099, May 1968.

31. J. B. Ainscough, *An Assessment of the IFA-116 and 117 Irradiations from Data Obtained from the In-Reactor Instrumentation*, HPR-129, April 1971.

32. *OECD Halden Reactor Project Quarterly Progress Report, July—September 1970*, HPR 128, November 1970.

33. *OECD Halden Reactor Project Quarterly Progress Report, April—June 1971*, HPR-140, August 1971.

34. F. List et al., "Fuel Column Shortening In Irradiated UO_2-Zr Fuel Pins," *BNES-73 Conference, 1975*, Paper No. 75.

35. M. Ichikawa et al., "Uranium Oxide Fuel Pin Elongation Behavior Under Irradiation," *Journal of Nuclear Science and Technology, 8, 9* September 1971, pp. 52-54.

36. H. M. Ferrari et al., "Fuel Densification Experiment in Westinghouse Pressurized Water Reactors," *BNES Conference, 1973*, Paper No. 54, CONF-731004.

37. M. A. Rigdon et al., "Babcock and Wilcox's Irradiation Program on Fuel Densification," *BNES Conference, 1972*, Paper No. 59, CONF-731004.

38. *OECD Halden Reactor Project Quarterly Progress Report, October - December* [illegible], HPR-130, February 1974.

39. A. Hanevik et al., "In-Reactor Measurements of Fuel Stack Shortening," *BNES Conference, 1973*, Paper No. 89, CONF-731004.

40. R. M. Berman et al., *Irradiation Behavior of Zircaloy-Clad Fuel Rods Containing Dished End UO_2 Pellets*, WAPD-TM-629, July 1967.

41. J. T. Engle and H. B. Meieran, *Performance of Fuel Rods Having 97 Percent Theoretical Density UO_2 Pellets Sheathed in Zircaloy-4 and Irradiated at Low Thermal Ratings*, WAPD-TM-631, July 1968.

42. W. F. Domenico and J. A. Ramsthaler, *IFA-429 Data Report No. 1*, TREE-NUREG-1009, December 1976.

43. C. R. Hann et al., "Experimental Verification of Nuclear Fuel Rod Stored Energy Calculations," *Enlarged Halden Programme Group Meeting, Sanderstolen, Norway, March 8-12, 1976.*

44. C. R. Hann et al., "A Comparison of Pretest Predictions With Preliminary Data from NRC/PNL Halden Assembly IFA-431," *Fourth Water Reactor Safety Research Information Meeting, Gaithersburg, Maryland, September 28, 1976.*

45. C. R. Hann et al., "Application of Experimental Data to Reduction of Stored Energy Uncertainty," *Fourth Water Reactor Safety Research Information Meeting, Gaithersburg, Maryland, September 30, 1976.*

46. Z. R. Martinson and R. K. McCardell, *Power-Cooling-Mismatch Test Series Test PCM-2 Test Results Report*, TREE-NUREG-1038, February 1977.

47. W. J. Quapp et al., *Irradiation Effects Test Series Test IE-1 Test Results Report*, TREE-NUREG-1046, March 1977.

48. G. W. Gibson et al., *Characteristics of UO_2-Zircaloy Fuel Rod Materials from Saxton Reactor for Use in Power Burst Facility*, ANCR-NUREG-1321, September 1976.

49. N. Fuhrman et al., *Evaluation of Fuel Rod Performance in Maine Yankee Core I, Task C*, EPRI-NP-218, November 1976.

50. *Light-Water-Reactor Safety Research Program: Quarterly Progress Report, January - March 1976*, ANL-76-49, March 1976.

51. *Light-Water-Reactor Safety Research Program: Quarterly Progress Report, April - June 1975*, ANL-75-58, June 1975.

52. *Light-Water-Reactor Safety Research Program: Quarterly Progress Report, July - September 1975*, ANL-75-52, September 1975.

53. *Light-Water-Reactor Safety Research Program: Quarterly Progress Report, October - December 1975*, ANL-76-15, December 1975.

54. *Light-Water-Reactor Safety Research Program: Quarterly Progress Report, April - June 1976*, ANL-76-87, June 1976.

55. *Light-Water-Reactor Safety Research Program: Quarterly Progress Report, July - September 1976*, ANL-76-121, September 1976.

56. *Evaluating Strength and Ductility of Irradiated Zircaloy, Quarterly Progress Report for April - June 1975*, BMI-1935, June 1975.

57. *Evaluating Strength and Ductility of Irradicted Zircaloy, Quarterly Progress Report for July -September 1975*, BMI-1938, September 1975.

58. *Evaluating Strength and Ductility of Irradiated Zircaloy, Quarterly Progress Report for October -December 1975*, BMI-1942, December 1975.

59. *Plutonium Utilization in Boiling Reactors, Phase II, Semiannual Report, July - December 1971*, NEDO-19747, December 1971.

60. S. Y. Ogawa and D. L. Zimmerman, *Plutonium Utilization in Boiling Reactors, Phase II, Post Irradiation Examination of Four Fuel Rods After One Cycle of Operation in Big Rock Point Reactor*, NEDO-10387, July 1971.

61. H. R. Freeburn et al., *Light Water Reactor Fuel Rod Modeling Code Evaluation*, EPRI-NP-369, March 1977.

62. F. H. Megerth et al., *Zircaloy-Clad UO_2 Fuel Rod Evaluation Program*, GEAP-10371, June 1971.

63. R. Ueda et al., *Irradiation Testing of IFA-106 and IFA-107*, JAERI-MEMO-4344, February 1971.

64. D. M. Bishop and W. E. Baily, *Nondestructive Examination of Plutonium Recycle Fuel Rods Irradiated to 30,000 MWd/t*, NEDO-12552, December 1974.

65. S. J. Dagbjartsson et al., "Investigations on Axial Gas Flow Within High Burnup Fuel Rods," *Proceedings of ANS Topical Meeting on Thermal Reactor Safety, Sun Valley, Idaho, July 31 - August 4, 1977.*

66. *D. R. Coleman* and E. T. Laats, *FRAP-T3: A Computer Code For Transient Analysis of Oxide Fuel Rods - Model Assessment Report*, NUREG/CR-0555, TREE-1320, February 1979.